**ALMA MATER STUDIORUM - UNIVERSITÀ DI BOLOGNA**

SCUOLA DI INGEGNERIA E ARCHITETTURA

DICAM

CORSO DI LAUREA MAGISTRALE
IN
**INGEGNERIA CHIMICA E DI PROCESSO**

TESI DI LAUREA

in

DOWNSTREAM PROCESSING OF BIOLOGICAL MOLECULES

# Adsorptive membranes for sustainable and accessible haemodialysis

CANDIDATO

Antonella Noto

RELATORE

Chiar.ma Prof.ssa Cristiana Boi

CORRELATORI

Chiar.ma Prof.ssa Maria Grazia De Angelis
Dr. Simone Dimartino
Thomas Fabiani

Anno Accademico 2021/22
III sessione di laurea

# ABSTRACT

The increasing number of patients with chronic kidney disease who require haemodialysis results in an increased consumption of water needed for the process. This is the main motivation for the study of new systems to regenerate spent dialysate especially from uremic toxins. Mixed matrix membrane adsorbents (MMMAs), consisting of a membrane of cellulose acetate and zeolite as a filler, have been studied and characterised to be used as an adsorbent material for waste metabolites, such as uremic toxins and especially urea, present in spent dialysate. The membranes have been shown to have satisfactory properties and characteristics; the mechanical resistance is sufficient to prevent membrane crushing and rupture up to a maximum pressure of 0.05 bar, and the permeability reaches values of 4200 L/(m2 h bar). The adsorbent is homogeneously dispersed in the membrane, and its skin layer is porous and less than 2 μm thick. In contrast, the morphology of the section is characterised by finger-like pores. Finally, MMMAs with 10 wt% zeolite show an equilibrium binding capacity of 17 mg/cm3. Particular interest was devoted to the study of the parameters that most influence membrane morphology in order to obtain membranes with the desired microstructure. The factors that influence membrane structure are many; among those analysed are the concentration of porogen and polymer, and the temperature of the coagulation bath. The bath temperature is definitely the factor that has the greatest impact on morphology.

Keywords: Haemodialysis, Water consumption, Uremic toxins, Zeolites, Silica, Cellulose acetate, Mixed Matrix Membranes adsorbers, Adsorption.

# Contents

# List of Figures

# List of Tables

# 1 Introduction

This thesis work was mainly carried out at the host site of the University of Edinburgh in the School of Engineering during an Erasmus period. The activities were supervised by Professors Maria Grazia De Angelis and Simone Dimartino with the collaboration of Professor Cristiana Boi, the project supervisor at the University of Bologna. All activities were carried out with the daily help of doctoral student Thomas Fabiani. The final part of the project was carried out in the Bioseparations laboratory of DICAM under the supervision of Prof. Cristiana Boi.

## 1.1 Chronic kidney disease

### 1.1.1 Kidney function and renal insufficiency

Chronic kidney disease (CKD) is a disease characterised by a progressive decline in kidney function over time, affecting 697.5 million people worldwide (Couser *et al.*, 2011).

Kidney removes compounds, known as uremic toxins (UTs), from the blood stream, as its primary function. Furthermore, kidneys continuously balance water and electrolytes, by selectively excreting or reabsorbing them, in response to changes in blood volume and osmolality. In addition, the kidneys serve as the primary location for the manufacturing of many hormones. (Yang and He, 2020)

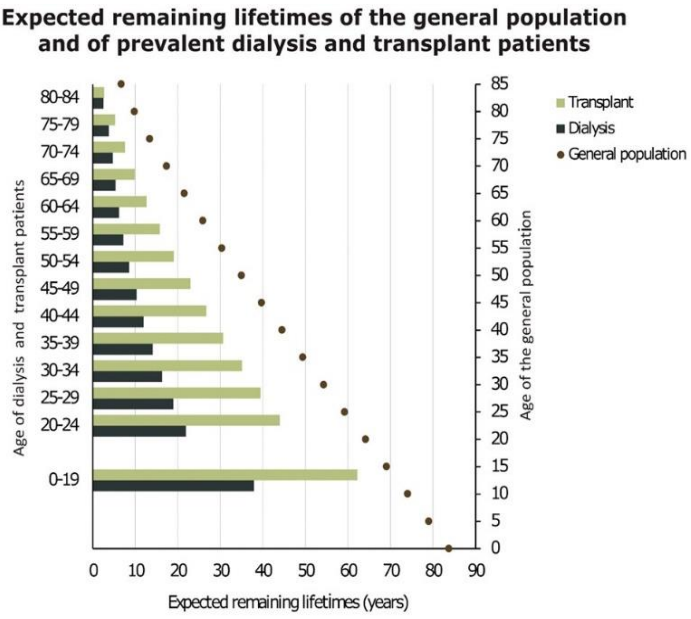


**Figure 1** Expected remaining lifetimes of the general population and prevalent dialysis and transplant patients.

Moreover, CKD is associated with extremely high morbidity and mortality even in its earlier stages (**Figure *1***).

CKD is divided into 5 stages that identify the magnitude of renal failure. The stages are associated with the value of a parameter called the Glomerular Filtration Rate (GFR), which indicates the volume of glomerular filtrate in the unit of time referring to an area of 1.73m$^2$. In a healthy adult, the GFR value is 100-120 ml/min. Stage 1, GFR>90 ml/min, is asymptomatic mild insufficiency without large reductions in GFR. Stage 2, GFR=60-89 ml/min, is often still asymptomatic insufficiency but with markedly reduced GFR values. Stage 3, GFR=30-45 ml/min, presents the first symptoms associated with a severe reduction in GFR values. Stage 4, GFR=15-29 ml/min, shows a severe clinical situation and a greatly reduced GFR. Finally, stage 5, GFR<15 ml/min, is called end-stage renal disease (ESRD) and is a condition of advanced renal disease requiring haemodialysis or transplantation. (Bauer, Melamed and Hostetter, 2008; miriana, 2021)

Mortality of ESRD patients can be 10 to 100 times greater than in age-matched controls with normal kidney function. This situation is even worse in most developing nations, where ESRD constitutes a “death sentence”, as renal replacement therapy is often unavailable or unaffordable: nearly 1 million people die with ESRD each year in developing nations.

The prevalence of ESRD increased significantly during the following several decades since it constitutes a growing global public health epidemic. (Couser *et al.*, 2011)

### 1.1.2 Transplantation and haemodialysis

Chronic kidney disease (CKD) usually results in the ESRD, requiring hemodialysis or transplantation as renal replacement therapies. (Couser *et al.*, 2011)

There has been a considerable increase in the population of people with ESRD; between 1998 and 2002, the prevalence of ESRD in Canada rose by 33%, whilst the incidence rose by 17%. Many ESRD patients are more likely to have health problems or other problems that preclude them from receiving a transplant due to the age of the ESRD population, so not all the patients (e.g. individuals with serious comorbidities) are eligible recipients for kidney transplant. Additionally, people who are eligible for transplants now have to endure longer dialysis wait times due to the lack of accessible organs for transplantation. For the majority of patients with ESRD, renal transplantation is the best form of renal replacement therapy now available, but unfortunately, the scarcity of donated organs continues to be a significant barrier, and problems with organ donation, retrieval, and preservation still exist. As a result, the most popular form of treatment for those with ESRD is dialysis.

Right now, over 2 million people worldwide are in hemodialysis, but it represent around one tenth of the patients requiring the treatment. (Yang and He, 2020)

### 1.1.3 The cost of hemodialysis treatment

Despite the fact that dialysis is the norm in many countries, the disproportionately high cost of treatment remains a major concern. For instance, even though only 0.092% of Canadians have ESRD, more than 1.2% of all health care spending ($1.8 billion) was spent in 2005 in Canada on treating patients with the condition. The United States and other countries have comparable statistics.

The significant number of patients receiving ESRD treatment further exacerbates the expense issue for each individual patient.

The prevalence of ESRD will continue to rise due to the rising number of people with chronic renal disease, as well as the global rise in both hypertension and diabetes mellitus. The number of persons requiring dialysis worldwide is predicted to exceed 2 million by 2010, and it is expected that treating this population will cost $1.1 trillion.

Haemodialysis comes in a variety of forms, including peritoneal dialysis, in-hospital haemodialysis, home haemodialysis, and overnight haemodialysis, each of which has its own benefits and drawbacks as well as costs and effectiveness. (Klarenbach and Manns, 2009; Couser *et al.*, 2011)

## 1.2 Hemodialysis

### 1.2.1 Toxin removal and ion balance

The uremic toxins (UTs) are a broad class of toxins that need to be removed from the blood. Low concentrations of these molecules do not constitute a toxicity factor for the human body (for urea, values below 20mM). Their concentration is kept below the maximum limits of toxicity thanks to elimination by the urinary system. When the kidneys no longer perform a regular physiological function, these molecules accumulate, increasing their concentration in the body and becoming toxic.

They are categorized as small soluble toxins (e.g. urea), middle soluble toxins (e.g. β-microglobuline) and protein-bound uremic toxins (e.g. indoxyl sulphate).(Weiner, Mitch and Sands, 2015; van Gelder *et al.*, 2020)

The reference concentration values used to assess the health of kidney function and the possible severity of the disease are urea nitrogen or azotemia, while urea concentration is rarely used. Urea nitrogen also called blood urea nitrogen (BUN) is the concentration of nitrogen contained in the urea molecule, while azotemia is the total concentration of non-protein nitrogen.

The amount of urea produced daily ranges between 14.4 and 28.2 g/d, according with the diet. This necessarily corresponds to the amount of urea that must be eliminated daily from the human body to ensure that urea concentration values are maintained in the range of 13-43 mg/dL, typical concentrations in a healthy patient. (Shinaberger *et al.*, 2006; van Gelder *et al.*, 2020)

Urea is the end product of the urea cycle, a set of reactions that take place in the liver and are aimed at metabolising nitrogenous waste products into ammonium. Ammonium is toxic at low concentrations and it is converted into urea, to be excreted by urination after the filtration process carried out by the kidneys. (Weiner, Mitch and Sands, 2015)

**Table 1** Concentration of urea, creatinine, BUN, azotemia in a healthy individual and a patient affected by CKD.

| **Parameter** | **Concentration healthy patient (mg/dL)** | **Concentration CKD patient (mg/dL)** |
|---|---|---|
| Urea | 13-43 | >43 |
| Creatinine | 0.84-1.21 | >1.21 |
| Urea nitrogen (BUN) | 6-20 | >20 |
| Azotemia | 15-50 | >50 |

**Table 1** shows some values of blood concentrations of reference for healthy patients, including urea and creatinine concentrations which should be in the ranges of 13-43 mg/dL and 0.84-1.21 mg/dL respectively. Other concentration values reported concern parameters often used as a reference for the assessment of renal function and are urea nitrogen and azotemia with values between 6-20 mg/dL and 15-50 mg/dL respectively. Higher concentration values than those indicated are characteristic of patients with CKD. (Hosten, 1990; Vanholder, Gryp and Glorieux, 2018; Miliani, 2020)

The concentration of urea accounts for about 50% of the total concentration of non-protein nitrogen, namely nitrogen not contained in protein molecules. Azotemia is defined as the total amount of nitrogen supplied by all uremic toxins, excluding protein nitrogen.

Blood concentrations of uremic toxins fluctuate within the ranges indicated in the **Table 1**, whereas in a CKD patient the UTs are not excreted and accumulate in the blood and therefore, the concentration of UTs increases until the next haemodialysis session. In addition, these values depend on many factors such as metabolism and diet of the individual.

During the dialysis process, UTs are diluted in the dialysate, decreasing their concentration in the blood stream. During the session, normal electrolyte levels are also restored, rebalancing the acid-base balance through the correct and specific composition of the dialysate used during the session. The dialysate is essentially a physiological salt solution that creates a gradient for the removal of unwanted solutes and maintains a constant physiological concentration of extracellular electrolytes **Table 2**. The concentrations of vital solutes added to the dialysate reflect those normally maintained in the body by the native kidneys. (Jane Y. Yeun, Brian Young, Thomas A. Depner e Andrew A. Chin, 2020; Azar and Canaud, no date)

**Table 2** Reference values for ions, salts, sugars and acidity in a healthy person and present in the dialysate.

| **Solutes** | **Concentration (mEq/L)** |
|---|---|
| Sodium | 135-145 |
| Chloride | 102-106 |
| Bicarbonate | 30-39 |
| Dextrose | 11 |
| Acetate | 2-4 |
| Magnesium | 0.5-1 |
| Potassium | 0-4 |
| Calcium | 0-3.5 |
| pH | 7.1-7.3 |

### 1.2.2 Hemodialysis treatment

Hemodialysis (HD) is an extracorporeal treatment based on the exchange of compounds in the blood stream through a semipermeable polymeric membrane with a buffered solution, called dialysate.

HD depletes UTs from the patient through a diffusion mechanism. Therefore, the clearance, i.e. the capacity of an organ to purify and dispose of a substance in the unit of time, is driven by the concentration gradient of solutes between the blood and dialysate, across the semipermeable membrane. For instance, urea diffuses from the blood to the dialysate compartment, lowering the body's overall urea quantity and blood urea concentration. In contrast, the gradient in bicarbonate concentration typically encourages the passage of this ion from the dialysate to the blood compartment, to restore the proper concentration of the anion.

The semipermeable membrane is responsible for the elimination of unwanted solutes and the removal of excess fluid, but at the same time it must ensure that it retains proteins and the suspended component of blood in the patient. The thickness, porosity, composition and surface area of a membrane determine its ability to eliminate solutes and remove water. In general, the thinner the membrane and the more porous the membrane, the more efficient the transport of solutes and fluids through the membrane. Urea clearance (60 Da) describes the membrane's ability to remove low molecular weight substances, β-2microglobulin clearance (11,8 kDa) indicates the ability to remove higher molecular weight substances, and the ultrafiltration coefficient ability to remove water. (Jane Y. Yeun, Brian Young, Thomas A. Depner e Andrew A. Chin, 2020)

Since solute removal is the primary goal of dialysis, this capacity should be extended to include substances up to a molecular weight of 50 kDa, because this value is the cut-off for the natural kidney. Therefore, the rejection of albumin (60 kDa) and the minimum retention of β-2microglobulin (11,8 kDa), whose removal is desired, are used as benchmarks for choosing the membrane cut-off. (Maduell, 2018)

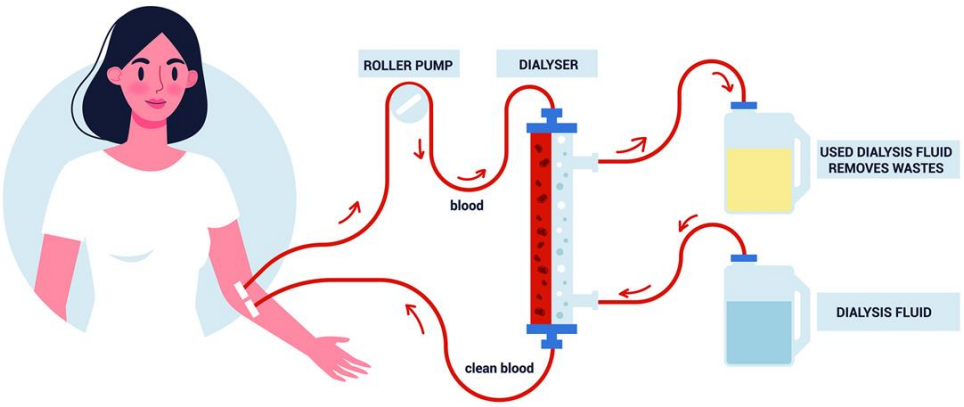


**Figure 2** Diagram of a conventional hemodialysis process.

The conventional haemodialysis process consists on the withdrawal of blood from the patient and, that is pumped, through an extracorporeal blood circuit, to a hollow-fibre membrane module, usually consisting of 10000-20000 fibres with a diameter of 0.2 mm and a length of 150 mm, called a dialyser. (Azar and Canaud, no date) The dialyser provides the necessary area for the exchange of matter between blood and dialysate. Often the required surface area is 0.8 - 2.1 $m^2$ and the flow of blood and dialysate through it are 250 and 500 mL/min respectively for a standard dialyzer (**Figure 2**). (*Hemodialysis - ClinicalKey*, 2020)

There are four different ways through which matter is exchanged:

1. *Diffusion*: Solutes migrate voluntarily and passively through the dialysis membrane
2. *Convection*: Solutes move voluntarily across the dialysis membrane. Scavenging of macromolecules is mostly accomplished by convection.
3. *Adsorption*: Adsorption is a process that involves attaching molecules from blood or plasma to a surface built into a module of an extracorporeal circuit. Fundamentally, adsorption happens because sorbents are hydrophobic.
4. *Ultrafiltration:* A solvent, such as water, can be pushed through a semipermeable membrane on a gradient of pressures, from higher to lower pressures. The pressure gradient may be caused by mechanical hydrostatic pressure or osmotic force. The molecules of the dissolved solute that are tiny enough to fit through the membrane pores are carried by the solvent. (Yang and He, 2020)

### 1.2.3 Delivery of haemodialysis

The conventional treatment is delivered in sessions of 4-5 h, two or three times per week, in a hospital or a dedicated clinic. (Raymond M. Hakim and Sharmeela Saha, 2013) For this reason, the patient is required to commute and be hospitalized for several hours per week, leading to a severe disruption of patient lifestyle. Moreover, UTs and electrolytes accumulate in the body in between the sessions, with a fast drop of their concentration during the session itself, resulting in a post-treatment hangover. In a similar way, the increase of blood volume, due to a reduced or absent diuresis, results a severe in vascular stress.

Treatment can be conducted at home overnight in order to reduce the downsides of in-clinic dialysis and improve the patient's living conditions. **Table 3** shows the two possible modes of frequency and duration of off-clinic treatment compared with the possible modes of in-clinic treatment.

**Table 3** Haemodialysis modalities: in-center and home-dialysis

| | | **Frequency** | **Duration** |
|---|---|---|---|
| Daily in-center | Conventional | 3 time a week | 4h each session |
| | Frequent | 6 time a week | 2-3h each session |
| Nocturnal at home | Conventional | 3 time a week | 4h each session |
| | Nocturnal | 6 time a week | 6-8h each session |

According to some statistics, patients undergoing home haemodialysis have experienced several positive effects:

- flexibility of scheduling haemodialysis sessions
- elimination of commuting between home and dialysis centre
- less medication
- less dietary restrictions
- better regulation of blood pressure and mineral metabolism
- reduction of left ventricular hypertrophy (15g in six months)

All these aspects help to improve the patient's quality of life, not only psychologically, but also medically. Ventricular hypertrophy (VH) is one of the most important and recurring negative effects in CKD patients due to the increase in blood volume as a result of failure to expel excess water and consequent accumulation of fluid between one haemodialysis session and the next in a discontinuous treatment.
Ventricular hypertrophy is a cardiac pathology in which the walls of the ventricle thicken due to increased muscle tone (hypertrophy), reducing the volume and capacity of the ventricular cavity. Structural alteration of the ventricle leads to functional alteration of the heart. VH can cause heart failure, arrhythmias and myocardial ischaemia and cardiac arrest. Therefore, the VH is an effect that not only reduces the quality of life, but especially the duration.

Many of the positive effects of nocturnal dialysis are due more to the time spent on dialysis and not to the increased amounts of urea removed. Night dialysis has been shown to have a much lower incidence of mortality than conventional dialysis and has survival rates comparable to those of transplant recipients. Unfortunately, home dialysis is still not widely practicable due to high equipment costs, because it requires the same equipment as in-center dialysis, which is not even mobile.(Stokes, 2011) Generally, home dialysis is a more patient-friendly solution, but it has proven to be very stressful for the patient's partners and family. (Mowatt, Vale and MacLeod, 2004)

According to some studies, home nocturnal haemodialysis (HNHD) is less expensive than traditional in-center haemodialysis, which is thought to cost between CAN$80,000 and CAN$95,000 per patient-year. In contrast to traditional in-center haemodialysis (IHD), where patients receive three treatments each week, a patient undergoing HNHD receives five to seven dialysis sessions each week. Thus, the HNHD offers more dialysis sessions than the IHD and at a cheaper overall cost, for three times as many sessions, the annual cost is estimated to be $10,000 less than for IHD. Reductions in costs for direct supplies for haemodialysis and the cost of depreciable products were more significant than increases in costs for personnel, overheads and support, admissions and procedures. The HNHD is always the less expensive choice, but the cost savings are only statistically significant if the patient uses the modality for at least three years. (Mcfarlane, Pierratos and Redelmeier, 2002)

In other words, haemodialysis at home does not cost more than at the centre, more hours of treatment are performed for the same cost and with different benefits on the patient's life and health.

The delivery of the treatment close to the patient is considered a fundamental target for the nephrology community but it is still a challenge due to the size of the equipment, the low portability of conventional machines and the need to supply water. Currently, the smallest home haemodialysis machines weigh 24 kg or 34 kg and require large volumes of dialysate, more than 20 L/treatment.(van Gelder *et al.*, 2018)

For these reasons, the aim in recent years has become to design new devices that are lightweight, small and do not require water supply, so that they can be portable and therefore worn by the patient. In addition, wearable devices, such as wearable artificial kidney (WAK) or portable artificial kidney (PAK), enable continuous haemodialysis treatment.

A continuous delivery of HD is preferred over conventional hospital haemodialysis and peritoneal haemodialysis because, unlike the former, it allows for the continuous excretion of uremic toxins, proteins and other metabolic waste products by mimicking the natural dialysis process carried out by a healthy kidney.

It prevents the accumulation of toxins, waste products and fluids, thus avoiding overloading and stressing other organs and in particular the cardiovascular system due to the onset of hypertension. In addition, unpleasant patient discomforts such as nausea are greatly reduced, increasing the patient's well-being. On the other hand, unlike peritoneal haemodialysis, there are no constraints on the duration of applicability of the process due to the reduced efficiency of the peritoneal membrane and the lower degree of blood purification per unit of time.

Two other benefits brought about by WAK are smaller fluctuations in the concentration values of salts and other solutes and, above all, smaller volumes of dialysate to be discarded and smaller volumes of water required for the process.(van Gelder *et al.*, 2020)

### 1.2.4 Dialysate preparation

Haemodialysis demands a large amount of water, required for the production of the dialysate.

A typical 4 hour HD requires 120 L of dialysate at a flow rate of 500 mL/min. (Yang and He, 2020) (van Gelder *et al.*, 2018) (Geremia *et al.*, 2021) Thus a patient receiving 4 hours of dialysis for 3 times per week uses around 18,000 litres of dialysis fluid per year (Tarrass *et al.*, 2010).

Dialysate fluid is a solution prepared dissolving salts in ultrapure water, according with a tailored proportion, according with the treatment plan. This is performed by adjusting the dialysate's chemical makeup, namely sodium chloride, sodium bicarbonate or sodium acetate, calcium chloride, potassium chloride, and magnesium chloride as its main ingredients. Glucose is usually included to prevent intradialytic hypoglycemia. (Yang and He, 2020)

Ultrapure water is produced through a water purification unit, consisting in adsorption (using activated carbon filters), softening, reverse osmosis, deionization, and exposure to UV radiation.(Health, 2020) Furthermore, the chemical, bacterial, and pyrogen composition of the dialysate water must adhere to stringent criteria.(Innovation, 2014) The patient's health depends critically on the quality of the water, since it gets in contact with the blood stream in the dialyser.(Yang and He, 2020)

Up to 25% of the water entering the water treatment system may be discharged down the drain for every litre of useful water used to create the dialysis fluid by the reverse osmosis system (Tarrass *et al.*, 2010)

The regeneration of dialysate represents a technical challenge that would enable the design of a miniaturized device, with the requirement of few litres of dialysate. Such an approach would make possible to design a portable artificial kidney (PAK) or a wearable artificial kidney (WAK).

## 1.3 Wearable Artificial Kidneys

The key point of the PAK/WAK technology is the in-line regeneration of the dialysate by removing waste solutes (uremic toxins, proteins and phosphate and potassium ions) and the

reintegration of salts and ions, necessary to maintain the physiological balance of the blood. (**Figure *3***)

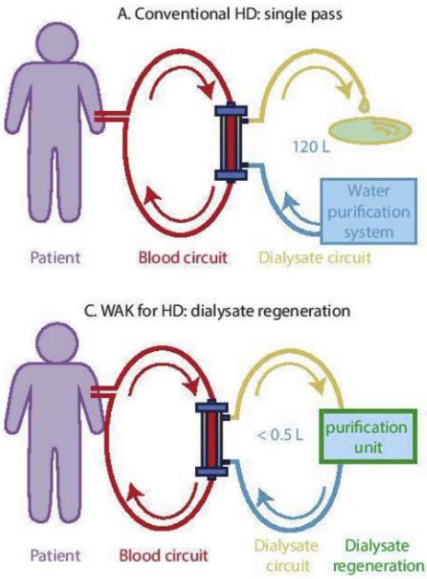


**Figure 3** Schematic of conventional h*a*emodialysis versus WAK haemodialysis.

Urea is the molecule of greatest interest because it is the toxin with the highest concentration (2 mM) of all the other UTs and because it is difficult to separate from the dialysate.

While most UTs are effectively captured by hydrophobic supports, urea is difficult to remove from water: water and urea have similar size and are both polar and weakly nucleophilic; not least, urea is extremely diluted in the dialysate (Olesberg, Arnold and Flanigan, 2004). For this reason, the bottleneck of dialysate regeneration is the removal of urea since the first attempts. (Lehmann, Marten and Gullberg, 1981).

### 1.3.1 State of art of PAK and WAK

The first wearable technology for haemodialysis developed, known as the REDY® system (Roberts *et al.*, 2000), was based on a multi-cartridge layout, consisting in:

- Activated carbon, to adsorb hydrophobic UTs, part of the urea and non-urea organic compounds.
- Urease immobilised on alumina support, converting enzymatically urea to ammonium and carbon dioxide.

30-50 g of immobilised urease are required to capture all urea at a concentration of 2-40 mM from a dialysate with a flow rate of 300 mL/min for a 4 h treatment. It is necessary to immobilise urease on solid media; there are different methods of immobilisation, either physical or chemical. Chemical immobilisation is the most preferable for WAK because physical immobilisation is weaker and easily reversible.(van Gelder *et al.*, 2020)

- An ion exchange to capture ammonium releasing sodium and proton, to convert carbonate in bicarbonate.

Such device entered the market on 1973, but it was withdrawn from the market during the 90s, due to safety issue. In fact, the READY system presented several problems. The ammonium produced by the conversion of urea was in higher quantities than urea, so 1 kg of zirconium phosphate was required to capture all the ammonium which was also more toxic than urea. But zirconium phosphate also bound calcium, magnesium and potassium which must necessarily be replenished to maintain the correct ionic balance in the patient and this required an additional reinfusion reservoir, which increased the weight of the device. Adsorbed cations were exchanged for sodium cations and the release of sodium in the dialysate caused hypertension. To avoid high sodium concentrations in the dialysate, a sodium-free dialysate reservoir could be used to dilute the released ions, but this was at the disadvantage of miniaturization. Finally, the release of aluminium ions from the AC caused osteomalacia (bone softening) and encephalopathy (brain injury). (van Gelder *et al.*, 2020)

The same system was improved during the last two decades, e.g. by Gura (Gura *et al.*, 2009), but they still rely on a reactive steps producing ammonium, hazardous for the patients. Other problems reported were excessive carbon dioxide bubbles in the dialysate circuit, the presence of gas bubbles in the blood circuit, blood clot formation in the blood circuit, and technical problems such as kinking of tubes and premature battery failure. (van Gelder *et al.*, 2018)

Another approach is based on electrochemical conversion of urea into gaseous products (nitrogen, hydrogen and carbon dioxide) that can easily be removed from dialysate by a bubble trap. But besides the mentioned gasses this technology has to cope with the formation of by-products, such as active chlorine species, chloramines, nitrogen oxides ($NO_3^-$, $NO_2^-$) and ammonia ($NH_3$), that need to be removed because they might be harmful due to their

high reactivity. A technology based on adsorption, rather than conversion of urea is intrinsically safer. (van Gelder *et al.*, 2020)

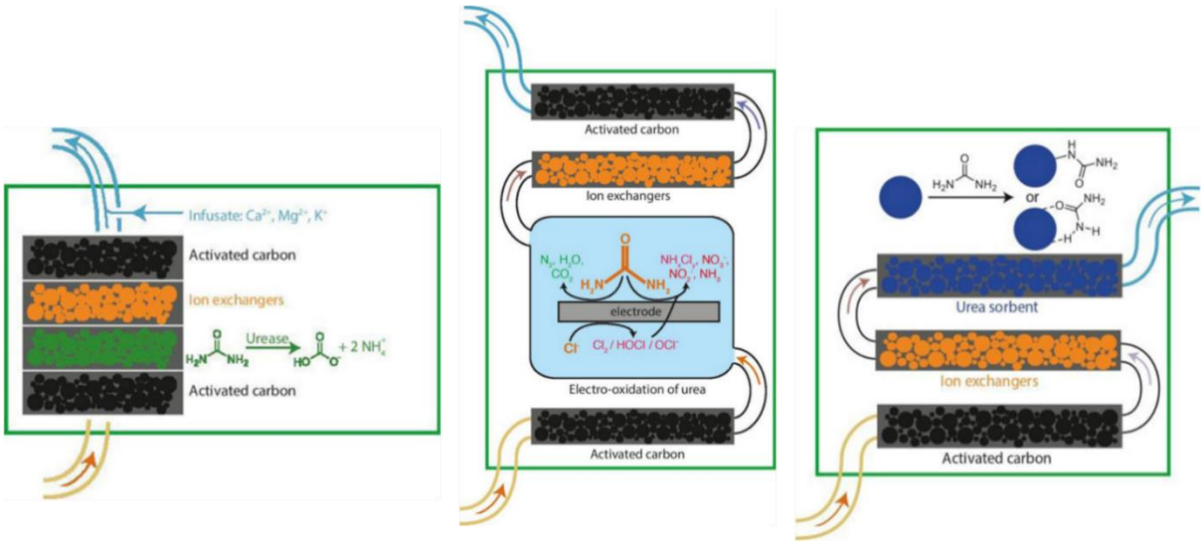


**Figure 4** WAKs and their mechanism of functioning. On the left, the REDY® system, in the center a WAK based on electrochemical oxidation of urea, on the right a WASK based on urea capture by a sorbent.

Adsorbents for urea must have a high adsorption capacity and reversibility of binding, this allows the amount of urea produced daily (240-470 mmol/d) to be removed by the dialysate.

**Table 4** contains some important constraints for the design of WAK devices and the desired characteristics.

**Table 4** Design constrains and design desirable features di un WAK device.

| WAK design constrains | WAK design desirable features |
|---|---|
| No reaction or leaching | Moderate cost |
| Chemical stability | Easily scalable |
| Regenerable | Autoclavable (easy sterilization) |
| Capture of 240-470 mmol/d of urea | |

The adsorbents most frequently used to capture urea are silica or zeolites, both materials bind urea with hydrogen bonds and dipole interactions and therefore the kinetics are fast, the

bond reversible and the adsorbent regenerable. Unfortunately, most urea adsorbents have a low adsorption capacity.

When the urea-adsorbent bond is non-covalent, the urea bound to the adsorbent is in equilibrium with the urea dissolved in the dialysate. As the urea concentration of the dialysate (10-30 mM (van Gelder *et al.*, 2020)) decreases during dialysis, the amount of urea bound per unit time (and thus removed from the dialysate) decreases over time, so the efficiency is reduced and the adsorption kinetics are slowed down over time.

Urea sorbents have to be bioincompatible, i.e. the material must not have toxic or injurious effects on biological systems, but not necessarily hemocompatible because the material will be in contact with the dialysate but not with the blood. In addition, it is necessary to prevent leaching by guaranteeing the stability of the adsorbent under dialysis conditions.

A WAK must necessarily:

- allow high flows of dialysate to be treated
- have low pressure drop to minimise the pressure applied and reduce the energy required
- ensure fast adsorption kinetics to quickly adsorb urea into the high-flux dialysate
- avoid dispersion of the adsorbent in the membrane module during the haemodialysis process

The use of a support in which the adsorbent is trapped, such as a mixed-matrix membrane (MMM), is a solution to satisfy the main requirements for a WAK device.

## 1.4 Mixed Matrix Membrane and adsorbents

### 1.4.1 Mixed Matrix Membrane (MMM) and their classification

A mixed matrix membrane (MMM) is a composite material made of a polymeric matrix in which micro or nanoparticles, so called filler, can be dispersed or incorporated. These fillers are often porous and come in a variety of forms, such as zeolites, activated carbon, or non-porous substances like titanium oxide and silica.

In principle, MMMAs have the potential to provide both the fabrication ease of a polymer and the stability of a ceramic material. They can also demonstrate greater permeability,

selectivity, fouling resistance, and chemical strength over a wide pH and temperature range. The filler is crucial to the effectiveness of separation whereas the polymeric matrix controls permeability. The inclusion of filler typically alters the membrane's morphology, which changes the transport phenomena and affects the membrane's overall performance. Collateral effects, such as pore obstruction and particle aggregation, might occur in MMMAs fabrication. Therefore, it is necessary to investigate an appropriate protocol for the desired application.

Polymeric membranes are cheap, easy to manufacture and versatile, but are chemically and mechanically not very resistant; on the other hand, ceramic membranes are very resistant but are expensive, difficult to manufacture and not very versatile. The MMMAs produced to date offer good mechanical strength, reduced fouling, high permeability and selectivity, and the mixed matrices allow for the specific removal of target components. MMMAs are a new topic of study that is still under investigation, but which has already found good success in several separation areas, such as gas separation or blood purification with the removal of toxins from human plasmas. (De Pascale, 2021)

MMMAs can be categorised according to the type of filler used:

1. *Inorganic filler MMMAs*:
   the filler interacts with the matrix through Van der Waals forces, covalent interactions, or hydrogen bonds. Inorganic fillers are a crucial component of MMMAs since they significantly aid in achieving the desired features, such as increasing flow, promoting selectivity, and reducing fouling and biofouling. The chemical incompatibility of inorganic fillers, which can result in gaps at the polymer-filler interface and compromise the MMMAs integrity and selective transport capabilities, is one of the main disadvantages of adding them to polymer matrixes.

2. *Biomaterial filler MMMAs*:
   have the benefit of being bio-based materials, the addition of biofillers improves MMMAs capabilities like mechanical resistance, fouling resistance, and permeability. They can be included in vesicles that are coated on the support or typically coated on the polymeric substrate.

3. *hybrid filler MMMAs*:
   have two distinct fillers added to the polymeric phase. These hybrid materials are integrated either to modify a particular quality of the pure membrane or to boost the MMMAs' overall effectiveness.

### 1.4.2 Mixed Matrix Membrane Adsorbers (MMMAs)

MMMAs are composite membranes for the adsorption process and they are based on the same principle of MMMAs. The composite material allows to obtain optimal physical-mechanical properties and a selective adsorption capacity at the same time, using adsorbing particles as a filler. MMMAs overcome the typical issues of traditional adsorbents: the porous polymer matrix allows to improve transport properties, guaranteeing stability. In comparison to traditional packed bed procedures, MMMAs offer uniform adsorbent distribution, low pressure drops, and short residence times, all of which reduce time and energy usage.

The dynamic adsorption of MMMAs depends on the trapped fillers, the pore size distribution and surface area, the ion exchange capability, and the adsorption properties of the particle. Mass transport in such systems may be divided into four contributions (**Figure 5**):

I. external mass transfer from the bulk solution to the membrane surface
II. diffusion trough the membrane pores in the membrane thickness direction (axial diffusion)
III. radial diffusion in membrane pores to reach the particles
IV. diffusion inside the pores of the adsorbent

In the case of MMMA, the limiting transport mechanism is axial diffusion; in the case of conventional adsorbents, the greatest resistance to matter transport is intraparticle diffusion (Yi Suen, 2015).

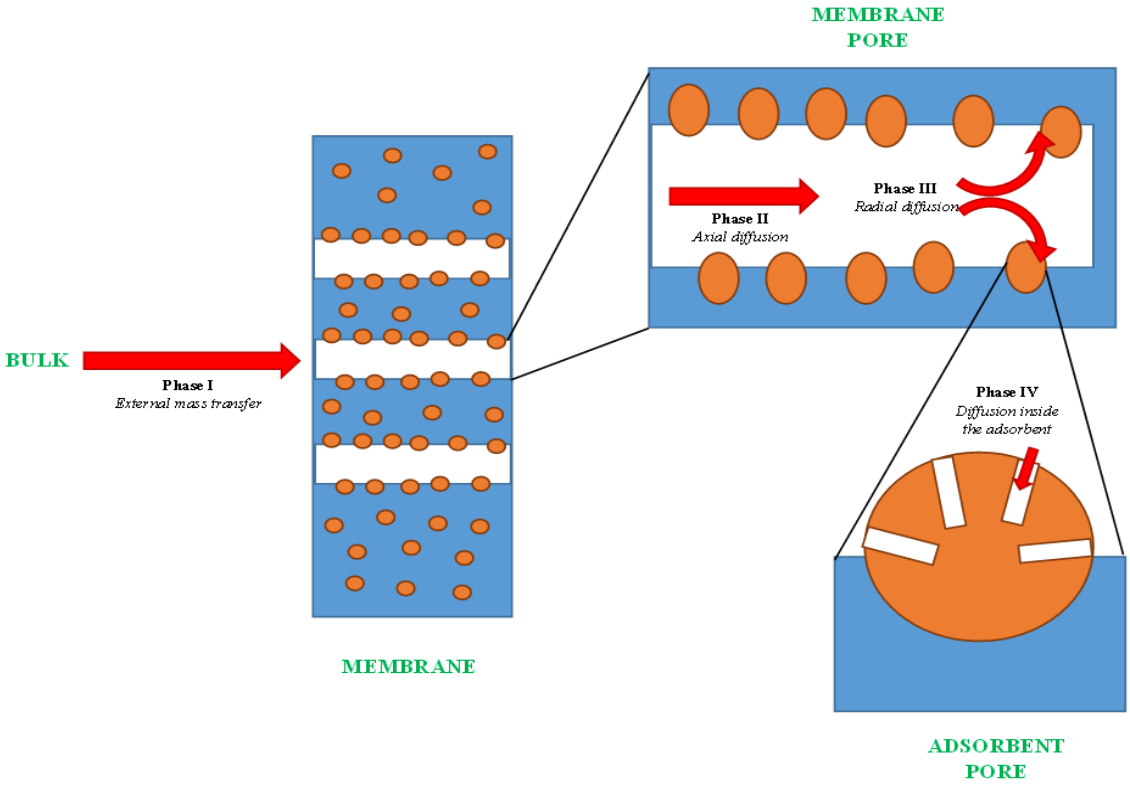


**Figure 5** Schematization of the phases of the mass transport mechanism.

### 1.4.3 Non-solvent induced phase separation for MMMAs fabrication

MMMAs may been adopted as a strategy for dialysate regeneration in haemodialysis. To integrate an effective sorbent for urea can be dispersed in a biocompatible porous polymeric matrix. The selection of adsorbent powders with a small particle size (micro or nanoparticle) and the fabrication of a highly porous polymeric support are critical to reduce the characteristic time for UTs to diffuse and bind to adsorption sites.(Avramescu *et al.*, 2003)

The Non-solvent Induced Phase Separation (NIPS) technique relies on the demixing of a polymer (dissolved in a solvent) induced by the presence of a third component, namely the non-solvent. Therefore, the coagulation phase consists in the demixing process, in which a polymer-rich and a polymer-lean phases forms. The polymer precipitates according with the equilibrium of the ternary system, that is influenced by many parameters, that results in a different morphology of the membrane. Particularly, an important role is played by:

- choice of polymer
- choice of solvent and nonsolvent

- composition of casting solution
- composition of coagulation bath
- temperature of the casting solution and the coagulation bath
- evaporation time if the solvent is volatile (high vapour pressure)

The process can be represented in a ternary phase diagram (***Figure 6***). The corners represent the pure components (solvent, non-solvent and polymer), the sides are the binary mixtures and the area of the triangle is the ternary mixture. Three zones delimited by a binodal and a spinodal boundary, the area to the left of the binodal boundary is the thermodynamically stable region, the area to the right of the spinodal boundary is the thermodynamically unstable region and the area between the spinodal and binodal is the metastable region.

The precipitation process is represented by a curve connecting two points on opposite sides of the triangle (solvent-polymer and non-solvent-polymer). The points on the sides depend on the concentrations of the components, the path determined by the curve connecting the points depends on other thermodynamic and kinetic factors. (De Pascale, 2021)

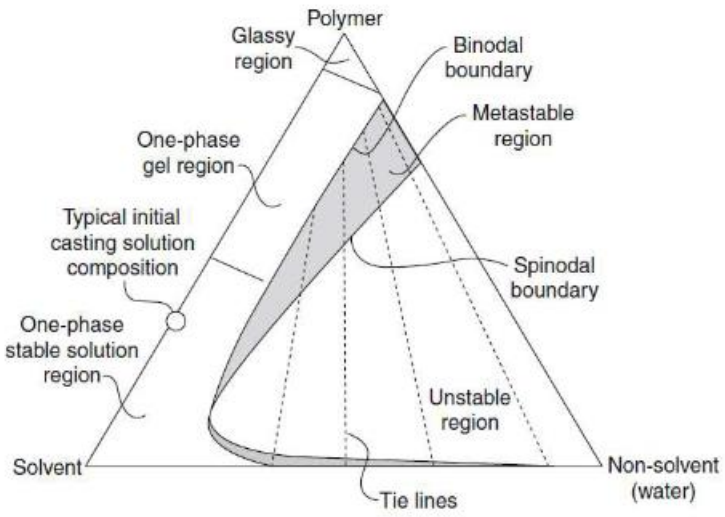


**Figure 6** Phase diagram of a three-component system.

The ternary diagram is also temperature-dependent.

The initial system generally consists in a mixture of polymer and solvent. Due to the addition of non-solvent to the initial system, the binodal curve is reached and the demixing phase

begins. The demixing process starting from the same initial solvent-polymer composition may be different depending on the casting conditions (**Figure 6**).

If demixing takes place above the critical point, the continuous phase is the polymer-rich phase and the dispersed phase consists of polymer-lean phase, whereas the former phases are reversed when demixing takes place below the critical point (**Figure 6**). In the case of demixing above the critical point, droplets of polymer-lean phase are formed as a dispersed phase in the continuous polymer-rich phase, which then precipitates. The coalescence of the droplets prior to precipitation causes the formation of pores.

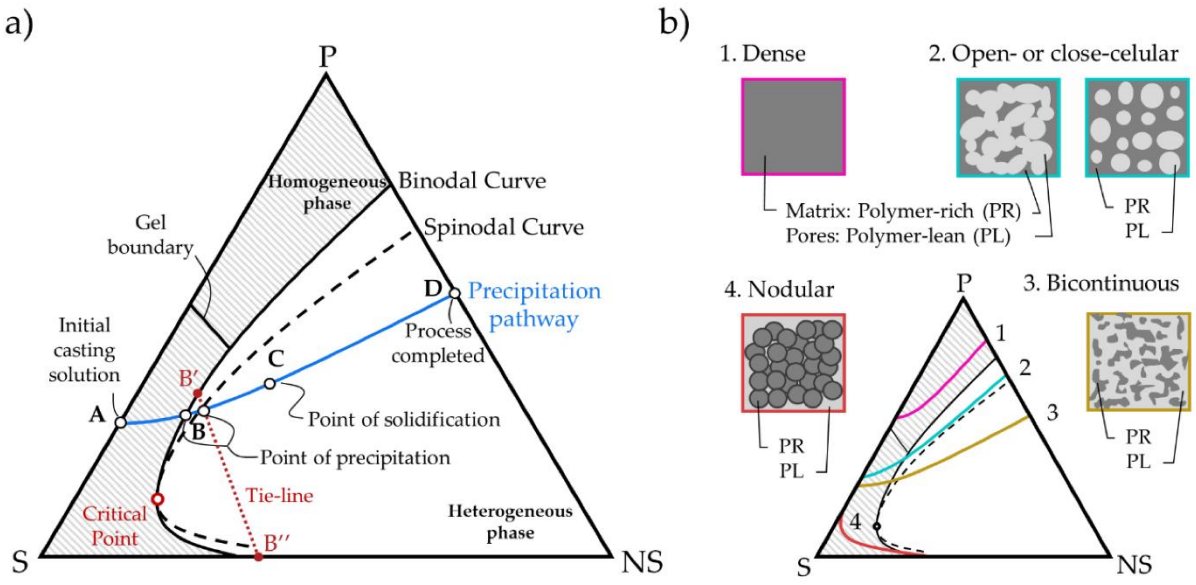


**Figure 7** The image on the left (a) shows a possible path of the precipitation process with characteristic phases. The image on the right b) shows the different demixing processes that can take place depending on the precipitation path and critical point. (Romay, Diban and Urtiaga, 2021)

Membrane casting using phase inversion methods, such as immersion precipitation, is a non-equilibrium process that requires the consideration of kinetics as well as thermodynamics. The local composition and its evolution over time is ruling the demixing process. However, due to the fast rate of composition change (typically less than 1 second) and the thickness of the film (200 µm), its composition cannot be precisely measured experimentally, but a theoretical description may be given. The final morphology of the membrane may also depend on the speed of the demixing process.

The exchange of matter is provided by the diffusion process.

The diffusion process begins at the film-bath interface and the composition starts changing there and as time passes, composition and demixing also takes place below the interface for increasing depths. Instantaneous and delayed demixing paths are reported in **Figure *8***.
The figure on the left shows that in the first moments of immersion the parts in the film below the top layer (t point) have crossed the binodal, indicating that liquid-liquid demixing begins immediately after immersion. This involves a large inflow of non-solvent, while the outflow of solvent is relatively small. This type of demixing usually yields a thin skin layer over a porous sub-layer with a finger-like structure containing large void spaces. In contrast, the figure on the right indicates that all compositions directly below the top layer are still in the one-phase region and are still miscible. This means that no demixing occurs immediately after immersion. It is expected that systems with delayed demixing exhibit membranes with a relatively dense skin layer along with sponge like sub-layer.(Mazinani *et al.,* 2017)

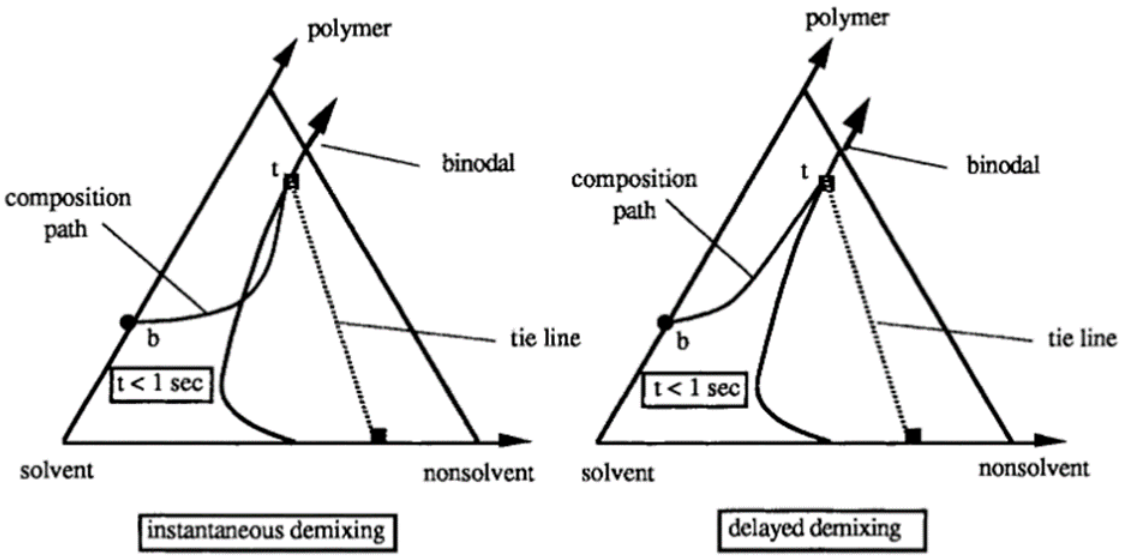


**Figure 8** Precipitation paths characterising instantaneous demixing in the image on the left and delayed demixing in the image on the right with respect to the unstable zone and the binodal curve.

Some considerations are made during the selection of operative parameters for casting:

- The solvent and non-solvent system should not present a miscibility gap at any composition.
- The polymer used constrains the choice of solvent and non-solvent. The polymer must be dissolvable in the solvent but not in the non-solvent and the solvent and non-solvent must be miscible with each other. The choice of solvent and non-solvent to be used with respect to a polymer is often made with reference to solubility. The most frequently used

parameter for assessing solubility is the Hildebrand delta ($\delta_H$). The Hildebrand parameter is a numerical estimate of the degree of interaction between chemical compounds, and can be a good indication of solubility, particularly for non-polar materials such as most polymers. Substances with similar $\delta_H$ values are miscible, so solvent and non-solvent must have similar $\delta_H$. Water is usually a common selection as a non-solvent. (Mazinani *et al.*, 2017)

- The amount of polymer used influences the density and porosity of the membrane. Density and porosity of the membrane decrease as the polymer concentration increases.
- Demixing can be delayed by introducing solvent into the coagulation bath together with the non-solvent. This method is adopted when the solvent and the non-solvent are very closely affinated; when the solvent is only slightly affinated to the non-solvent, it is not necessary because demixing is already delayed. The amount of solvent that can be added in the bath depends on the binodal curve that is approached as the solvent in the bath increases.
- It is also possible to add non-solvent in the casting solution, the maximum usable amount of non-solvent in the polymer depends on the binodal curve. The addition of the non-solvent in the casting solution can promote instantaneous demixing.

A very large number of combinations of solvent and nonsolvent are possible all with their own specific thermodynamic behaviour. Where a high mutual affinity exists ($\Delta\delta_H$[1] is high) a porous membrane is obtained, whereas in the case of low mutual affinity ($\Delta\delta_H$ is small) a nonporous membrane (or better an asymmetric membrane with a dense nonporous top layer) is obtained.

Furthermore, other parameters exist which have an influence on the type of membrane structure, the choice of solvent-nonsolvent is crucial. Fixing this parameter, still leaves a number of degrees of freedom in the system such as polymer concentration, addition of solvent to the nonsolvent bath, addition of nonsolvent to the polymer solution, the temperature of the coagulation bath and of the polymer solution and the addition of additives (low molecular weight, high molecular weight) to the casting solution or to the coagulation bath.

[1] $\Delta\delta_H$ is the interaction parameter between polymer/non-solvent systems which can be related to the solubility parameter difference.

The addition of hydrophilic additives, such as Polyethylene glycol (PEG), to the casting solution has a dual effect on membrane morphology.

The presence of PEG causes an increase in the thermodynamic instability of the casting solution and facilitates the formation of macrovoids, because the precipitation process occurs more rapidly. But on the other hand, PEG due to the increased viscosity of the casting solution, slows down the rate of diffusional exchange of solvent (e.g. N-Methyl-2-pyrrolidon or NMP) and non-solvent, and this leads to the suppression of these macrovoids and the formation of a denser structure. So the final structure depends on the superiority of instantaneous or delayed demixing.

Instead, decreasing the temperature of the coagulation bath reduces the mutual diffusivities between the non-solvent (e.g. water) and solvent (e.g. NMP) in the casting solution during the solidification process. This makes the precipitation process longer and causes the formation of thinner membranes. In addition, the limited nuclei (formed quickly after immersion of the cast film into the distilled water bath) to grow slowly. This results in the formation of a large number of small nuclei in every part of the cast film and causes the suppression of macrovoid formation, producing a denser membrane. On the contrary, when the temperature of the coagulation bath is increased, the formation of macrovoids is favoured, because precipitation is faster at higher temperatures.(Saljoughi, Amirilargani and Mohammadi, 2010) (Saljoughi, 2009)

The formation of macrovoids in asymmetric membranes takes place in the porous zone below the thin dense layer, known as the skin layer. Macrovoids are generally undesirable because they reduce mechanical strength. Macrovoids are often present when the demixing process is instantaneous, in delayed demixing their formation is less frequent. The parameter that most influences the formation of macrovoids is the solvent-non-solvent combination; when the affinity and miscibility between the components of the couple increases, the presence of macrovoids also increases, regardless of the type of polymer used. To avoid the formation of macropores, one can act on the choice of solvent-non-solvent couple, the demixing speed by introducing solvent into the bath or non-solvent into the casting solution, and the addition of additives. Additives are preferred to delayed demixing because this causes the skin layer to form. (Mulder, 1996)

## 1.5 Aim of this work

This work aims to identify, analyse and optimise the parameters that influence the properties and the structure of a MMMAs, to be used as a regeneration unit of dialysate in haemodialysis.

As explained in Chapter 1.4, MMMAs are very versatile composite membranes; their properties can be easily modified by changing their constituent components, as well as their concentrations or even the conditions adopted during their manufacture. The characteristics and properties assumed by mixed-matrix membranes depend on many variable parameters, as a result of which it is possible to obtain membranes with the characteristics required for the specific application under consideration, optimising the parameters.

MMMAs for dialysate regeneration in the haemodialysis process must have sufficient mechanical strength to prevent rupture or squeezing of the membrane at pressures of around 1 bar. They must have high permeability values, not less than 2000-3000 L/($m^2$ h bar), but must also have high porosity.

The porosity has to guarantee a large surface area over which the adsorbent particles are embedded and exposed. The high surface area allows to expose the adsorbent and overcome the mass transport limitations. The presence of interconnected porosity would contribute to this latter purpose because it would reduce the resistance to urea transport in the membrane.

Cellulose acetate (CA) is a polymer widely used in membranes manufacturing, furthermore, together with polysulphone, is one of the materials used for the production of dialysers for haemodialysis. CA and its derivatives are suitable for membranes fabrication due to ease in manufacturing, their high salt rejection, they are relatively inexpensive, highly hydrophilic, non-toxicity and with good biocompatibility and renewability.

CA is an ester of cellulose, obtained by reacting cellulose with acetic anhydride and acetic acid in a sulfuric acid environment. According to the grade of acetylation (varying from 29% to 44.8% normally) mono-, di-, triacetate of cellulose can be produced. CA could be prepared at room temperature using sulfuric acid as catalyst. Therefore, cellulose acetate was the first high performance asymmetric membrane prepared and commercialized. (De Pascale, 2021)

For this work, all the membranes prepared are cellulose acetate-based membranes.

### 1.5.1 Fillers

Performances of adsorbent materials are crucial for the fabrication of MMMAs. There are many types of adsorbents and for application in haemodialysis, where uremic toxins have to be adsorbed from an aqueous solution.
The adsorbents that were considered in this work are mesoporous silica and zeolites to replace the conventional activated carbon used as adsorbents. The choice to use these new adsorbents was driven by the low capacity of AC to adsorb urea and its non-regenerability, in addition the choice was supported by the other benefits brought by the properties of Silica and Zeolites.

Mesoporous silica has a complex structure of hexagonal channels, similar to those characterising zeolites, and a large surface area. The surface area can easily be chemically modified to increase the adsorption capacity for a target molecule and the pore size can be modified, so silica is a very versatile material. In addition, unlike zeolites, there are usually no atoms of Al in the chemical structure that can be non-biocompatible and therefore unsafe elements for biomedical application.

The mesoporous silica SBA-15 was chosen as an adsorbent because of its large pore diameter and it could be functionalised without risking pore closure. (Cheah, Sim and Yeoh, 2016) In fact, SBA-15 is a porous material whose surface can be chemically modified, and can therefore be functionalised as required, and it also has a large surface area in the range of 600-850 $m^2/g$, it depends on the temperature at which it was synthesised.(Galarneau *et al.*, 2001) Generally, when silica is used as an adsorbent, it is functionalised with amine or phosphoryl because pure silica has lower adsorption capacities and is less thermally and mechanically stable. Functionalised silica with amine groups showed to bind urea and creatinine with a hydrogen bonding between the N atom of the amine group and the hydrogen of the urea, which greatly increases the adsorption capacity at the expense of the available surface area, which decreases in functionalised silica. (Nguyen *et al.*, 2021)

In detail, the SBA-15 used has a particle size <150 μm, a hexagonal pore shape and with a pore size of 10 nm, the maximum surface area is 650 $m^2/g$.

For our purposes, zeolites were chosen as adsorbents too, they have a micro/nano porous structure and are aluminosilicate minerals. Over 40 different types of frameworks can be

found in nature, or they can be produced through industrial synthesis. The porous structure of zeolites often holds a variety of cations ($Na^+$, $K^+$, $Ca^{2+}$, $Mg^{2+}$, and others) that are eager to exchange when in contact with solutions. They are frequently contaminated with metal, quartz, and other minerals. The oxygen atoms in the tetrahedrons $TO_4$ (T= Si, Al, P, etc.) that make up the zeolite lattice are shared with neighbouring tetrahedrons. Tetrahedral units are arranged to form regular structures in increasingly intricate geometries, such as chains or rings. Zeolites are renowned as molecular sieve materials because of their ability to separate molecules according to their sizes with precision. Their regular molecular-scale pore structure distinguishes them, and the size of the channels determines the largest species that may enter the pores. Since the rings in the zeolite lattice are occasionally not symmetrical due to the strain generated by the bonding between the units required to create the overall structure, the channels are not always cylindrical. Zeolites made synthetically have the benefit of being uniform and pure and by changing the synthesis process, different results can be obtained depending on the requirements.(Wernert *et al.*, 2005)

For the removal of toxins to be successful, the adsorptive particles' characteristics are essential. As a result, the pore size distribution can be tuned to alter the adsorbent's performance. Porous adsorbent materials offer enormous potential when it comes to removing uremic toxins. They can be functionalised or the cations can be changed and thus personalised to adsorb a particular molecule or group of compounds. To fully utilise their adsorption potential in a haemodialysis procedure, numerous efforts must be made.

Regarding zeolites, as mentioned above, there are a huge variety of zeolites. Their morphology and pore size are a factor in their selectivity, but in addition it is possible to functionalise them to improve their selectivity for a specific target. The zeolites chosen, *Zeolite Ferrierite Ammonium*, *Zeolite Y hydrogen*, *Zeolite β hydrogen and Zeolite ZSM-15*, are all very hydrophobic because they are the ones that adsorb the most toxins. The zeolites used are very fine (particle size is less than 2 μm) powders that facilitate dispersion in the membrane and increase the surface area available to capture urea. Their surface area is between 400-800 $m^2/g$ and are both mechanically and fouling resistant, in addition it can be easily regenerated.

# 2 Materials and Methods

## 2.1 Materials

The materials required for the production of a membrane dope are:

- *Cellulose acetate* (CA) (*Sigma-Aldrich, Merck*) is used as a polymer:
molecular weight is 30 kDa, acetyl substitution degree is 2.4 in the form of powder and density 1.3 g/cm$^3$ at 25°C

- *Polyethylene glycol* (PEG) (*Sigma-Aldrich, Merck*) is chosen as a porogen:
molecular weight is 400 Da with a density of 1.128 g/cm$^3$

- *Glycerol* (GLY) (*AnalaR® NORMAPUR®, Slaughter*) is another porogen used as an alternative to PEG:
molecular weight is 92.1 Da and the density is 1.26 g/ cm$^3$, bidistilled 99,5 %

- *1-methyl-2-pyrrolidone* (NMP) (*Sigma-Aldrich, Scientific Laboratory Supplies*) is the solvent:
density is 1.03 g/cm$^3$, anhydrous, 99.5%

- *Deionized water* (DW) is the non-solvent.

Adsorbents used for the testing are:

- *Zeolite Y hydrogen (Thermo ScientificTM, ThermoFisher scientific)*:
Si/Al mole ratio is 80:1 and Specific Surface Area (S.A.) is 780 m$^2$/g

- *Zeolite Ferrierite ammonium (Thermo ScientificTM, ThermoFisher scientific)*:
Si/Al mole ratio is 20:1 and S.A. is 400 m$^2$/g

- *Zeolite β hydrogen (Thermo ScientificTM, ThermoFisher scientific)*:
Si/Al mole ratio is 360:1 and S.A. is 620 m$^2$/g

- *Zeolite ZSM-5 ammonium* (*Thermo Scientific™, ThermoFisher scientific*):
Si/Al mole ratio is 200-400:1 and S.A. is 400 m$^2$/g

- *SBA-15* and *Calcined Silica SBA-15 (Glantreo, Ireland)*

For the production of mixed matrix membranes adsorbers (MMMAs), only two of the above types of zeolites have been used.

Absorption capacity was tested with the following uremic toxins:

- *Urea (ACS Reagent, Sigma-Aldrich, Merck)*:
molecular weight 60.06 g/mol

- *Creatinine (Sigma-Aldrich, Merck)*:
molecular weight 113.12 g/mol, anhydrous ≥98%

## 2.2 Adsorbent powder Characterization

### 2.2.1 UV-Spectrophotometry

UV spectroscopy is an analytical technique based on the absorption of ultraviolet radiation (UV) by a sample. The amount of UV light absorbed by a molecule is proportional to the concentration of the absorbing species and the length of the light path through the sample. This relationship is described by the Lambert-Beer law, which states that the absorbance (A) of a solution is directly proportional to the concentration (c) of the absorbing species and the path length (l) of the sample:

$$A = \varepsilon c l \tag{2.1}$$

Where ε is the molar absorptivity, a constant that describes the ability of a molecule to absorb UV light at a particular wavelength.

UV spectroscopy is commonly used to analyse the electronic transitions of chromophores, which are molecules that absorb UV or visible light. Chromophores typically contain double bonds or aromatic rings, which have delocalized electrons that are capable of absorbing UV light. The absorption spectrum of a molecule can provide information on the identity and concentration of the chromophores present in the sample.

The unit of measurement used for photometric analysis is the 'optical density' denoted by OD.

The analysis is carried out on a sample volume of 2 µL with a NanoDrop 2000/2000c spectrophotometer (Thermo Fisher Scientific). By means of a pipette, the sample volume is collected and transferred as a drop to the pedestal of the instrument. Having lowered the arm that overlaps the drop and the sensor, the test is started.

As first, for the quantification of urea and creatinine, calibration curves were calculated at wavelength ranging from 199 nm to 210 nm and 220 nm to 250 nm respectively. The optimal wavelength was selected, to ensure linearity and enhance sensitivity. In this case, the solution analysed is the supernatant consisting of urea PBS solution obtained after the adsorption processes on the adsorbent and subsequent separation of the adsorbent powder and Urea-PBS solution by centrifugation (for details of the separation and centrifugation process see the following paragraph 0). The urea-PBS solution in which an MMMAs was immersed is also analysed, after the adsorption process on the membranes.

### 2.2.2 Centrifugation and filtration

It is an apparatus that speeds up the separation process between bodies of different densities by exploiting centrifugal acceleration, so that a centrifugal force is applied that is far greater than the gravitational force.

An Eppendorf rotor centrifuge was used. Test tubes with 50 mg of adsorbent dispersed in a volume of 1000 µL of urea PBS solution were centrifuged at 10000g for 15 minutes. The supernatant was used for spectrophotometric quantification of urea.

Another separation method used are non-sterile 0.20 µm cellulose acetate syringe filters (Incofar). Filters are used as a separation method integrated with centrifugation to ensure that traces of adsorbent too small to precipitate by centrifugation are removed from the supernatant to be analysed. Filters alone are not used as a separation method to avoid clogging by the adsorbent powder, which would all be in suspension without the prior centrifugation process. Therefore, after centrifugation of the samples, the supernatant obtained is collected with a syringe on which the filter will be mounted. The filtrate is analysed by UV readings (see previous paragraph 2.2.1).

### 2.2.3 Static Binding Capacity

The objective of a static binding test is to assess the binding capacity of zeolites (Zeolite Ferrierite Ammonium, Zeolite Y hydrogen, Zeolite β hydrogen, Zeolite ZSM-5**)** and mesoporous silica SBA-15 toward urea and creatinine, in phosphate buffer solution (PBS).

PBS was prepared according to the "Cold Spring Harbor" protocol ('Phosphate-buffered saline (PBS)', 2006). 1 L volume of solution was prepared. Specifically, 8 g NaCl, 0.2 g KCl, 1.44 g $Na_2HPO_4$ and 0.24 g $KH_2PO_4$ were weighed and placed in a 1000 mL flask into which a volume of 800 mL DI water was added. The flask was stirred at room temperature T=22°C, when the reagents were totally dissolved, DI water was added to reach the final solution volume of 1000 mL. Finally, it was checked that the pH was 7.2-7.4. The PBS was stored in a glass laboratory bottle.

The binding capacity $q_{ads}$ (mg/g) is defined as the mass of the target molecule adsorbed at equilibrium divided by the mass (of volume) of the stationary phase.

$$q_{ads} = \frac{m_{ads}}{m_{solid}} \tag{2.2}$$

Specifically, 50 mg of powder was weighted on a precision scale and placed it in a 1500 µL Eppendorf tube, followed by the addition of 1000 µL of previously prepared urea-PBS solution at different urea concentrations, in the range of 0-7 mg/mL. The test tubes were first vortexed and then kept shaking for 24 h on a roller shaker to ensure equilibrium is reached.

The samples were centrifuged at 10000g for 15 min in an Eppendorf rotor centrifuge. Finally, 10 µL of the supernatant is withdrawn with a micropipette and analysed by spectrophotometer.

The tests were carried out at 22°C. The value of urea detected by the spectrophotometer is the amount of urea present in solution at equilibrium and thus the amount of urea not adsorbed by the powder. Therefore, the amount of urea adsorbed is the difference between the mass of initial urea in solution and the mass of urea in the supernatant at equilibrium (for details paragraph 3.1).

The same protocol was used for creatinine.

The mass of toxin adsorbed at equilibrium is calculated as follows:

$$m_{ads} = V_{sol}\,(C_0 - C_{eq}) \tag{2.3}$$

Where $V_{sol}$ is the volume of toxin solution used, $C_0$ is the initial toxin concentration and $C_\infty$ is the equilibrium concentration in solution. $C_{eq}$ is obtained as

$$C_{eq} = OD\,(lambda)\,m + q \tag{2.4}$$

where OD is the average optical density obtained from the spectrophotometric measurement at wavelength equal to *lambda*. Three OD measurements of the same samples were carried out and averaged to ensure reproducibility. While, *m* and *q* parameters were obtained from the calibration line.

The amount of toxin adsorbed $q_{ads}$ (mg/g) is defined as the mass of toxin adsorbed, $m_{ads}$, on the mass of absorbent powder (zeolites) used $m_{solid}$.

$$q_{ads} = \frac{m_{ads}}{m_{solid}} \tag{2.5}$$

The *m* and *q* values should be readjusted by performing a new calibration each time a spectroscopic analysis is performed and especially when the Urea-PBS solutions used for testing are reproduced, because the values of *m* and *q* change with the specific solution produced. However, it was found that the *m* and *q* values do not change much, with the third digit being affected.

The error in the measurement (run in duplicates or triplicates) is reported as standard deviation, reported as error bars in the charts. The standard deviation is defined as the difference between the average calculated over all squared values and the square of the average of the original values and calculated as:

$$\sigma_x = \frac{\sum_{i=1}^{N} x_i^2}{N} - \left(\frac{\sum_{i=1}^{N} x_i}{N}\right)^2 = \sqrt{\frac{\sum_{i=1}^{N}(x_i - \overline{X})^2}{N}} \tag{2.6}$$

where $x_i$ is the value of each sample and N the number of samples.

The standard deviation was calculated with the aid of the Excel calculation programme using the command 'STDEV.P'.

The standard deviation is a dimensional quantity whose unit of measurement is the same as the quantity for which the deviation calculation is performed (in this work, mg/g, mg/mL, µm and %wt).

### 2.2.4 Kinetic of adsorption on adsorbent powder

Tests were carried out on the zeolite to obtain adsorption kinetics in order to analyse the adsorption capacity as a function of the contact time of the adsorbent with the target molecule in solution. The parameter used for evaluation is once again the binding capacity $q_{ads}$ (mg/g).

In this work, the adsorbent tested is zeolite (Zeolite Ferrierite Ammonium, Zeolite Y, Zeolite β and Zeolite ZSM-5) and the target molecule is urea in solution with PBS at a specific concentration of 7 mg/mL. The samples are prepared and the tests conducted in the same way as described in the previous section 2.2.3. Specifically, several identical samples are prepared and placed in contact with the urea solution. After vortexing, each sample is centrifuged at increasing time intervals from the moment of contact and the supernatant is analysed by spectrophotometer. The first adsorption value is obtained after 5 min of contact between zeolite and urea-PBS solution, the second at 10 min, the third at 20 min, and so on until 3 h of contact are reached, which is generally sufficient time to reach equilibrium for the tested zeolites.

The tests were repeated twice for each type of zeolite under the same conditions, but adding the filtration step using 0.2 µm CA syringe filters after centrifugation and before spectrophotometric analysis. When filters are also used as an additional separation method, the centrifuge is set at 10000g and 1 min.

## 2.3 Membranes and MMMAs fabrication

Membranes were produced via non-solvent induced phase separation (NIPS) technique. (Mulder, 1996; Mazinani *et al.*, 2017; De Pascale, 2021)

Porogen and polymer (cellulose acetate) were dissolved in the solvent (NMP) by gently stirring the solution at 60°C (by mean of a hot plate and a water bath). The porogen was dissolved first, then the polymer is added gradually, since as the amount of polymer increases, the viscosity increases, slowing down the dissolution of the powder. If a large amount of polymer is immediately immersed and contacted with the solvent, it forms agglomerates and pockets of solid polymer within the liquid phase. These phenomena make mixing difficult, the dissolution of the polymer in the solvent is slower and the solution not homogeneous.

The solution was stirred at a fixed temperature for at least 10-12 h. The solution was let cool to down and the presence any precipitate is checked. The solution was centrifuged at 1000 g for 5 min to remove air bubbles, if necessary.

The membrane is cast using a micrometric knife with adjustable thickness (Elcometer 3580 Casting Knife Film Applicator 175 mm, UK). The solution was poured onto a flat glass surface and immediately casted gently with the knife. The polymer layer obtained on the glass, at the desired thickness of 400 µm, is immediately immersed in a water coagulation bath, in this case distilled water is the non-solvent.

Membranes were cast at different temperatures of the coagulation bath, namely 22°C, 40°C and 50°C. The coagulation bath temperature is an important parameter that influences the membrane characteristics. (Saljoughi, 2009; Saljoughi, Amirilargani and Mohammadi, 2010)

In the bath, the polymer precipitates and forms the structure of the porous membrane, exchanging solvent and non-solvent with the coagulation bath, until the membrane detaches from the glass.

The membrane sheet was cut in parts by using a blade and die cutter. The membrane was visually inspected to spot defects and imperfections.

The membranes manufactured were washed four times with DI water, to remove completely PEG or GLY and NMP from the membrane and stored in Petri dishes to preserve them from bending.

In most of the membranes produced, the porogen used is PEG, but in the H and I membranes, GLY was used as the porogen. The decision to use another type of porogen is due to the possibility of changing the morphology of the membrane by changing the porogen. Although glycerol has a density very similar to that of PEG, 1.26 g/mL compared to 1.128 g/mL of PEG, it has a much smaller molecular mass, 92 Da compared to 400 Da, and above all has a much higher viscosity than PEG.

The different chemical-physical properties of the two molecules (**Table 8**) allow for different interactions with the non-solvent (DI water) and thus to produce membranes with different morphology and mechanical properties.

Mixed matrix membranes adsorbers (MMMAs) are composite membranes produced analogously, but in which a filler, in this case adsorbent powder, is blended to the casting solution. The quantities of filler introduced were 5%, 10% and 15% by weight.

In this case, the filler was added to the solution of NMP and PEG or GLY before the polymer, kept stirring at 60°C for at least 30 min, to ensure the formation of a homogeneous suspension. Thereafter, the polymer was added gradually. The mixture was kept stirring and at fixed temperature for at least 12 h.

The other details of the membrane production procedure remained the same as those described above.

The impact of concentration of polymer, of concentration and type of porogen were investigated. The experimental scheme is summarized in **Figure 9**.

Membrane M is fabricated according to a previous work performed in our lab (De Pascale, 2021). The membranes M, A and B maintain the same CA/PEG mass ratio of 1.7, but with decreasing polymer concentration. In contrast, membranes G, C, F D and E maintain the same polymer (CA) concentration, but changing the porogen concentration (PEG), moving to the right of the **Figure 9** the porogen concentration decreases. In membranes H and I, glycerol (GLY) was used as a porogen instead of PEG.

For every casting solution the effect of the coagulation bath temperature was explored.

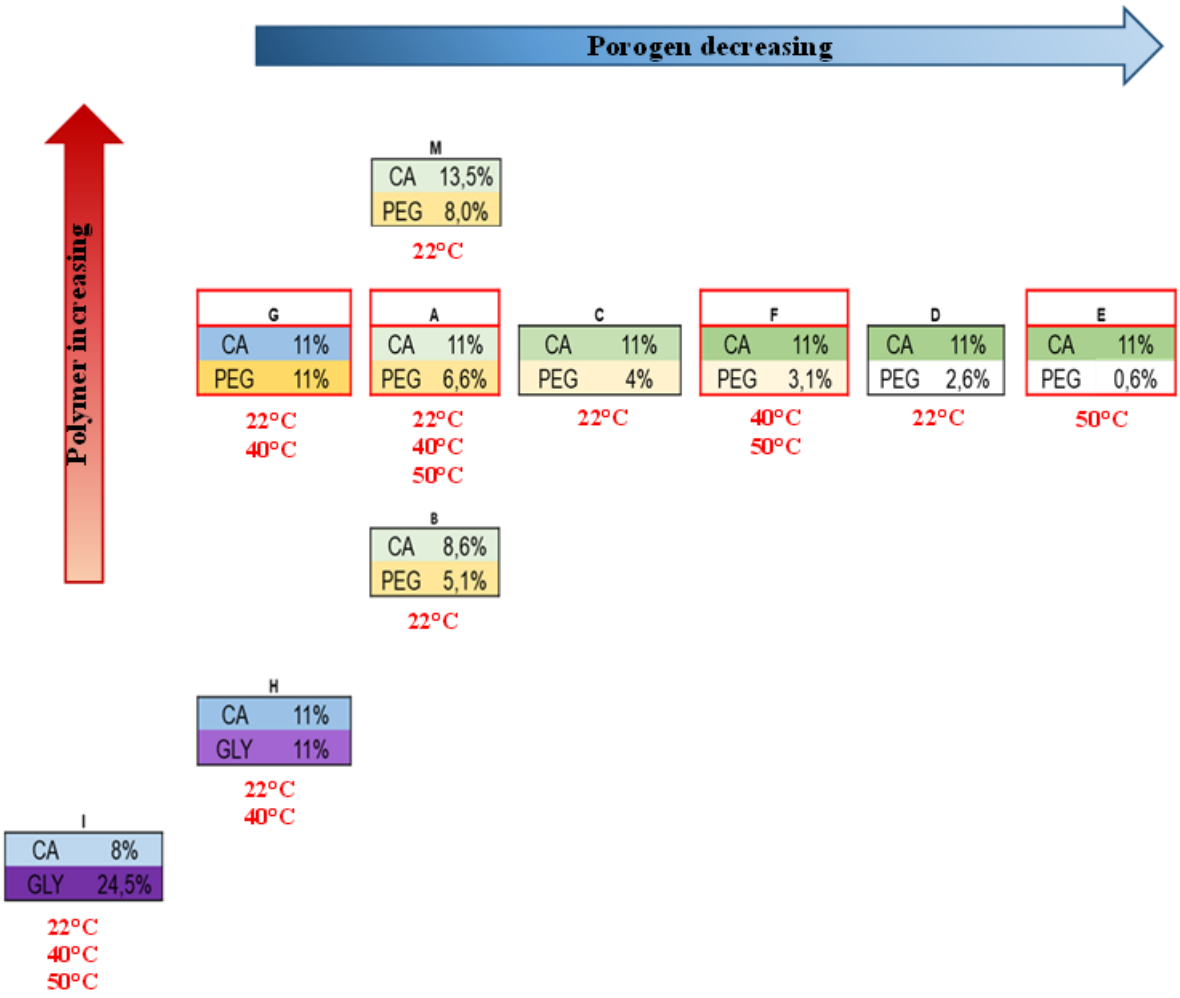


**Figure 9** shows all the membranes produced, with different concentrations and at different temperatures.

**Figure 9** Diagram of membranes produced with the bulk compositions of polymer and porogen. In red, membranes with PEG as porogen cast at different bath temperatures $T_{bath}$ (°C).

The impact of the type of filler used and the amount of adsorbent introduced into solution in the microstructure and the features of the mixed matrix membranes adsorbers (MMMAs) are investigated by the experimental scheme reported in **Table 5**.

In this work, the adsorbents used as fillers in MMMAs were only two types of zeolites, although adsorption tests were carried out on the powders of all the proposed adsorbent materials in the *"Materials"* section. The choice of fillers to be used in the MMMAs was dictated by the best performance, for the purposes of this study.

In **Table 5** membranes AA, AB, AC are the type A membranes at a temperature of 22°C (**Figure 9**) into which *Zeolite Y* was introduced as a filler at increasing mass concentrations, 5% 10% 25%.

The membranes FB and IB have the concentrations of type F and I membranes at a temperature of 50°C and 40°C respectively (**Figure 9**) into which *Zeolite Ferrierite Ammonium* was introduced at a concentration of 10% by mass.

**Table 5** Different types of MMMAs produced.

| Sample | Membrane | Concentration Ratio % | CA/porogen ratio | Filler | Concentration [wt%] | Temperature of bath [°C] |
|---|---|---|---|---|---|---|
| AA | A | CA 11,1%; PEG 6,6% | 1,7 | Zeolite Y | 5 | 22 |
| AB | A | CA 11,1%; PEG 6,6% | 1,7 | Zeolite Y | 10 | 22 |
| AC | A | CA 11,1%; PEG 6,6% | 1,7 | Zeolite Y | 25 | 22 |
| FB | F | CA 11,1%; GLY 3,1% | 3,6 | Zeolite Ferrierite Ammonium | 10 | 50 |
| IB | I | CA 8,2%; GLY 24,5% | 0,3 | Zeolite Ferrierite Ammonium | 10 | 40 |

## 2.4 Membrane characterization

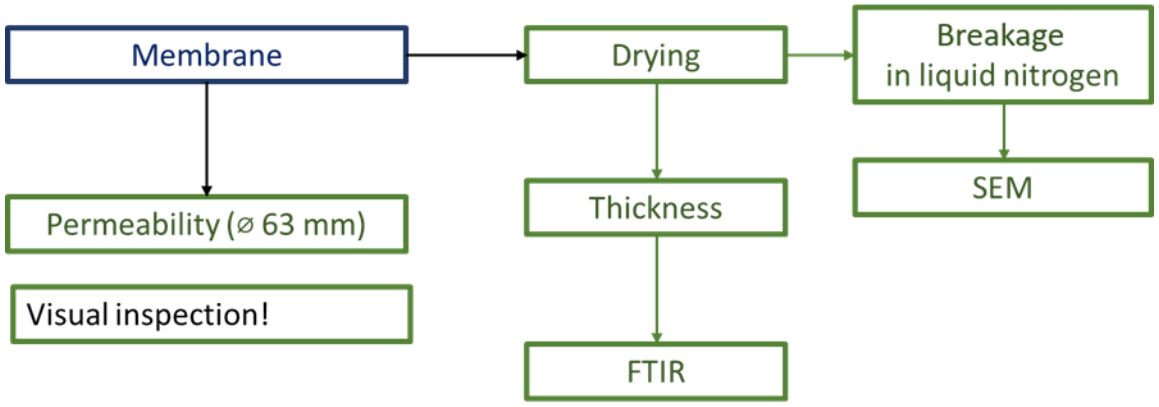


**Figure 10** Analyses carried out on the membrane.

### 2.4.1 Visual inspection

Visual inspection was carried out on the samples to detect imperfections, holes or cracks that may be generated during casting. This analysis involves observing the surface of the membrane without the aid of instrumentation. It is important to carry out the visual analysis before permeability tests, because the presence of imperfections makes the permeability values unreliable; when imperfections were detected, the permeability test was not carried out.

### 2.4.2 Permeability

Permeability describes the flow of a fluid through a porous medium and is defined by Darcy's:

$$< v > = \frac{k\,\Delta p}{\mu_0\,L} = \frac{\Delta p}{\mu_0\,R} \tag{2.7}$$

where k is the filter permeability (it is function of porosity, pore size, structure), $\mu_0$ is the viscosity of the liquid fluid through the medium (permeate), L is the thickness of the porous medium layer, ΔP is the pressure drop across the layer and the R is (L/k), in other word it is the flow resistance of the layer.
For the Darcy law described above, the hypotheses of laminar motion, Newtonian fluid and one-dimensional motion are assumed.
In this case, the layer is MMMA and the fluid is DI water.

The flux through the membrane with a given Δp may be calculated as the variation of permeate collected over time per unit of surface.

$$J = \frac{1}{A}\frac{d\,V}{d\,t} \tag{2.8}$$

Relating the fluid velocity to the rate of permeate volume accumulation, the following is obtained:

$$< v > = \frac{\Delta p}{\mu_0\,R} = \frac{1}{A}\frac{d\,V}{d\,t} \tag{2.9}$$

Therefore, permeability is defined as:

$$k = \frac{1}{\mu_0 R} = \frac{\frac{1}{A}\frac{dV}{dt}}{\Delta p} \tag{2.10}$$

Permeability is a key parameter in the manufacture of MMMA because it is an indicator of the hydraulic resistance of the membrane. In order to guarantee a certain flux, the pressure drops are constrained by the size of the pump circulating the dialysate, that needs to be small and efficient. For this reason, pressure drops needs to a fraction of 1 bar. The use of a MMMA unit is crucial to satisfy this requirement, that would be challenging with a traditional packed bed.

The test was conducted on a circular membrane with a diameter of 63 mm, previously punched, placed in a permeability cell (Amicon® Millipore, UK) (**D** in **Figure 11**) using DI water.

In the set-up represented in **Figure 11**, the pressure on the membrane is the hydraulic head $h\rho g$, that is the column of liquid in the cell plus the column of liquid above the cell in the system. The value of the pressure at which the test is conducted is varied by changing the height $h$ of the cell relative to the top of the small vessel.

The pressure on the membrane needs to be constant throughout the test, namely keeping the liquid level above the membrane constant, while providing the necessary flowrate.

The siphon connects a large-diameter vessel, behaving as a reservoir (**A** in **Figure 11**), with a small container, behaving as a buffer (**B** in **Figure 11**). The water can drip from the top buffer vessel. In this way, the level (and therefore the pressure) is kept constant, the excess flow rate flowing from A to B overflows and the system remains in steady state, smoothing the variation in level observed in the reservoir ( **Figure 11**). The vessels differ in size because this affects the sensitivity of the system; the larger diameter vessel is less sensitive to changes in the liquid level.

The system weights over time the mass of DI water permeated through the membrane, by mean of a digital balance. The weight measures are saved on a computer in real time.

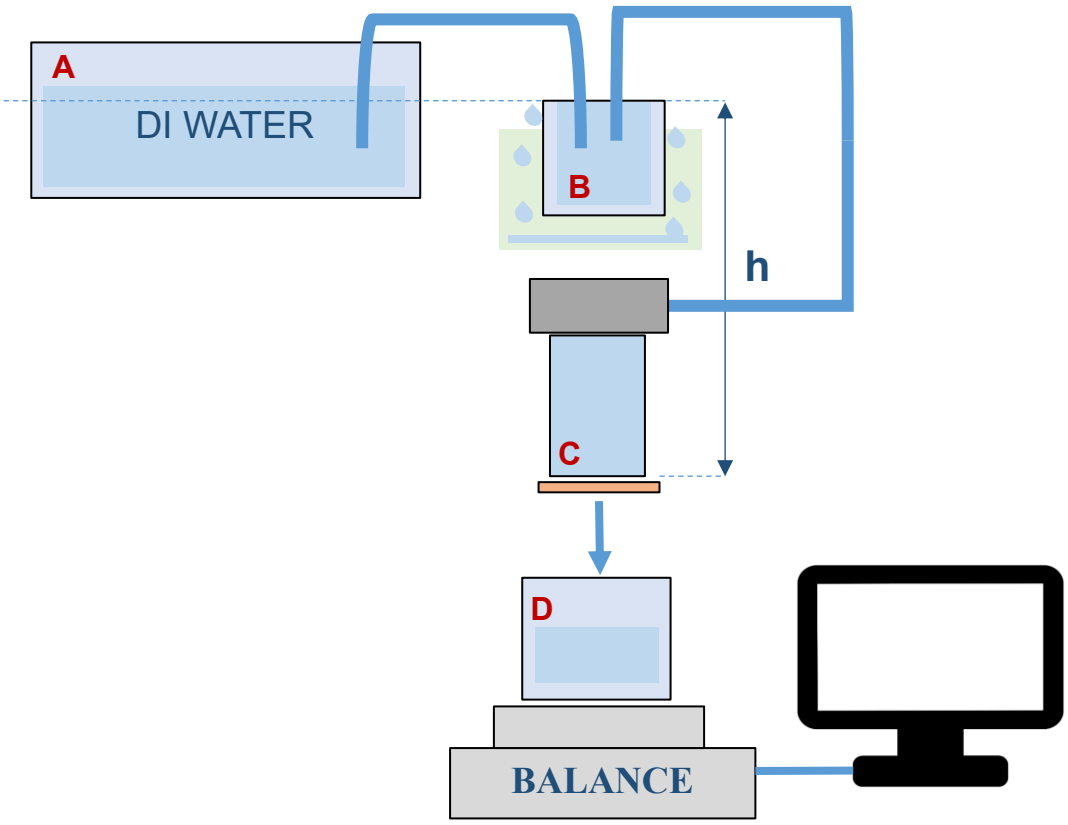


**Figure 11** Hydraulic permeability tests set-up.

### 2.4.3 Drying

Membranes were dried by exposing the samples to air in a room temperature environment of T= 22°C overnight. The membranes were placed vertically on special supports, so that all membrane surfaces were in contact with air and a homogeneous drying process was guaranteed.

### 2.4.4 Thickness

The measurement of membrane's thickness is an important parameter required to develop a membrane process. The thickness is measured with a plate micrometer on dry membranes.

The measurement is repeated five times on different points of the same membrane sample to take into account possible non-homogeneity of the membrane thickness and to obtain an average thickness value. This test can be destructive when the dry membrane is broken by the plates during measurement.

Another, less accurate method used for thickness measurement is the analysis of images obtained with Scanning Electron Microscope (SEM) of the membrane section (details of the

SEM analysis are given in section 2.4.7). The arrangement of the sample in relation to the lens is of fundamental importance here. In order for the thickness measurement to be conducted correctly, the membrane cross-section must be oriented orthogonally to the direction of the lens, so that measurement errors due to perspective are avoided.

The latter method is very useful when membranes fold in on themselves during the drying process and do not allow the thickness to be measured using a micrometer.

### 2.4.5 Water sorption and porosity

By taking mass measurements of wetted membranes, it is possible to calculate the membrane's capacity to adsorb water. The water sorption is calculated as follows:

$$m_{ads,H_2O} = \frac{m_{wet} - m_{dry}}{m_{dry}} \quad (2.11)$$

where $m_{wet}$ is the mass of the wet membrane and $m_{dry}$ is the dry mass of the same membrane.

Since the membrane is porous, it can be assumed that the amount of water absorbed by the membrane occupies the membrane pores, therefore porosity can be calculated by referring to the amount of water absorbed. It is also possible to roughly calculate the porosity of a membrane as follows:

$$\varepsilon = \frac{m_{wet} - m_{dry}}{m_{wet}} \quad (2.12)$$

### 2.4.6 Fourier Transform InfraRed Spectroscopy (FTIR)

Infrared (IR) spectroscopy is an absorption spectroscopic technique used to characterise materials by analysing chemical bonds. The technique is based on the principle that a molecule absorbing an infrared photon assumes an excited vibrational state. Vibrations can cause two possible changes in the chemical bond, stretching (stretching) or changing the bond angle (bending). In the spectra graph, the abscissas are the photon wave number and the ordinate the transmittance. In the spectrum, two zones can be distinguished: 'functional

groups' and 'fingerprints', in the former are the stretching and bending bands, in the latter are the characteristic bands of each molecular species.

Spectroscopy is achieved by an interferometer that detects all frequencies of IR radiation. There are two mirrors one fixed and one moving, the waves reflected by the moving mirror can generate constructive or destructive interference with the waves reflected by the fixed mirror, thus an interferogram is obtained. The Fourier transform, hence the name FTIR, makes it possible to move from the time domain to the frequency domain.(“FTIR.pdf”)

**Figure 12** FTIR components and operating mechanism.

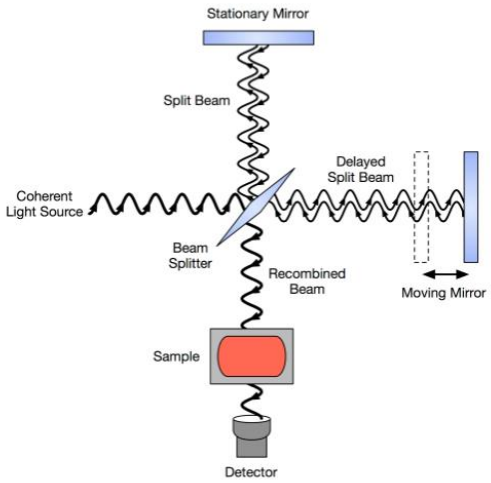


The objective is to analyse the composition of the membrane produced and to verify that the membrane after casting and washing consists of only cellulose acetate and is free of traces of porogen and solvent. Specific machinery is required to perform the analysis. The test is conducted on dry samples, the sample did not receive any chemical-physical treatment prior to the FTIR test and this is a destructive test.

An important element present in FTIR is the internal reflection element (or ATR crystal), which consists of a crystal with a high refractive index. Attenuated total reflection is a technique often used in conjunction with infrared spectroscopy. The IR beam first passes through the crystal and then through the sample. The advantage of ATR is that samples with any state of aggregation can be analysed accurately without the need to subject them to treatment.

The test is carried out by placing a previously dried fragment of membrane in the specific spot identified by a well, where the ATR crystal is present. The tip is placed on top of the

sample, exerting a small amount of pressure to ensure close contact with the ATR and avoiding the interposition of air. In this case, the dry sample is very fragile and is therefore reduced to very small fragments due to the pressure exerted.

Within seconds, the spectrum is shown on the interface.

### 2.4.7 Scanning Electron Microscope (SEM)

Scanning electron microscopy is a technique used to inspect the surface of a sample and is preferred to the optical microscope because it has a much higher resolution. The inspected surface has a small area of the order of nanometres. The operating principle of the SEM is to exploit the interaction between electrons and the sample to produce images. The SEM consists of an electron source, electromagnetic lenses, electron detectors and a chamber in which to place the sample. Electrons are produced by a tungsten filament. The sample placed in the chamber is hit by an electron beam; secondary electrons (SE), backscattered electrons and X-rays are obtained from the interaction with the sample. The SEs originate from anaelastic shocks in which the sample emits electrons, whereas if the shocks are elastic, the sample deflects the primary electrons producing the scattered electrons (BSE). SEs give information in the form of images on surfaces, BSEs give information on structures.(De Pascale, 2021)

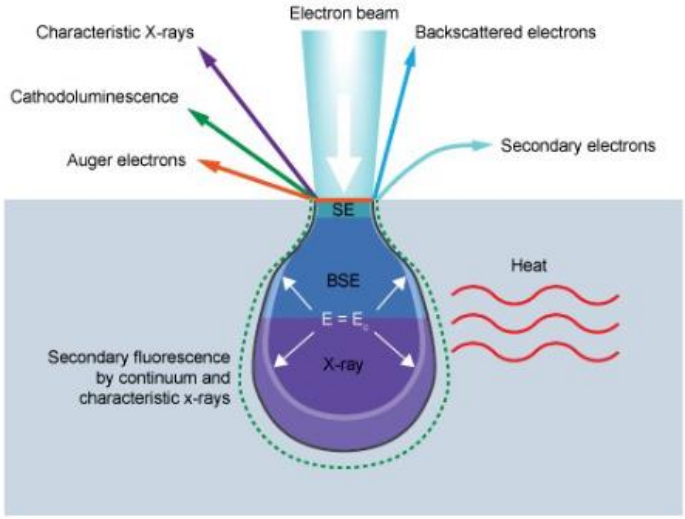


**Figure 13** Typology of electrons generated by the interaction between electron beam and sample.

SEM allows to inspect surface and cross-section of the membrane and its morphology, size and dispersion of pores both in the thickness.

The analysis was carried out on dry samples, broken by immersion in liquid nitrogen to ensure a brittle fracture of the material, to expose the cross-section. This procedure was followed to ensure pores not undergoing plastic deformation, caused by the stresses generated during the fracture, resulting in artifacts in the imaging.

Specifically, the sample was immersed in liquid nitrogen for few seconds, holding the membrane with tweezers and then breaking it. This procedure requires ad-hoc personal protective equipment.

In the case of MMMAs, the size and dispersion of the filler in the membrane matrix can be analysed. SEM was used on powders to assess their particle size and their geometry.

In this case, the membranes have not undergone any gold coating before the test and they were positioned and fixed on a stud with synthetic rubber adhesive that is placed into the SEM chamber. The samples were 45° oriented unless the analysis was aimed to the thickness measurement, in such case the samples was arranged at an angle of 90°.

The microscope chamber was sealed and evacuated from air before the analysis.

### 2.4.8 Static Binding Capacity of MMMAs

Static adsorption tests on mixed-matrix membranes were carried out to evaluate the adsorption capacity of the MMMAs.

The parameter used for the evaluation of the adsorption capacity is the Binding Capacity $q_{ads}$ (mg/(g cm$^3$)) defined as the mass of adsorbed target molecule over the density of adsorbent in the membrane:

$$q_{ads} = \frac{m_{ads}}{\rho_{solid}} \tag{2.13}$$

where $\rho_{solid}$ is the density of adsorbent powder in the membrane, defined as mass of adsorbent over membrane volume:

$$\rho_{solid} = \frac{m_{solid}}{V_{MMMA}} \tag{2.14}$$

Another definition of $q_{ads}$ (mg/cm$^3$) is the mass of the adsorbed target molecule over volume of membrane tested:

$$q_{ads} = \frac{m_{ads}}{V_{MMMA}} \tag{2.15}$$

The membranes used for the analysis were die-cut with a diameter of 2.5 cm, therefore, the membrane volume is calculated as the volume of a cylinder whose thickness was obtained by micrometer measurements.

Sample preparation involves drying the membranes, the MMMA and the corresponding membrane (same composition and same $T_{bath}$) without filler. The dry membranes are weighed with an analytical balance to obtain the mass; knowing the mass of the same membrane with filler and without filler, it is possible to accurately calculate the mass of zeolite actually trapped in the membrane. Therefore, assuming that the amount of polymer contained in a polymeric membrane is the same as that contained in the MMMA, whose polymer and porogen concentrations in the dope solution are the same as in the membrane without filler, the mass of adsorbent in the sample is calculated by difference as follows:

$$m_{adsorbent} = m_{MMMA} - m_{mem} \tag{2.16}$$

where $m_{MMMA}$ is the mass of the membrane with filler and $m_{mem}$ is the mass of the membrane without filler.

Then the MMMAs samples are placed inside 20 mL beakers, a volume of 4000 µL of urea-PBS solution at a concentration of 1.6 mg/mL is added to the beaker.
It is necessary to ensure that the membrane is fully immersed in the volume of solution. The beakers are covered with 'parafilm' to prevent evaporation and placed on an orbital shaker at a speed of 200 strokes/minute for at least 18 h.
Finally, the urea-PBS solution after the time required to reach equilibrium is taken from the beaker and analysed on the 'nanodrop' spectrophotometer, according to the protocol described in Section 2.2.1.

# 3 Results and discussion

## 3.1 Mesoporous silica and zeolites adsorption tests

Adsorption tests are aimed at assessing the potential of the mesoporous silica SBA-15 and the zeolites Ferrierite Ammonium, Y hydrogen, β hydrogen and ZSM-5, in order to identify the adsorbent material best suited to adsorb urea and creatinine.

The off-set is measured on PBS and calibration was done on the toxin-PBS solutions at different concentrations, in a concentration range of 0-7 mg/mL and 0-1 mg/mL of urea and creatinine respectively.

For urea, a wavelength of 202 nm showed to be the optimal measurement condition because it maximises the sensitivity of the measurement and ensures linearity in the range of interest. This is deduced from the spectra of urea at different concentrations and the calibration curves at different wavelengths that are attached in the appendix (**Figure A.1**, **Figure A.2** and **Figure A.3**).

In the case of creatinine, the optimal wavelength is 243 nm. This is the wavelength at which the linear regression for the calibration curve in the concentration range of interest is best (in appendix **Figure A.5** and **Figure A.6**).

Parameter *m* and *q* for the calibration curve is given in **Table 6** .

**Table 6** Parameter values of the urea and creatinine calibration curve used for sample analysis.

| **Parameters** | ***λ (nm)*** | ***m*** | ***q*** | $R^2$ |
|---|---|---|---|---|
| **Urea** | 202 | 16.67 | 0.445 | 0.9972 |
| **Creatinine** | 243 | 0.346 | -0.007 | 0.9967 |

The value of parameter *q* is negative due to the off-set calculated on PBS.

### 3.1.1 Mesoporous silica SBA-15 adsorption tests

Mesoporous silica SBA-15 adsorption toward urea was tested. Adsorption tests were performed on both untreated and calcined silica.
The SBA-15 to be calcined was subjected to a heat treatment at 500°C for 5h.

Adsorption isotherms were obtained, at a room temperature of 22°C, of the untreated silica and the calcined silica on two different uremic toxins, both urea and creatinine (**Figure 14** and **Figure 15**).

The urea adsorption on SBA-15 does not show a monotonic increasing trend with equilibrium concentration. Furthermore, measured adsorption in this work, does not agree with results in literature (Nguyen *et al.*, 2021). According to (Nguyen *et al.*, 2021) pristine SBA-15, adsorbs 200 mg/g of urea with an equilibrium concentration of 1.9 mg/mL. Not least, **Figure 14** shows that calcination of SBA-15 does not have any impact on the adsorption.

A binding capacity of 5 mg/g is measured at an equilibrium concentration of 0.5 mg/mL and 0.7 mg/mL. The experiments, run in duplicates, show standard deviation ranging between 0.2 and 1 mg/g for SBA-15 (and a maximum of 2 mg/g for calcined SBA) therefore the measurement is affected by an instrumental error, due to low sensitivity.

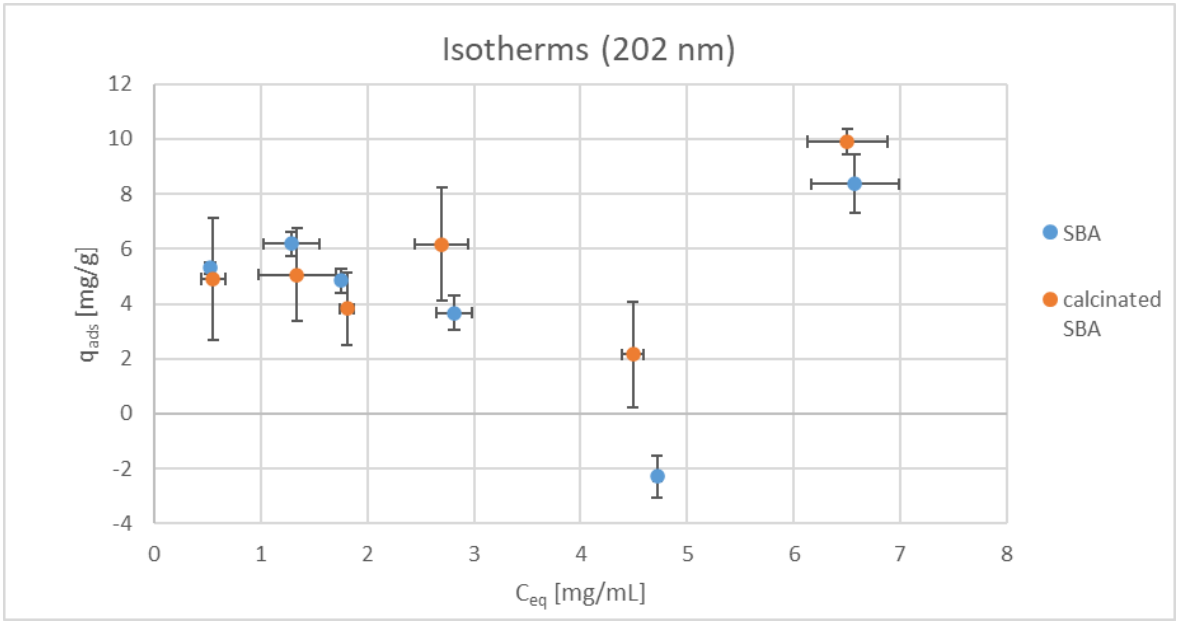


**Figure 14** Adsorption isotherm of urea on SBA-15 and calcinated SBA.

For creatinine isotherms (**Figure 15**) such as urea, the trend is not increasing and the adsorption values are very low, in fact the highest adsorption value reached is 1.4 mg/g with an equilibrium concentration of 0.42 mg/mL. According to (Nguyen *et al.*, 2021), in which the adsorption test was carried out for a range of concentrations higher than those used in **Figure 15**, pristine SBA-15, adsorb 2.5 mg/g of creatinine with an equilibrium concentration of 0.5 mg/mL. Also in this case untreated SBA-15 and calcined SBA-15 there is no difference in adsorption. Conversely from urea tests, the creatinine adsorption test values are more repeatable, with the standard deviation in the range of 0.005-0.02 mg/g.

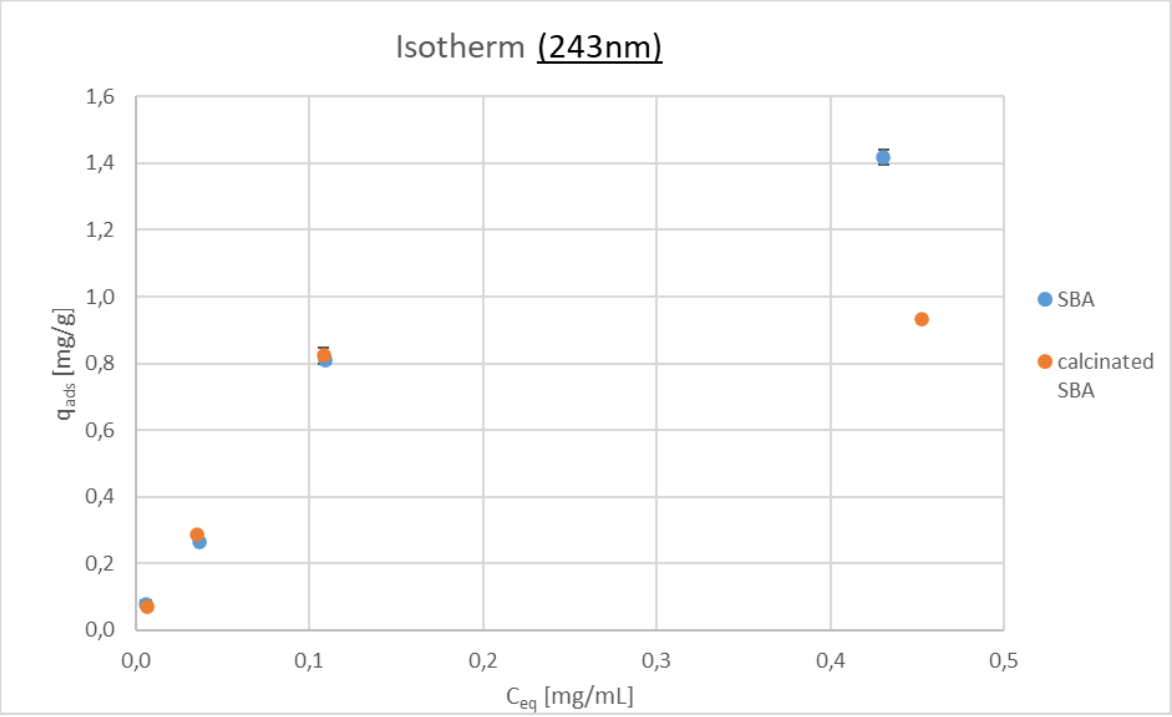


**Figure 15** Adsorption isotherm of creatinine on SBA-15 and calcinated SBA.

In conclusion, the adsorption of urea and creatinine on SBA-15 is an order of magnitude lower than the value reported in literature. The discrepancy in the results might be ascribed to:

- different analytical protocol for the quantification of urea and creatinine (e.g. HPLC)
- different material used (e.g. different synthesis process)

Since the SBA-15 does not satisfy the required adsorption capacities, it was not selected as filler in the fabrication of MMMAs.

### 3.1.2 Zeolites adsorption tests

The following table shows the characteristics of the tested zeolites; they are hydrophobic zeolites because they are of greater interest in our case; in fact, this type of zeolite adsorbs more toxin.

**Table 7** Characteristics of zeolites used for static adsorption tests.

| Zeolite | Si/Al Mole ratio | Specific Surface Area S.A. [$m^2/g$] |
|---|---|---|
| Ferrierite Ammonium (ZFA) | 20:1 | 400 |
| Y, hydrogen (ZY) | 80:1 | 780 |
| B, hydrogen (Zβ) | 360:1 | 620 |
| ZSM-5 | 200-400:1 | 400 |

The zeolites tested did not undergo any treatment or functionalisation.

The zeolite *Ferrierite Ammonium* (ZFA) and *zeolite Y* (ZY) showed the highest adsorption capacity towards urea, with $q_{ads}$ in the range of 26-16.5 mg/g and 12-5.3 mg/g, respectively, for a range of urea concentrations at equilibrium between 0 and 6 mg/mL (**Figure *16***). ZFA and ZY are also the zeolites with the lowest Si/Al ratio, 20:1 and 80:1, respectively.

The presence of aluminium atoms in the framework structure make the zeolite less hydrophobic, but aluminium atoms in the framework make the zeolite less safe to be used in medical applications. For this reason, zeolites need to be dealuminated.
However, ZFA and ZY zeolites showed a smaller particle size, according to SEM images in **Figure *17***.
The $q_{ads}$ values of the *ZSM-5 zeolite* are null because the amount of urea adsorbed is very low and therefore not detectable by the instrumentation.

In all cases, measurements are very repeatable, as shown by the error bars. The standard deviations of the binding capacity measurements are within a range of 0.1-1.1 mg/g.

Zeolites ZFA and ZY have been incorporated into membranes as fillers to produce MMMAs.

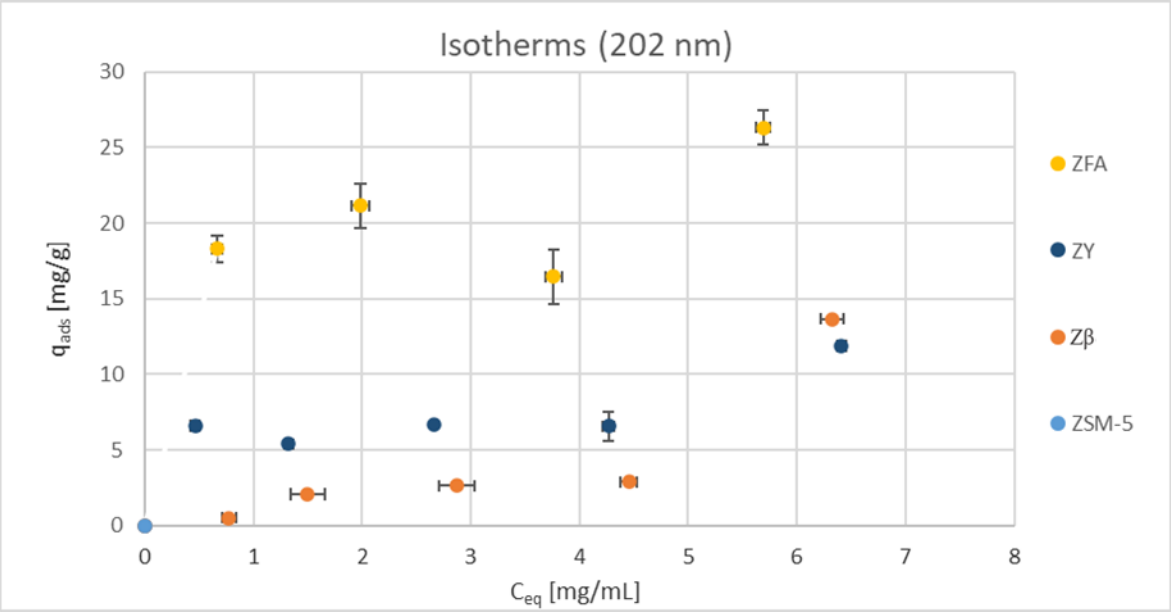


**Figure 16** Adsorption isotherm of urea on zeolites.

Finally, to complete the characterisation of the adsorbent, SEM imaging was used to obtain qualitative information on the morphology and size of the zeolite. The SEM images show that as the Si/Al ratio increases, the size of the zeolites decreases (***Figure 17***).

For all the powders, the formation of agglomerates of particles caused by contact with moisture is noticeable. The size of the clusters is not homogeneous, the largest size of a cluster being on average 6 µm compared to the average particle size which is less than 2 µm in all types of zeolites.

Despite the presence of clusters, it was found that the powder used as a filler is well dispersed in the membrane because during the formation of the casting solutions, the powder aggregates manage to dissolve in the solvent. This is observed and discussed in detail in section 3.7.

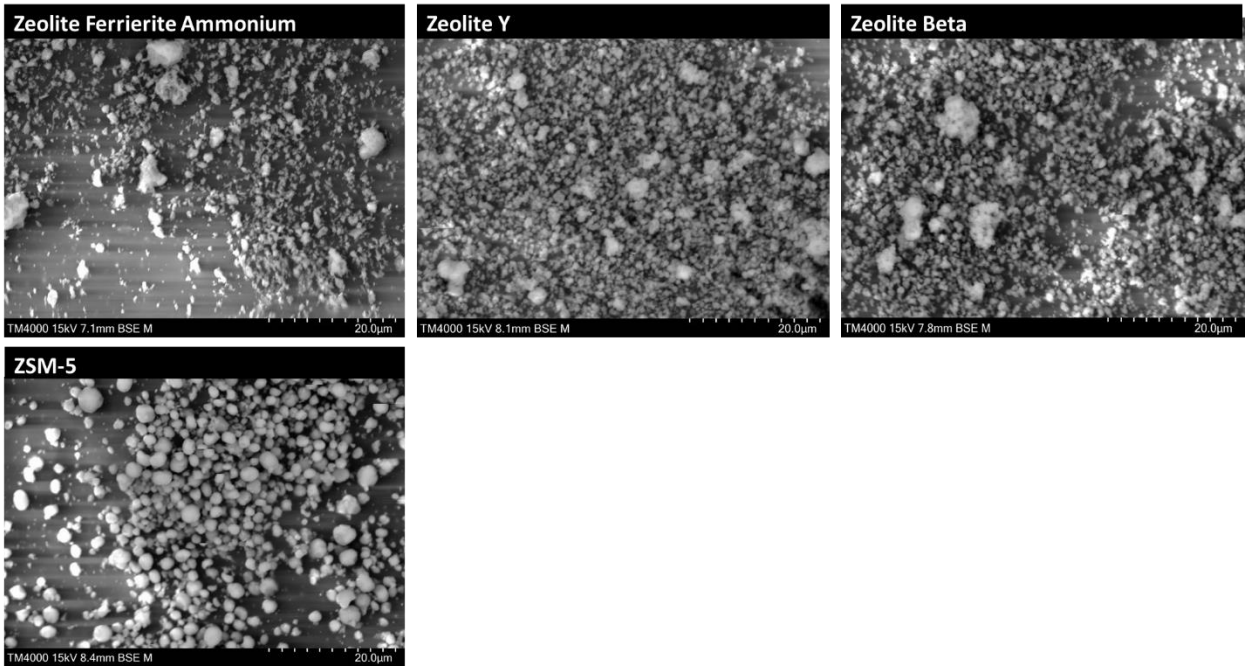


**Figure 17** SEM imaging of powders. Si/Al mole ratio: Zeolite Ferrierite Ammonium 20:1, Zeolite Y 80:1, Zeolite Beta 360:1, Zeolite ZSM-15 200/400:1

### 3.1.3 Adsorption kinetics on powder

The adsorption kinetics of the four zeolites listed in **Table 7** were tested. The zeolites did not undergo any treatment prior to analysis.

**Figure 18** shows the adsorption kinetics of the zeolites ZFA, ZY, Zβ and ZSM-5, which only underwent the centrifugation process at 10000g and 15 min to separate the adsorbent powder from the urea-PBS solution.

All the zeolites do not show the regular trend of expected adsorption kinetics, i.e. a very rapid increase of adsorption capacity until reaching a constant equilibrium value that will remain so over time. Instead, an initial rapid increase in $q_{ads}$ values is observed and after reaching a maximum value, $q_{ads}$ values decrease and finally oscillate around the equilibrium value which corresponds to the adsorption value reached at steady-state. The adsorption values reached at steady-state in the kinetics tests on all the zeolites are very close to the values obtained from the static adsorption tests (triangle symbol in the graph).

Specifically, although the trend is the same for all zeolites, the ZY and ZSM-5 zeolites reach a maximum value of 17 mg/g after about 12 min, for longer times the values are in the range of 10-15 mg/g until they reach the steady-state value of 15 mg/g. As far as Zβ is concerned,

it reaches a maximum value after 12 min of 25 mg/g slightly above the previous values, and for longer times it oscillates between values of 20 and 15 mg/g until it reaches the same value as ZY and ZSM-5 at steady-state. Finally, ZFA has significantly higher values than the other zeolites, reaching a maximum value of 40 mg/g after 12 min and for longer times oscillating between 35 and 30 mg/g until reaching steady-state with a $q_{ads}$ value of 30 mg/g.

In conclusion, all zeolites show the same trend in $q_{ads}$ as a function of time, the ZY, Zβ and ZSM-5 zeolites having very similar $q_{ads}$ values in contrast to ZFA, which has significantly higher values.

**Figure 19** shows the adsorption values of all the zeolites which in this case were subjected to the additional process of filtration with syringe filters after centrifugation at 10000g for 1 min and before being examined at the "nanodrop". In the graph, a homogeneity between the adsorption values of the different zeolites can be observed. In fact, all the zeolites assume $q_{ads}$ values close to the average value of 33 mg/g, except for ZY which has slightly different values. In addition, all the zeolites reach the steady-state with the same adsorption value of approximately 33 mg/g, this value being much higher than the values obtained without the use of syringe filters (**Figure 18** or triangles in **Figure 19**).

Thus, the inhomogeneity and the distribution of the values in a larger range in the case of **Figure 18** are caused by an incomplete separation process using the centrifuge only, the centrifugation is not sufficient to precipitate all the powder in the pellet and traces remain in the supernatant. For this reason, the values obtained by spectrophotometry are altered by the presence of powder traces in the supernatant sample analysed. Therefore, filtration by means of syringe filters is necessary to ensure complete separation between the pellet and the supernatant and to avoid powder traces in the sample analysed at the 'nanodrop', making the analysis reliable.

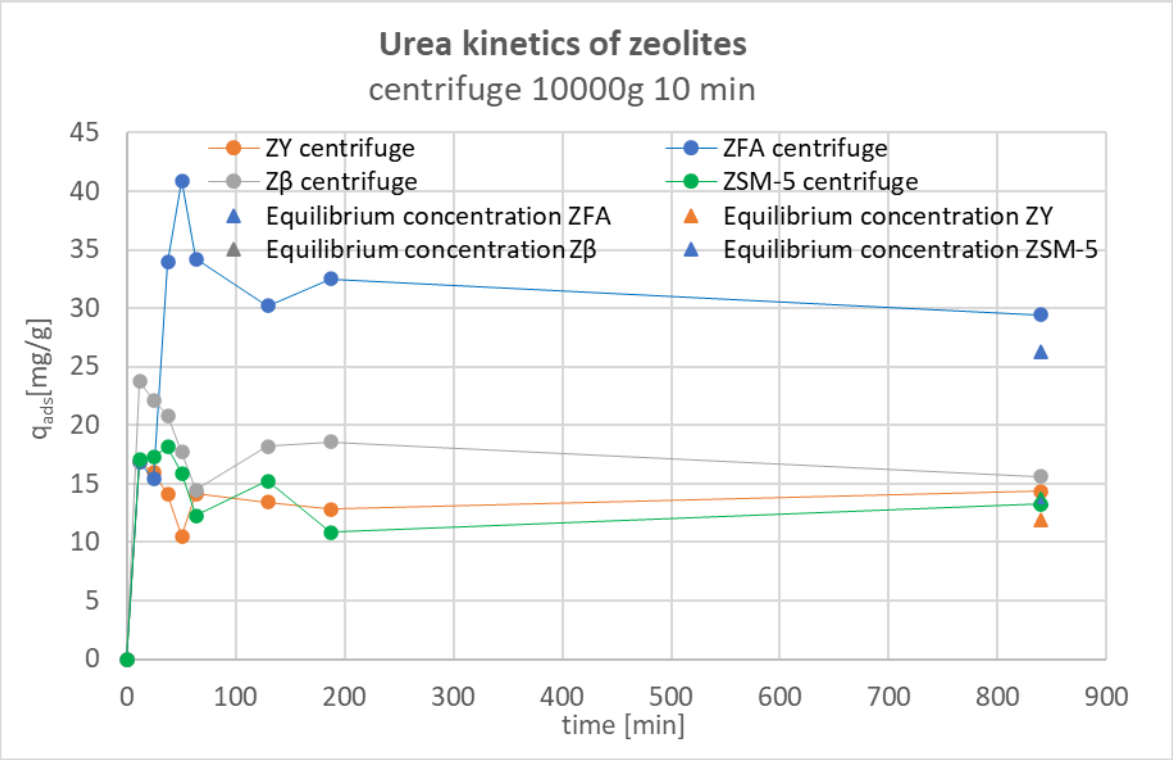


**Figure 18** Adsorption kinetics on zeolites ZFA, ZY, Zβ and ZSM-5 on which only the centrifugation process was carried out prior to spectrophotometer analysis.

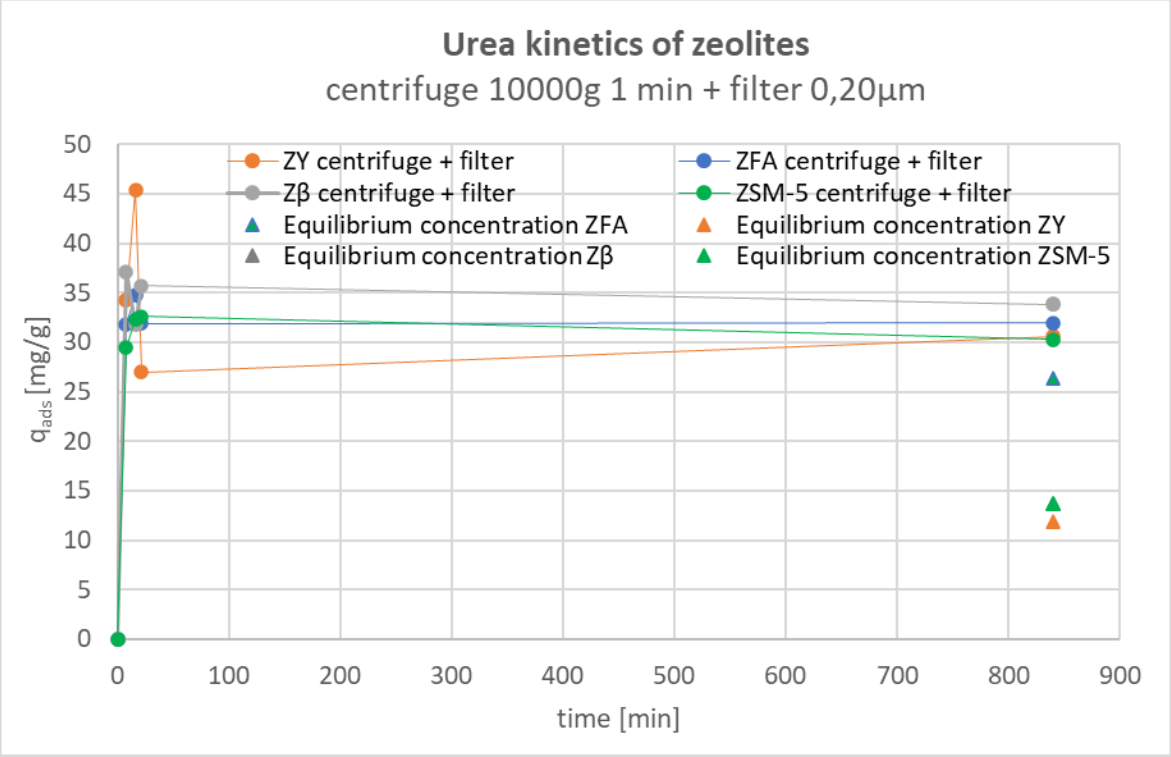


**Figure 19** Adsorption kinetics on zeolites ZFA, ZY, Zβ and ZSM-5 on which both centrifugation and filtration processes were performed prior to spectrophotometer analysis.

Finally, each graph in ***Figure 20*** shows the results of three different kinetic adsorption tests carried out on the same type of zeolite, what differs between the tests is the separation process used. The first test was carried out on samples that were subjected to centrifugation only, the second test is a replica of the first test and the third test involves the use of both centrifugation and filtration processes. In this way, it is possible for the same zeolite to easily compare the values obtained in different tests and thus assess the repeatability of the test and the effect of the separation process on the results.

For all zeolites, it is shown that the test is repeatable, in fact the first test and the second test, which are conducted under the same conditions, show very similar results. In contrast, the results obtained from the third test are very different from the others and therefore the separation process has a strong effect on the adsorption values.

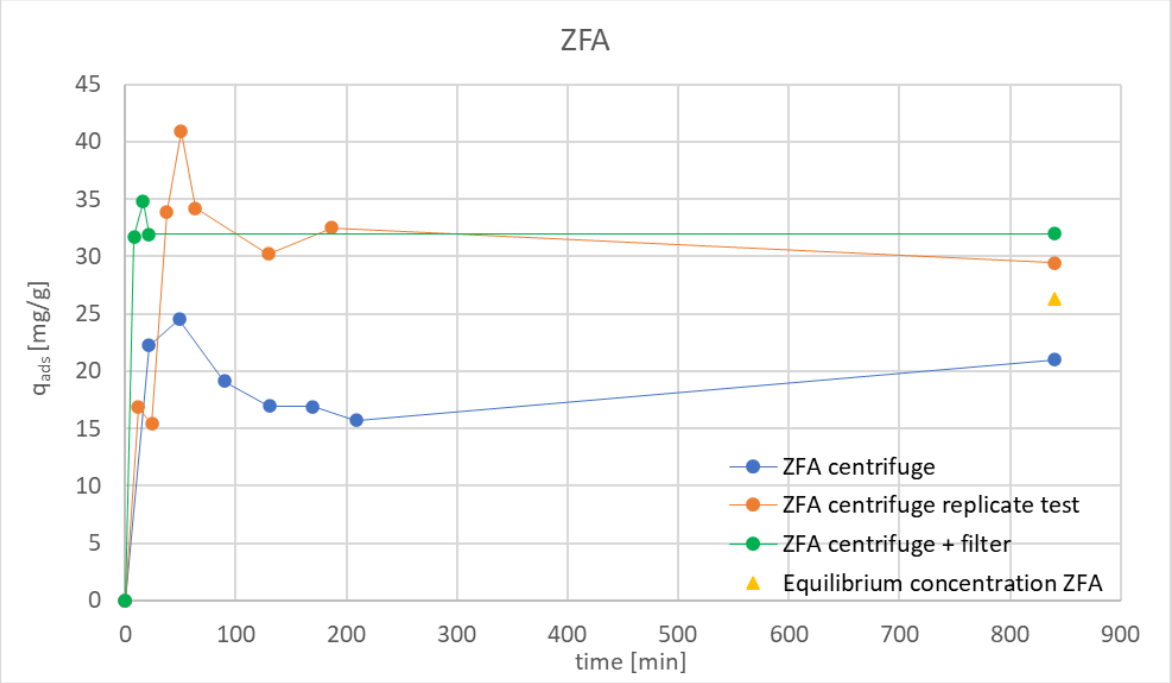

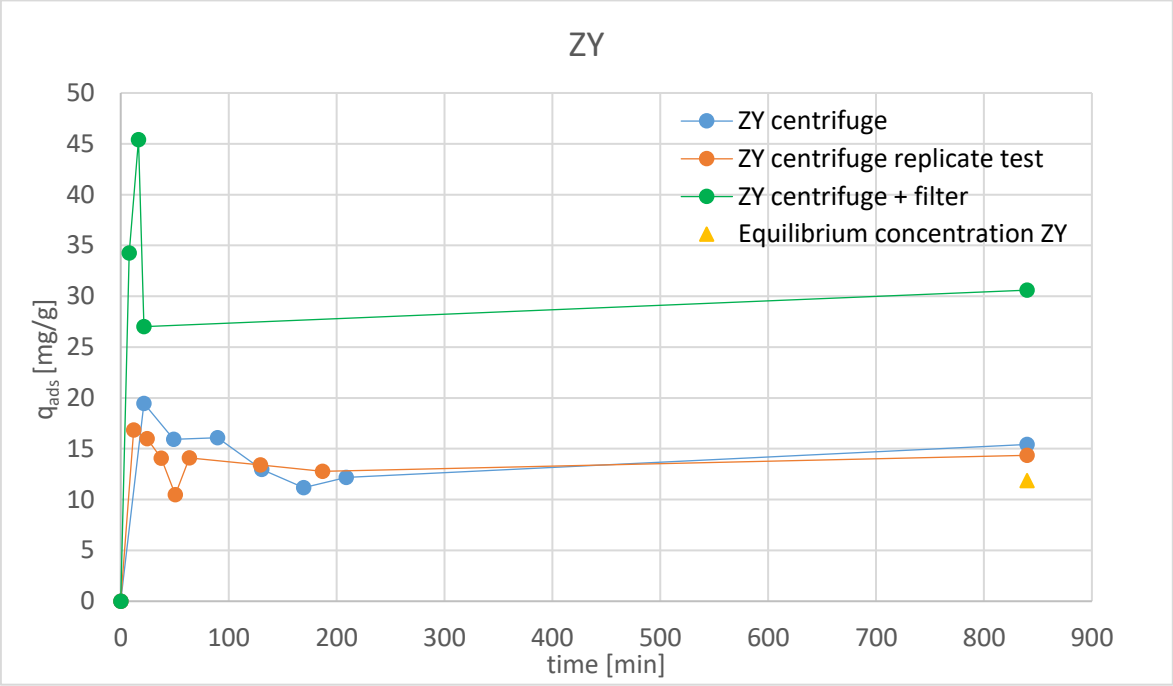
ZY
ZY centrifuge
ZY centrifuge replicate test
ZY centrifuge + filter
Equilibrium concentration ZY
$q_{ads}$ [mg/g]
time [min]
0
5
10
15
20
25
30
35
40
45
50
0
100
200
300
400
500
600
700
800
900

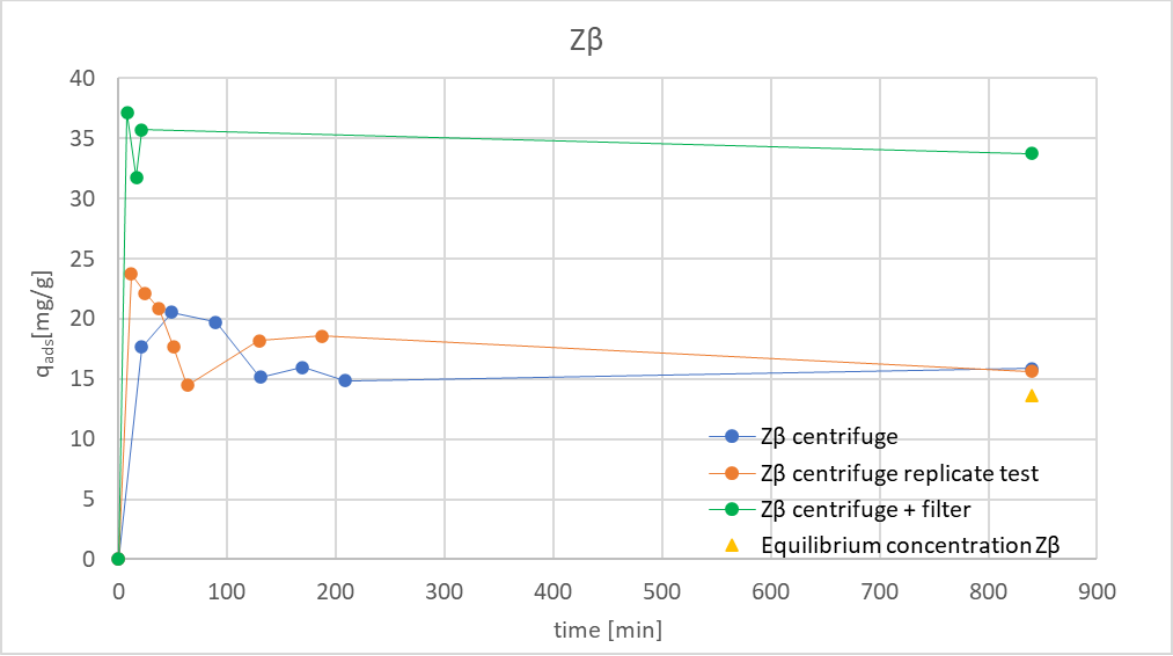
Zβ
Zβ centrifuge
Zβ centrifuge replicate test
Zβ centrifuge + filter
Equilibrium concentration Zβ
$q_{ads}$ [mg/g]
time [min]
0
5
10
15
20
25
30
35
40
0
100
200
300
400
500
600
700
800
900

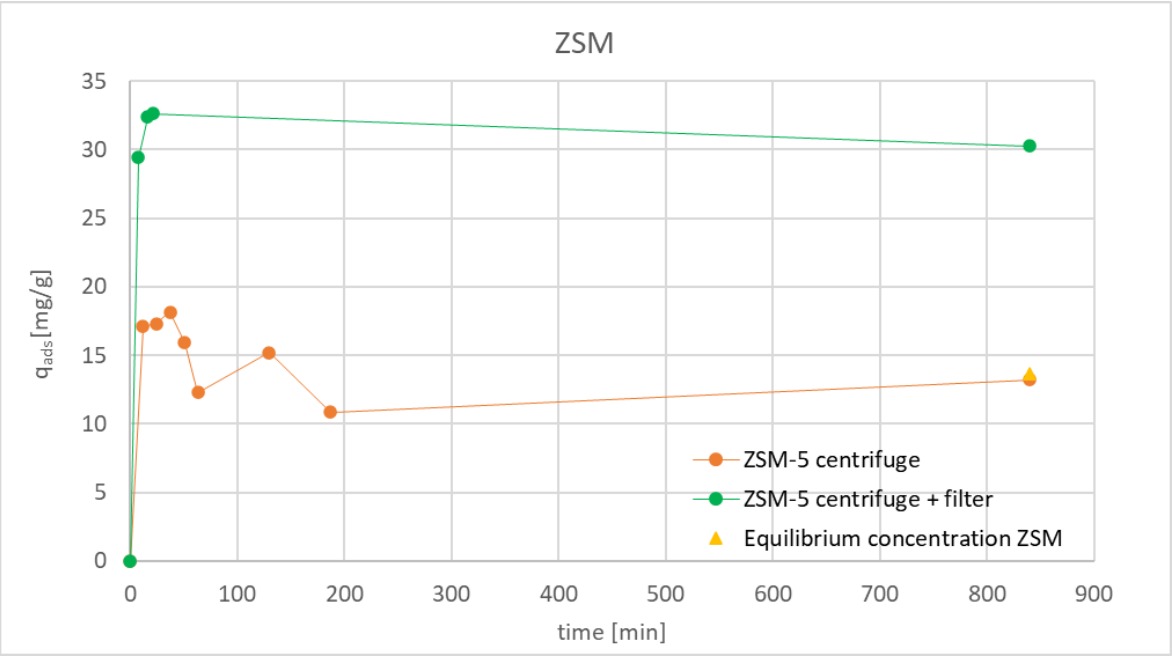


**Figure 20** Comparison of kinetic adsorption values obtained from three different tests, categorised on the basis of zeolite type. In the first test only the centrifuge is used, the second test is a repetition of the first test and in the third test both the centrifuge and filters are used like separation process.

## 3.2 Thickness

The thickness set on the casting knife is 400 µm for all membranes.

The thicknesses of membranes A (CA 13.5% PEG 8.5%), B (CA 10% PEG 5.9%), C (CA 13.5% PEG 5%) and D (CA 13.5% PEG 3%) casted in a coagulation bath at room temperature of 22°C, were obtained using a plate micrometer.

**Figure 21** shows the average values of five measurements made on the same sample. The samples shown in the diagram that have the same letter in their name (e.g. A1, A2, A3, A4 and B1, B2, B3) belong to the same dope solution, whereas the samples with the same letter and different number belong to different membranes obtained from the same dope solution, finally the samples with the same letter and same number are different fragments that belong to the same membrane (**Figure 22**).

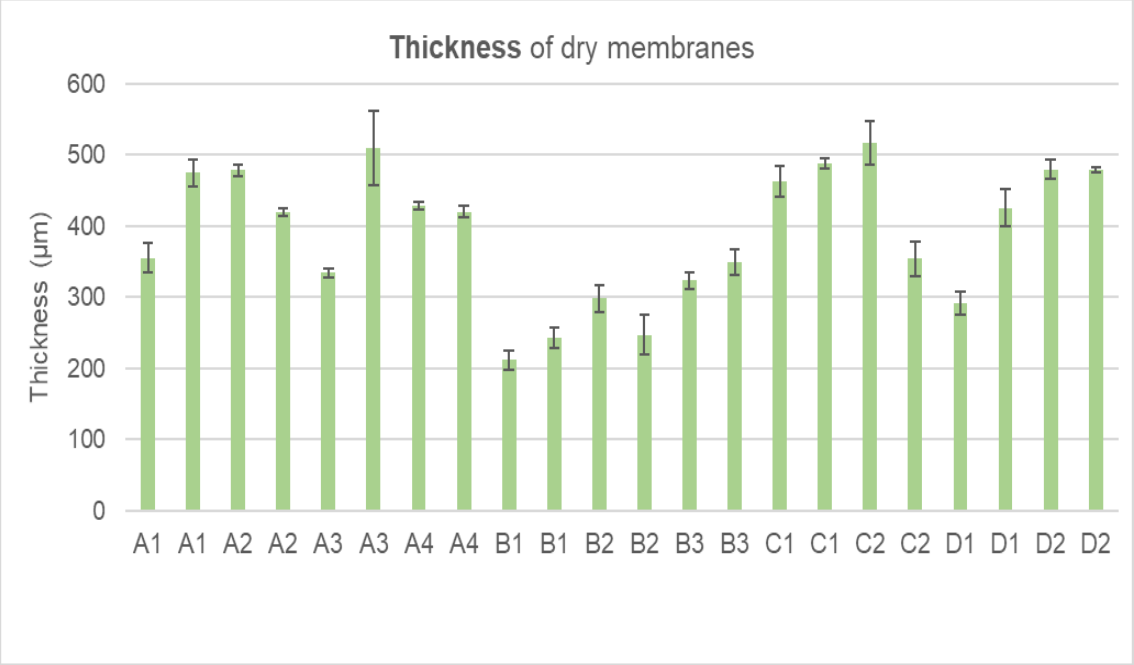


**Figure 21** Thickness measurements on dry membranes with a plate micrometer.

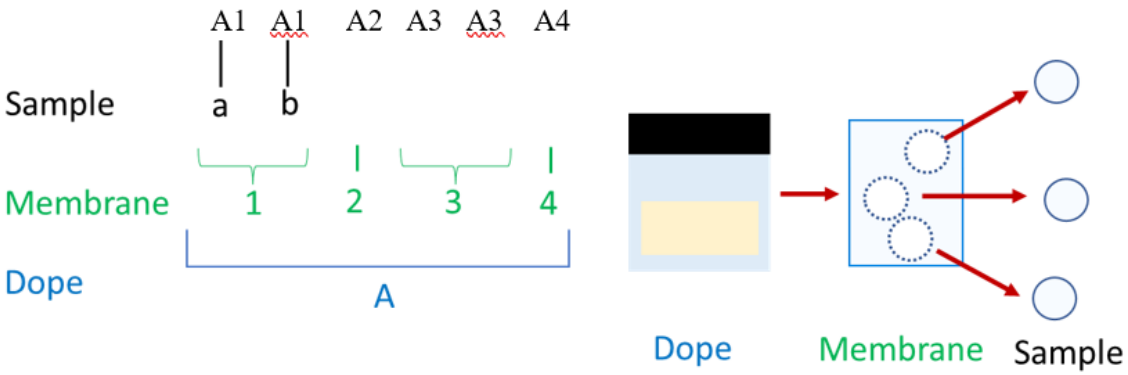


**Figure 22** Representative scheme of how the thickness measurements on the samples were carried out with the micrometer.

**Figure 24** shows the average values of the thicknesses of all different membranes as a function of coagulation bath temperature.

From the results shown in the **Figure 24** it can be stated that membrane B (CA 10% PEG 5.9%) has an average thickness value of 290 µm and is less thick than membrane A (CA 13.5% PEG 8.5%) which has a value of 410 µm. This difference may be related to the different concentration of polymer used, observing a reduced thickness when a lower concentration of CA is used. On the other hand, membrane A, C (CA 13.5% PEG 5%) and

D (CA 13.5% PEG 3%) have a similar thickness value of approximately 410 µm, as these membranes have the same amount of polymer by weight.
The percentage error on the measurements on the same membrane ranges of 3%-16%.

It can be seen from the **Figure 21** that there is variability in thickness among different points on the membrane (A1, A1 and A3, A3 in the figure) and not only among different batches of the same dope solution. This variability in thickness is the cause of the percentage error values obtained.

Except for membranes A, B, C, D and AA AB, the thickness of all other membranes was obtained from SEM images.

The micrometer measurement revealed to be inaccurate o ineffective in measuring the thickness of membranes that do not dry as flat sheets. For this reason, SEM imaging was used to assess the thickness, despite its lower accuracy. In fact, this latter technique leads to an underestimation due to the angle of the membrane section in the SEM chamber. However, the thickness values obtained by the SEM imaging proved to be very close to those measured with a micrometer, provided that the membranes are well oriented in the SEM chamber. In fact, measurements of the thickness of membranes AA and AB were carried out both with the plate micrometer and from SEM images, ensuring that the sample section was oriented at the correct angle (90°). It was verified that the thickness value obtained from the SEM image matched the value measured with the micrometer up to the third digit on a measurement in the order of µm.

Interestingly, membranes less than 400 µm thick (with a thickness around 250 µm or less), tend to wrap and to not dry as flat sheet.

Cross-sectional images of some of the membranes produced with their respective thickness measurements are shown for demonstration purposes, with reference to the scale (visible at the bottom left of the image). Shown is membrane I (CA 8.2% GLY 24.5% NMP 75.3%) cast at different bath temperatures (22°C and 40°C) and an MMMA with the same composition as the previous ones and with 10% ZFA as filler.

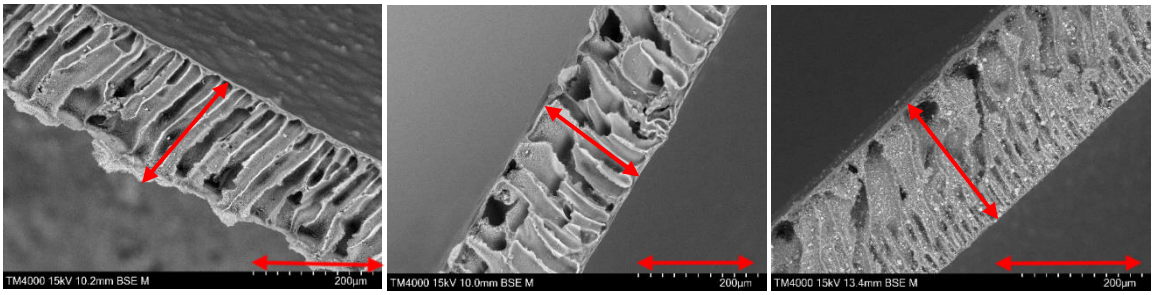


**Figure 23** Measurement of membrane thickness I at $T_{bath}$=22°C, $T_{bath}$=40°C and MMMA IB from SEM section image.

Measured thicknesses regardless of the method used are reported in **Figure 24**, details about each membrane compositions are collected in **Table 9**.

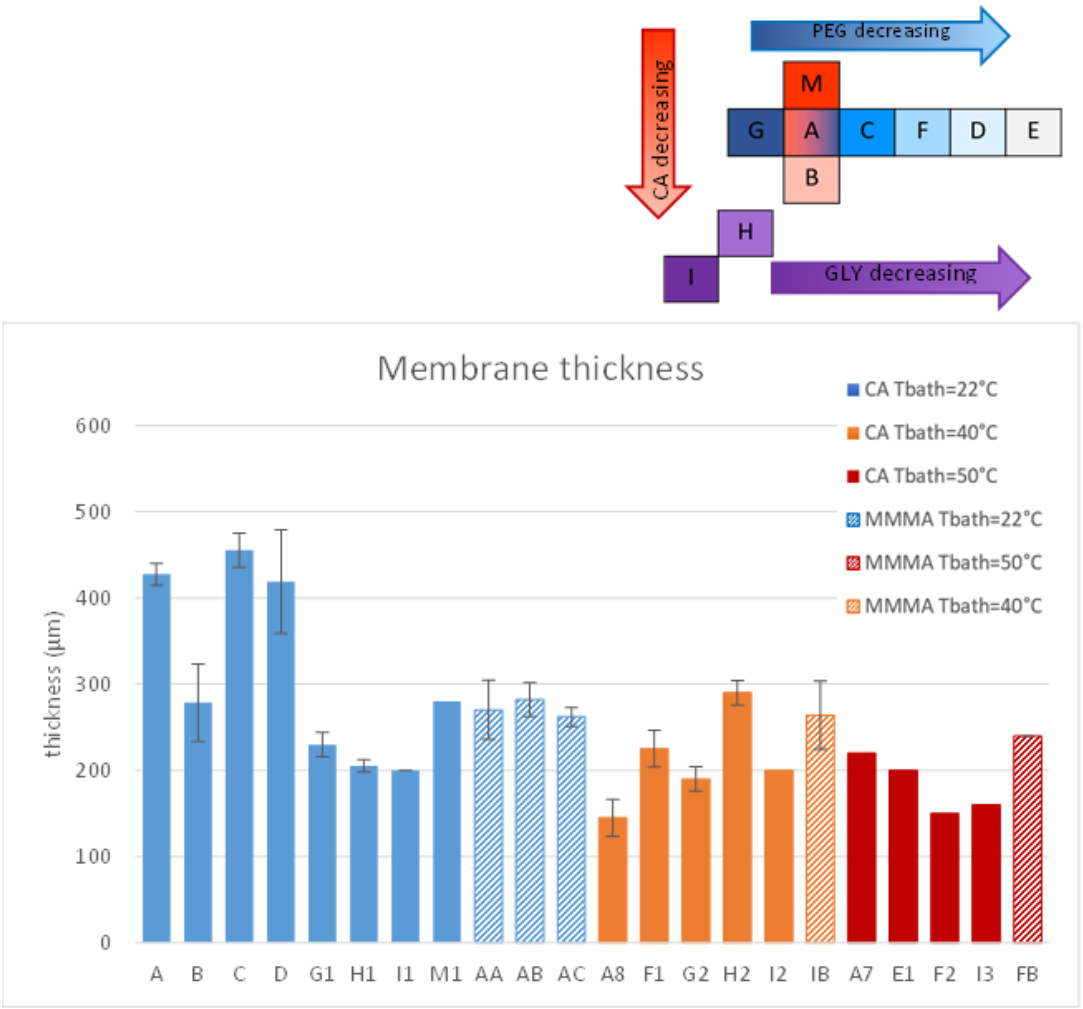


**Figure 24** Average thickness of all membranes as a function of coagulation bath temperature.

It can be asserted that the temperature of the coagulation bath has not a strong influence on the thickness of the membrane. In fact, membranes with the same composition, but fabricated with different bath temperatures, have very similar thicknesses, such as membranes G1, G2 or membranes I1, I2 and I3. Finally, the dispersion of zeolites in the membrane results in an increase of the thickness, e.g. MMMA IB has a thickness of around 260 µm compared with 200 µm of the pristine membrane I2, or MMMA FB has a thickness of 240 µm compared with 150 µm for the membrane without filler F2.

## 3.3 Water sorption and porosity

Water sorption is usually used to estimate an approximate porosity of the membrane, by differential weighting of wet and dry samples. However, this method showed to be imprecise because it is difficult to measure only the amount of water that is truly absorbed. In fact, small droplets or films of water may cling to the membrane's surface due to surface tension, without actually being absorbed. Additionally, when attempting to remove excess droplets from the surface, an excessive amount of water may be subtracted from the membrane through a mechanical drying process involving absorbent paper.

For this reason, water absorption has been calculated for only a few membrane types, A, B, C and D, in order to obtain indicative water absorption values.

**Figure *25*** shows the water sorption of membranes A, B, C and D cast in a coagulation bath at $T_{bath}$=22 °C.

From the results it can be noticed that membrane B absorbs more water than the other membranes, about 4.5 mg/mg (mass of water absorbed per mass of polymer) compared to 2.9 mg/mg for membrane A. This is explained because membrane B has less polymer than A while maintaining the same polymer/porous ratio. It is important to evaluate the error bars, which have a significant range of 0.9-1.9 mg/mg of the standard deviation values. The largest error occurs for membrane B. Due to the width of the error bars, it can be stated that all of the membranes analysed in the diagram have a similar average uptake capacity, around 3.5 mg/mg, specifically for membranes C (CA 13.5% PEG 5%) and D (CA 13.5% PEG 3%), which have the same amount of polymer as membrane A (CA 13.5% PEG 8.5%) and a smaller amount than membrane B (CA 10% PEG 5.9%) but have decreasing amounts of porogen.

In conclusion, the water absorption capacity is little influenced by the membrane composition, it has a slight dependence on the polymer concentration used.

The porosity shown in **Figure *25*** are in agreement to the relative water absorption values, with porosity percentages of 74% for A and 78% for B. In conclusion, membrane B has more porogen and less polymer, so the membrane is more porous and is able to absorb more water. As far as membranes C and D are concerned, their porosity values are also very similar if we take into account the important error on the measurement of membrane D. In fact, the errors in the measurements are within a range of 0.3% and 2%, excepting for membrane D whose percentage error is 4.4%.

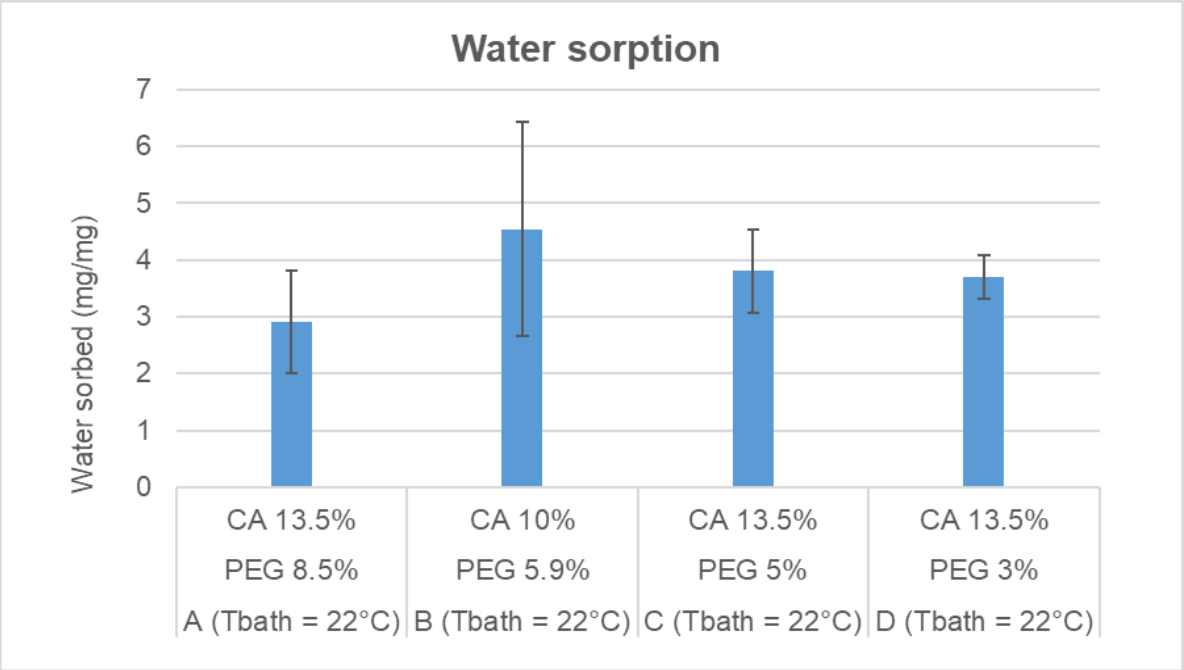


**Figure 25** Water sorption of membranes A, B, C and D cast with a coagulation bath temperature of T= 22°C.

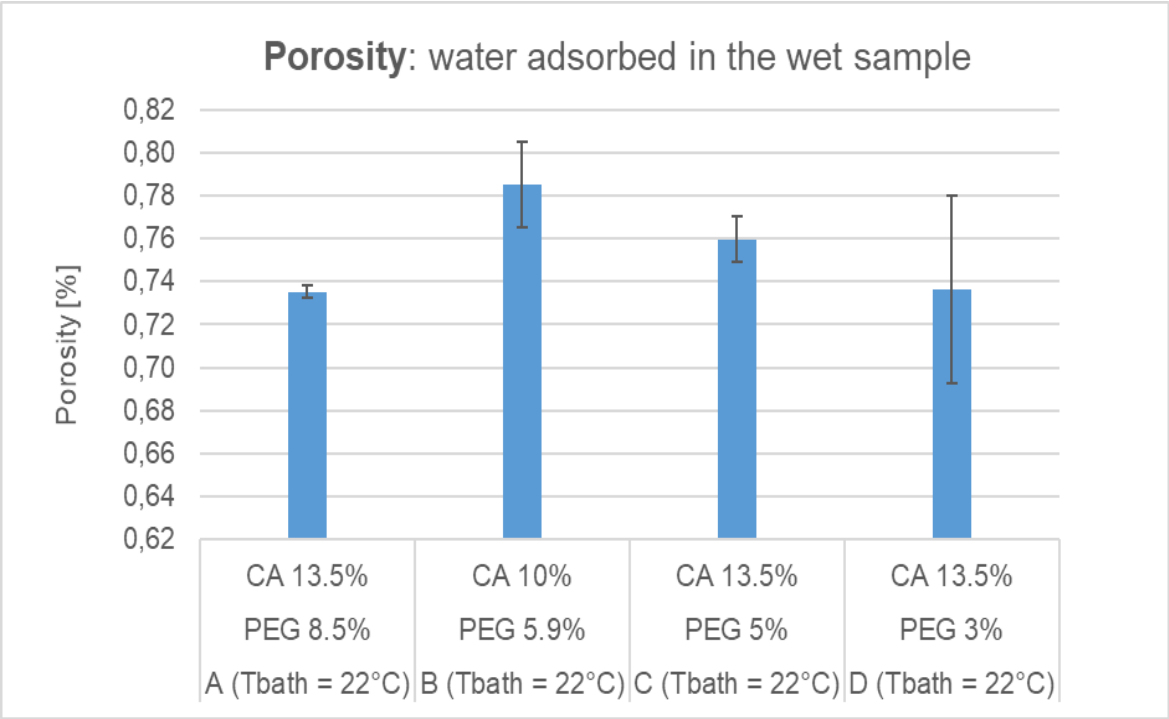


**Figure 26** Porosity values of membranes A, B, C and D obtained on the basis of the mass values measured on the dry and wet membrane. The membranes were castrated in a coagulation bath at a room temperature of T=22 °C.

## 3.4 FTIR spectroscopy test on membranes

FTIR was used to check the complete removal of solvent and porogen from the membrane after repeated rinsing. NMP possesses "N-C" bonds, while PEG has ether groups in its structure, that are not present in CA.

The effective removal of solvent from the membrane sample was confirmed, since the spectra of the CA powder and the membrane samples present peaks at the same wavelength (1100, 1250, 1350 and 1750 $cm^{-1}$). Furthermore, the spectra of the membranes and the spectra of the cellulose acetate powder are superimposed in **Figure 27**, showing that only the functional groups that are also present in the polymer are present in the membrane with the same ratio of amplitude. This proves that the membrane has no excess of ethers groups, that would show residual PEG in the structure.

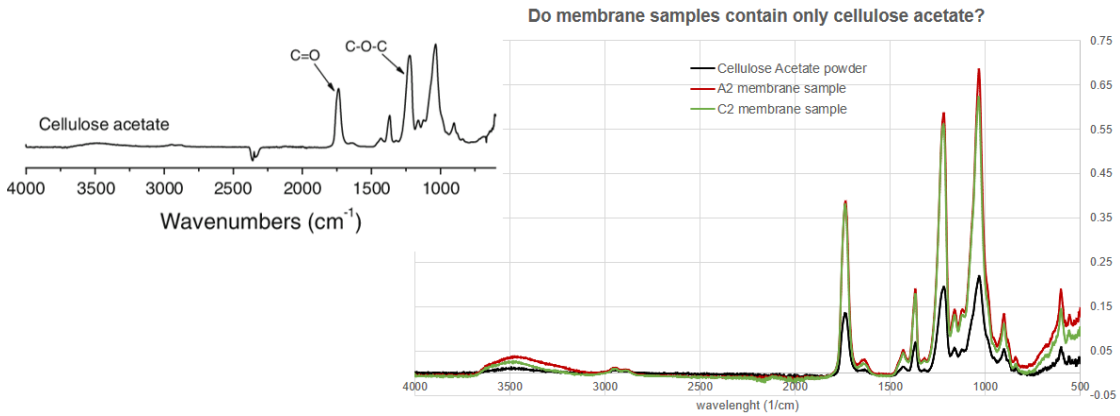


**Figure 27** FTIR spectra of samples showing the effective removal of solvent and porogen.

## 3.5 Impact of porogen and polymer concentrations on the membrane features

The production of membranes with different concentrations of CA and PEG or GLY was aimed at analysing how the polymer and porogen influence membrane characteristics. Hydraulic permeability and imaging on membrane cross-section and surface were monitored.

Permeabilities of membranes with different concentrations of PEG and CA are reported in **Figure *28*** (coagulation bath temperature $T_{bath}$=22°C), in which they are represented as the slope of the flux over pressure drop curve. The amount of PEG does not influence membrane permeability, in fact the permeability values of membranes ranging from 2.6% to 11% PEG (C1, D3, G1 and A6) are similar.

On the other hand, the permeability of the membrane decreases from 4270 L/($m^2$ h bar) to 2080 L/($m^2$ h bar) with the increasing of CA concentration in the solution from 11% (M2) to 13.5% (A6) of polymer, keeping the CA/PEG mass ratio constant. The membrane M has lowest permeability over all the others (C1, D3, G1 and A6).

A polymer concentration of 8.6% (B) results in a thin and fragile membrane, over which a permeability test cannot be carried out.

The permeability values for G1, A6, C1, D3 and M2 membranes agrees with what the SEM imaging shows (**Figure *29*** and **Figure *30***). Membranes G1, A6, C1 and D3 have a cross-section morphology and pore distribution, both in thickness and on the surface, that are

similar as are the permeability values. Thus, the amount of PEG does not influence the membrane morphology either. In contrast, M2 is a denser membrane with a thicker skin layer and has an uneven pore distribution in thickness with smaller pores near the skin layer and macrovoids at the bottom. These two differences result in lower permeability values than G1, C1, D3 and A6 membranes.

From the analyses, also discussed below, it appears that the permeability values are strongly dependent on:

- thickness of the skin layer:
  is responsible for the main pressure drop across the membrane and therefore reduces the permeability
- size of pores and their distribution on the surface:
  a greater number of pores and homogeneous distribution increase the permeability
- morphology of the section, i.e. the shape of the pores in the thickness

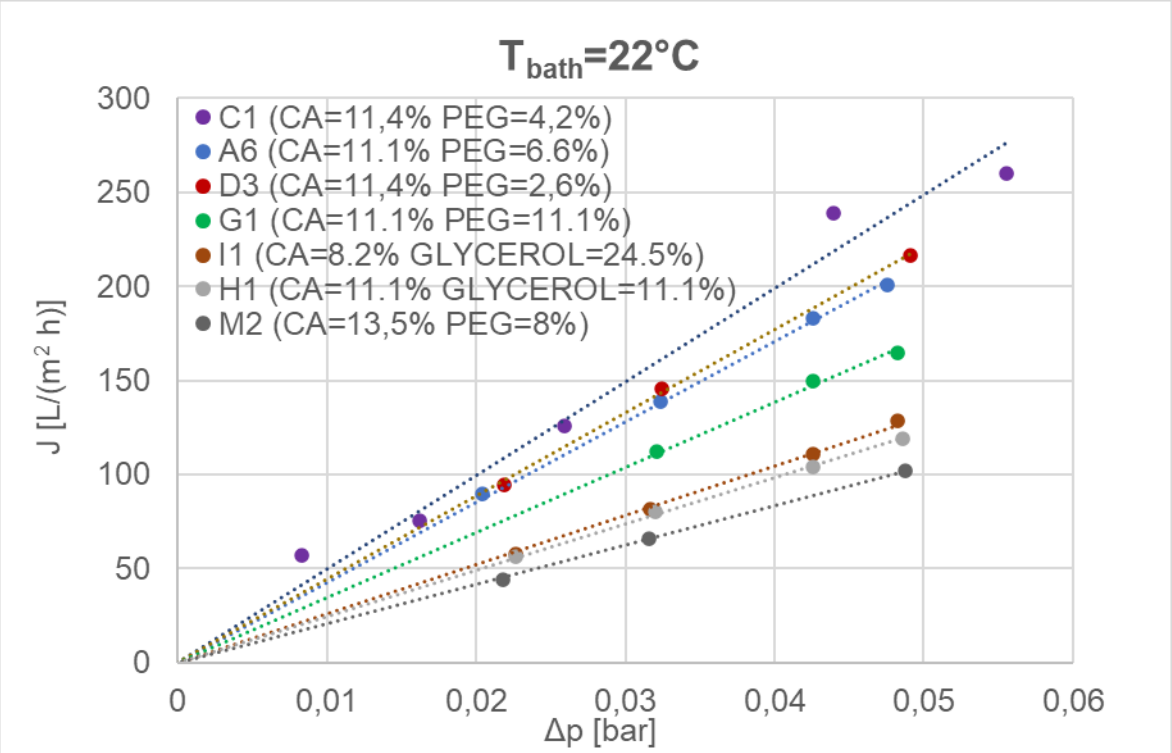


**Figure 28** Water flux vs pressure as a function of the amount of porogen and CA.

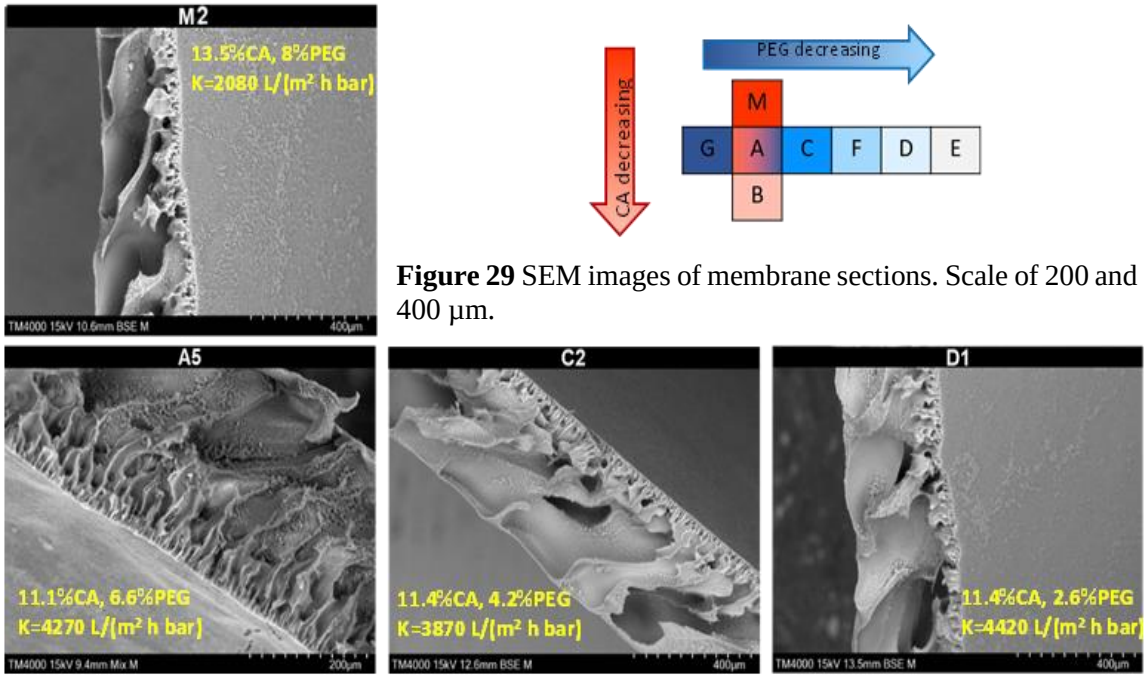


**Figure 29** SEM images of membrane sections. Scale of 200 and 400 µm.

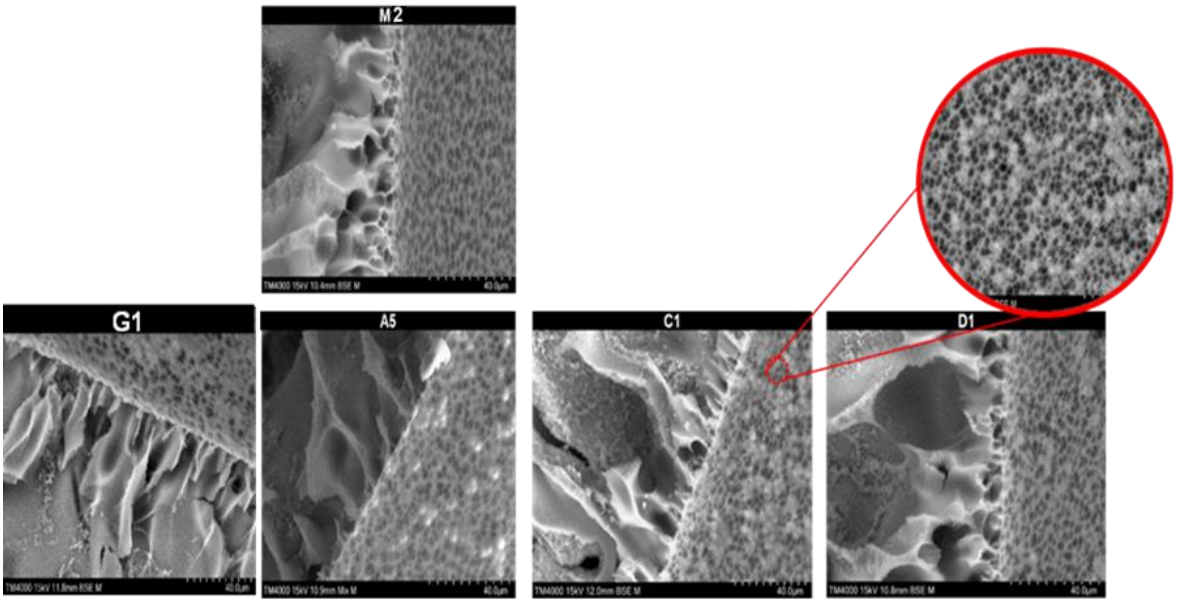


**Figure 30** SEM images of membrane surface and skin layer details, scale of 40 µm.

Even in membranes in which glycerol was used as a porogen, the permeability was not influenced by the mass percentage of the porogen and polymer (**Figure *28***), in fact the I1 and H1 membranes have the same permeability value although they have a CA/GLY mass ratio of 1 and 0.3 respectively, i.e. almost three times higher in I1.

The cross-section images obtained by SEM (**Figure 30** e **Figure 31**) justify the similar permeability values of the H1 and I1 membranes because it is observed that the cross-section morphology and the shape of the pores more specifically as well as their distribution remain the same for the two membranes.

Specifically, the membranes have a very thin skin layer with a dense, homogenous distribution of pores with an average diameter of less than 4 µm. In the membrane section, close to the skin layer, there is a poorly developed and inhomogeneous 'finger like' porosity; on the other hand, in the bottom of the membrane section, large macrovoids are observed, reaching up to 200 µm of diameter.

In general, the permeability is not affected by the concentration of porogen, regardless of the type of porogen used PEG or glycerol.

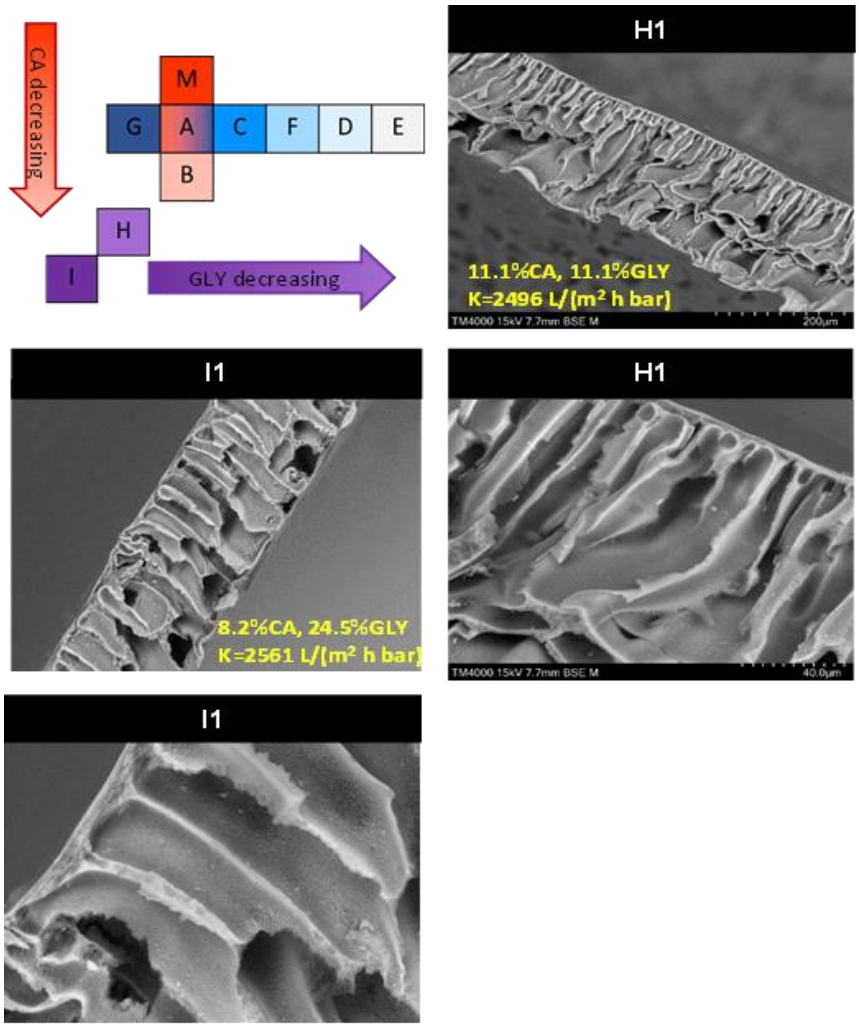


**Figure 31** SEM images of membrane sections. Scale of 200 and 400 µm.

Finally, **Figure *31*** shows that membranes obtained by using different porogens, but with the same or similar AC/porogen ratio as the membranes in **Figure 30** (e.g. G1 and H1 or C1 and I1) have different characteristics. In fact, membranes with PEG as porogen have higher permeability values than membranes with glycerol as porogen.

From the images obtained by SEM, it is evident that the skin layer is thicker and the pores on the surface are homogeneously distributed but smaller in size (cannot be observed with the same scale of reference) compared with membranes with PEG as porogen. These differences explain the lower permeability of membranes with GLY as porogen because their skin layer offers more resistance to flow. From **Figure 31** in the membrane section, a very homogeneous finger like porosity is observed, the channels constituting it are regular and with an average size of 16 μm. The pores are interconnected and their pore walls are very thin and not very dense with microporosity. At the bottom of the membrane are macrovoids of small size, on the order of 50 μm.

The different permeability between the membranes is related to the different morphology, that results from the different demixing during the coagulation phase. This effect comes from the different physiochemical properties of glycerol and PEG, reported in **Table 8**. Glycerol has a viscosity one order of magnitude higher of PEG 400, while density is similar. On the other hand, PEG is more hydrophilic than glycerol, dissolving more than 100 times better in water.

Due to its higher viscosity, higher molecular weight and higher hydrophobicity, glycerol is hindered from escaping the membrane pores during the demixing phase. This is what explains the morphology of the membrane section. In fact, PEG being less viscous and more hydrophilic allows for a faster demixing process, especially at the beginning when there is a high concentration gradient between the polymer phase and the coagulation bath. This justifies the very thin skin layer and the "finger like" porosity at the top of the section. In the bottom of the section there are macrovoids because PEG before finally moving away from the membrane stagnates at the bottom in pockets and then slowly exits. This phenomenon is justified by the concentration gradient between the bath and the polymer, which is now reduced, and also by the transfer of solvent-porogen and DI water between membrane and bath that is only allowed through the top surface of the membrane. Instead, the bottom surface is in contact with the supporting glass, which prevents the mass transfer for almost the entire demixing phase, until the membrane detaches itself from the glass when the

coagulation process is almost complete. In contrast, GLY, due to its chemical-physical properties (high viscosity, high hydrophobicity), leaves the membrane immersed in a DI water bath more hardly. Therefore, the demixing process is not much faster in the initial phase than in the final phase. This explains why the pore morphology is similar throughout the membrane thickness and no macrovoids occur.

Generally, the skin layer and the 'finger like' porosity characterise the surface in contact with the bath and not the bottom of the membrane in contact with the glass because in the area of the top of the membrane the exchange starts much faster than at the bottom. Exchange is slowed down along the thickness of the membrane because it is unidirectional, only from the top to the bottom, and because the concentration gradient and the driving force decrease with thickness. In general, finger like porosity is characteristic of fast mass transfer, whereas “sponge like” porosity is characteristic of very slow matter exchanges.

**Table 8** Physiochemical properties of glycerol and PEG-400

| | **PEG 400** | **Glycerol** |
|---|---|---|
| **Kinematic viscosity** [cSt] | 90.0 | 1120.6 |
| **Dynamic viscosity** [Pa s] | 0.10152 | 1.412 |
| **Density** [kg/m$^{3}$] | 1128 | 1260 |
| **logP** | -4.8 | -2.32 |

In all the membranes tested, permeability remains constant, with a linear trend of flux over increasing pressures, up to a pressure of 0.049 bar. Even after 5 h of flushing at the maximum pressure, the fabricated membranes do not undergo any morphological change, such as squeeze or rupture, that would change the permeability values with increasing pressure.

**Table 9** List of membranes produced with details of compositions, polymer/porogen ratio, permeability and bath temperature.

| Sample | Concentration Ratio % (CA:PEG/GLY:NMP) | CA/Porogen ratio | Permeability [L/(m$^2$ h bar)] | $T_{bath}$ [°C] |
|---|---|---|---|---|
| M | 13,5:8:78,5 | 1,7 | 2080,8 | 22 |
| A | 11,1:6,6:82,3 | 1,7 | 4270,68<br>8777,06<br>16256,92 | 22<br>40<br>50 |
| B | 8,6:5,1:86,3 | 1,7 | / | 22 |
| C | 11,4:4,2:84,4 | 2,7 | 3870,15 | 22 |
| D | 11,4:2,6:86 | 4,5 | 4420,36 | 22 |
| E | 11,1:0,6:88,3 | 18,5 | 16231,37 | 50 |
| F | 11,1:3,1:85,8 | 3,6 | 9862,27<br>14319,91 | 40<br>50 |
| G | 11,1:11,1:77,8 | 1 | 3466,52<br>5775,47 | 22<br>40 |
| H | 11,1:11,1:77,8 | 1 | 2496,52<br>4124,25 | 22<br>40 |
| I | 8,2:24,5:75,3 | 0,3 | 2561,19<br>4593,55<br>7115,07 | 22<br>40<br>50 |

## 3.6 Impact of coagulation bath temperature on permeability and morphology of membranes

**Figure *32*** shows the permeability of the membranes as a function of the temperature of the coagulation bath, each membrane (excluding E) was casted at a different bath temperature. The graph shows the flux as a function of operating pressures during the test, so the slope of the line represents the permeability. The membranes tested (A, E, F and G) had different compositions but all had PEG as porogen.

It is clear from the graph that the bath temperature greatly influences the permeability of the membrane; as the temperature increases, the permeability increases. Going from a temperature of 22°C to a temperature of 40°C, the permeability has an increase of about 56.7%, from a value of 4270 to 9862.3 L/($m^2$ h bar), while varying the temperature from 40°C to 50°C, the permeability has an increase of 39.3%, varying from 9862.3 to 16257 L/($m^2$ h bar). Thus, permeability is more sensitive to changes in bath temperature at low temperatures.

In contrast, the concentration of porogen has a slight influence on the permeability at the fixed temperature of the bath. In particular, when the concentration of the porogen increases the permeability decreases. In fact in detail from **Figure *34***, varying the mass percentage concentration of PEG by 40%, from 6.6% to 11.1% at $T_{bath}$=22°C, the permeability is reduced from 200 to 160 L/($m^2$ h bar), by 20%, whereas varying it of 50% at low concentrations from 3.1% to 6.6% at $T_{bath}$=50°C the permeability is reduced from 800 to 700 L/($m^2$ h bar), by 12.5%.

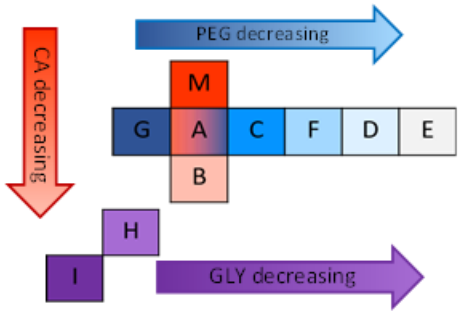


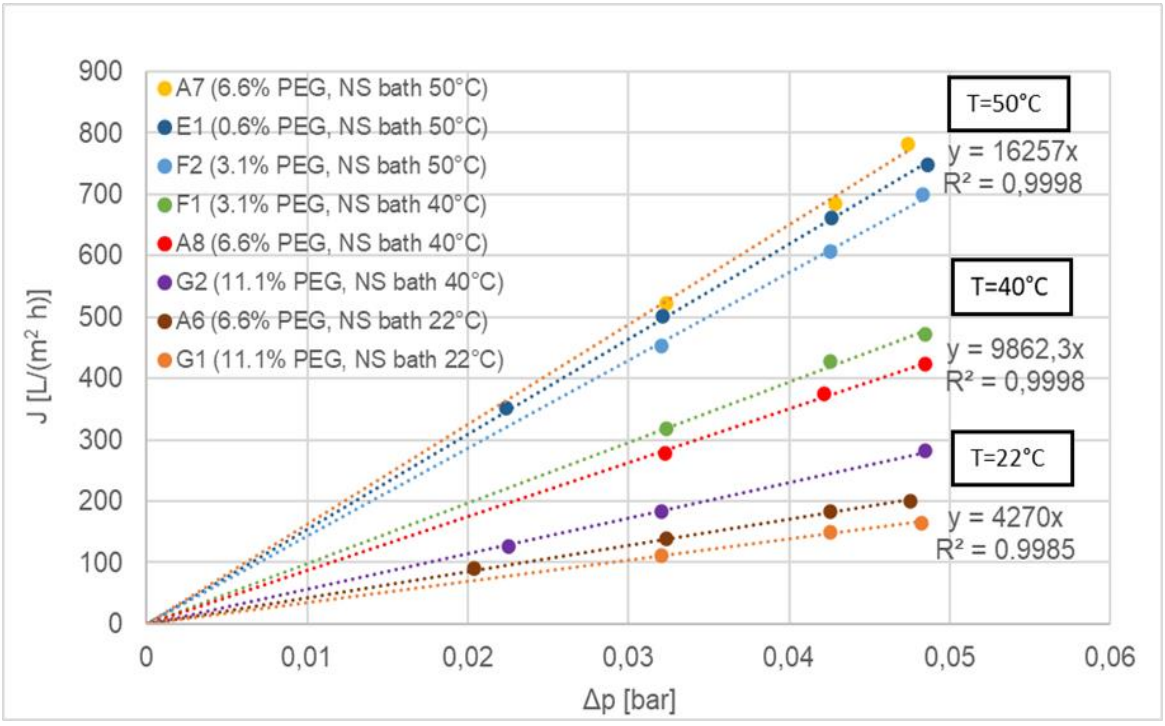


**Figure 32** Flux vs pressure drop at different bath temperature: membranes prepared with PEG as porogen.

In **Figure *33*** permeabilities of membranes fabricated using different bath temperatures and different porogens are shown. The permeability is the slope of the flux over pressure drop curve.

The type and amount of porogen used does not influence the trend of permeability with temperature, in fact permeability increases when the temperature is increasing regardless of whether GLY or PEG was used and at what concentration. However, membranes with PEG as porogen show higher permeabilities than membranes with GLY as porogen. In fact, membranes G2 and H2 (same composition and temperature) have permeabilities of 5775.5 and 4112.4 L/($m^2$ h bar) respectively. Membranes G, H and I are listed in descending order of their permeability values.

Finally, the CA/GLY ratio does not influence the permeability of membranes at the same bath temperature. In fact, the membranes H1 and I1 at $T_{bath}$=22°C have very similar permeability values (2494.5 L/($m^2$ h bar)), the same for membranes H2 and I2 at $T_{bath}$=40°C (4112.4 L/(m2 h bar)).

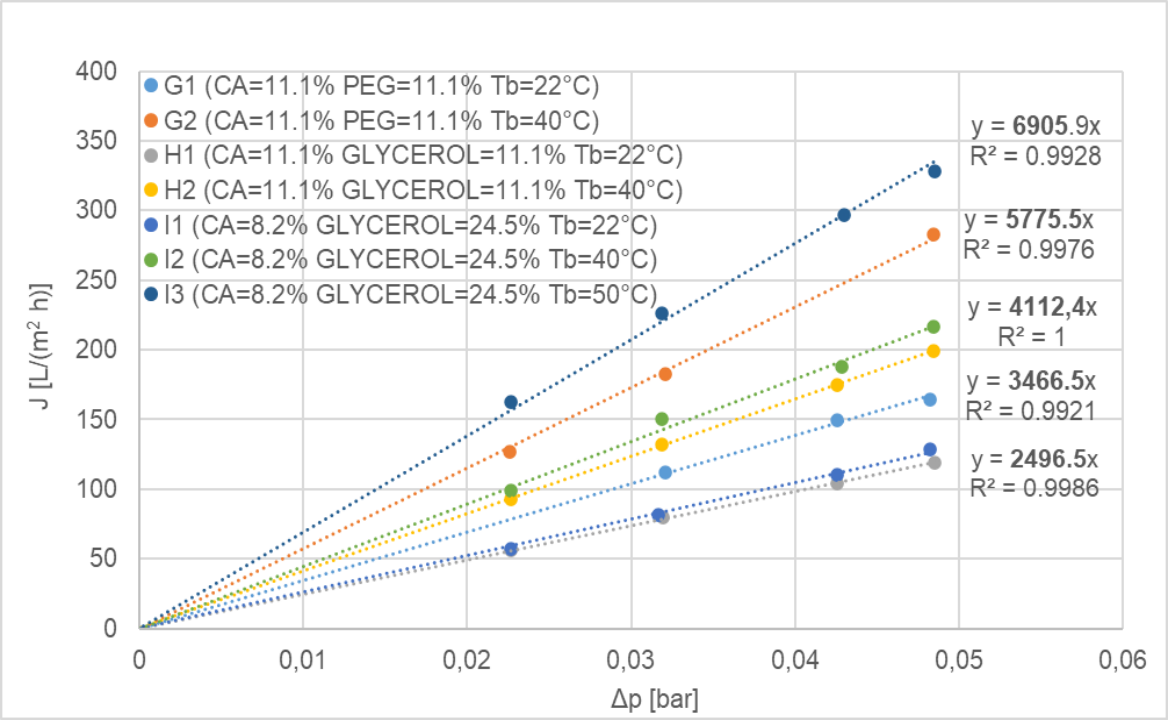


**Figure 33** Flux vs pressure drop of membranes (G, H and I) with the same composition but different porogen and coagulation bath temperature.

In conclusion, the temperature of the coagulation bath is a factor that strongly influences membrane permeability values, but it does not change the dependency relationship between the amount and type of porogen and permeability values, already described in detail in section 3.5.

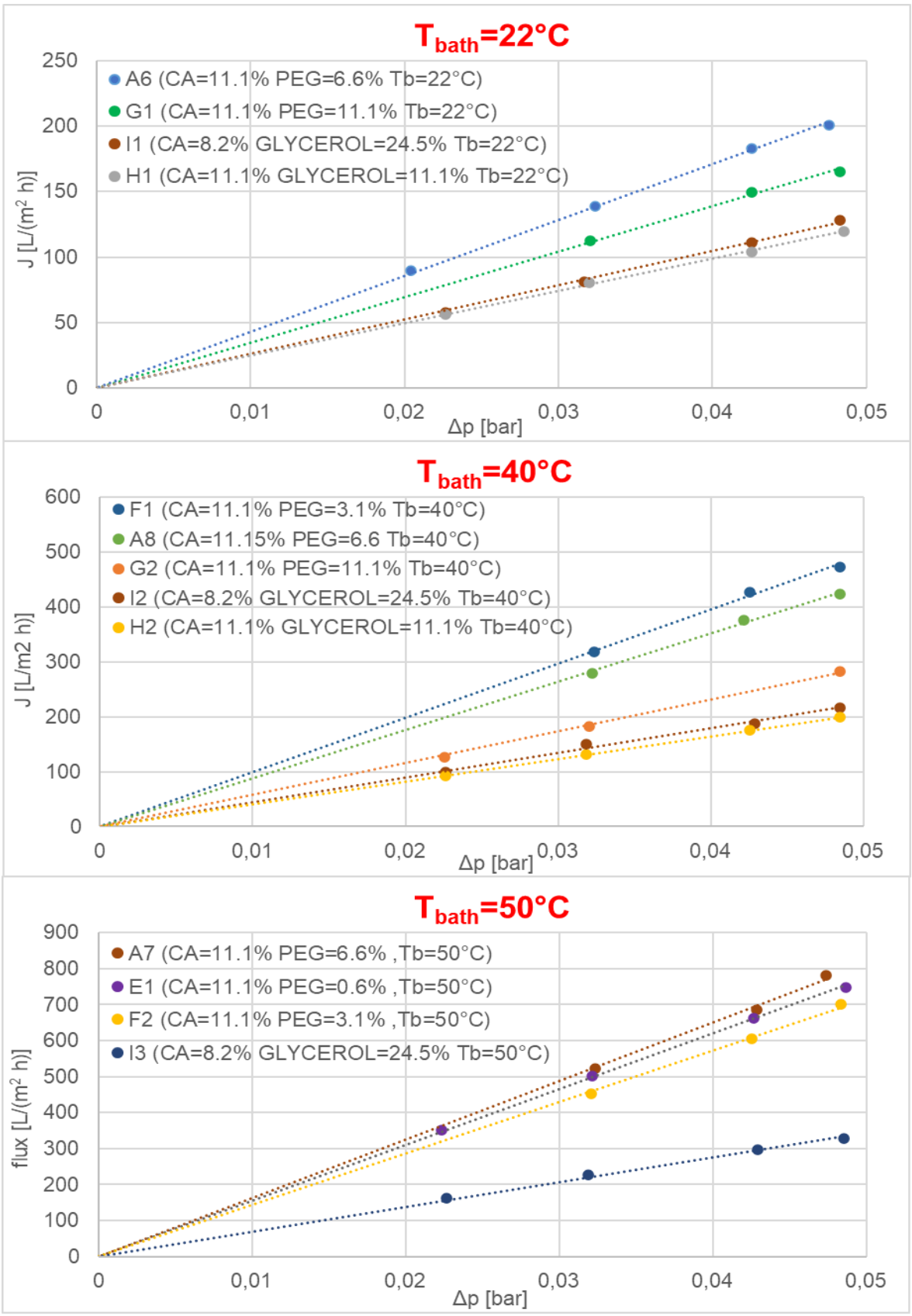


**Figure 34** Flux vs pressure drop of all membranes manufactured at coagulation bath temperatures of 22°C, 40°C and 50°C.

**Figure *35*** shows sections of membranes cast at different bath temperatures obtained by SEM. The images are organised from up to down as a function of increasing bath temperature. Moving vertically means analysing membranes with the same composition but different bath temperatures. Moving horizontally, membranes with a different composition but cast at the same bath temperature are analysed, so from left to right the porogen concentration decreases. Finally, the membranes on the left of the image G, F and E have PEG as a porogen and on the right the membranes H and I have GLY as a porogen.

Since that the detailed description of morphology has already been discussed in paragraph 3.5, in the following description will be limited to the differences in morphology arising from the variation in coagulation bath temperature during the membrane casting process.

In accordance with the increasing trend in permeability with both temperature from the images, a strong change in membrane morphology is observed from the images regardless of the type of membrane analysed. In fact, for all membranes with increasing bath temperature they show an increase in the size of the macrovoids at the bottom of the membrane and this is the main cause of the increase in permeability values.

Specifically, in membrane G (11.1%CA, 11.1%PEG) the differences in the cross-section are evident only at the bottom of the membrane, where at $T_{bath}$=40°C the macrovoids unite to form larger cavities. While the morphology of the skin layer and the part of the membrane immediately below remains unchanged (same dispersion of the porosity and thickness). For the F membrane (11.1%CA, 3.1%PEG) the same variations in morphology as for the G membrane can be observed. Moreover, for the F membrane is clear how the macrovoids at the bottom of the membrane at $T_{bath}$=40°C have walls that clearly define the macrocavity, whereas at $T_{bath}$=50°C they are no longer defined and the individual macrovoids can be distinguished, but a single large void layer can be observed between the skin layer and the bottom of the membrane.

As far as membranes with GLY as porogen are concerned, the membrane H (11.1%CA, 11.1%GLY) also shows a melting in the macrovoids at the bottom of the membrane that form much larger cavities, justifying the increase in permeability. Unlike membranes with PEG as porogen, the finger-like porosity that characterises the membrane immediately below the skin layer is much more homogeneous and extends to half the thickness of the membrane at $T_{bath}$=22°C. At $T_{bath}$=40°C an increase in the size of the macrovoids at the bottom is

observed, as for membranes with PEG as porogen (G, F and E), however the finger like porosity persists in the section for greater depths (up to 160 µm).

Finally, membrane I (8.2%CA, 24.5%GLY) at $T_{bath}$=22°C is characterised by a finger like porosity that develops throughout its entire thickness and in the bottom of the membrane a few macrovoids are evident (no more than 60 µm) compared to the other membranes. At $T_{bath}$=40°C the macrovoids are absent and the porosity has the form of a regular cylindrical channel that crosses the entire thickness of the membrane. At $T_{bath}$=50°C the membrane drastically changes its morphology and, like all the other membranes mentioned above, it acquires a morphology characterised by the presence of large cavities at the bottom of the membrane.

In conclusion, increasing the temperature of the coagulation bath has the same effect on the morphology of all the membranes analysed and acts on the morphology of the bottom of the membrane, while leaving the morphology of the top of the membrane mostly unchanged. At $T_{bath}$=50°C the morphology of all membranes tends to be similar especially for membranes with PEG as porogen. In fact because of the similar morphology of the F and E membranes at $T_{bath}$=50°C they have very similar permeability values (14320 and 16231 L/(m$^2$ h bar) respectively) and for the same reason the effect of the other parameters, e.g. the amount of porogen, on the permeability are milder at high coagulation bath temperatures as shown **Figure *34***.

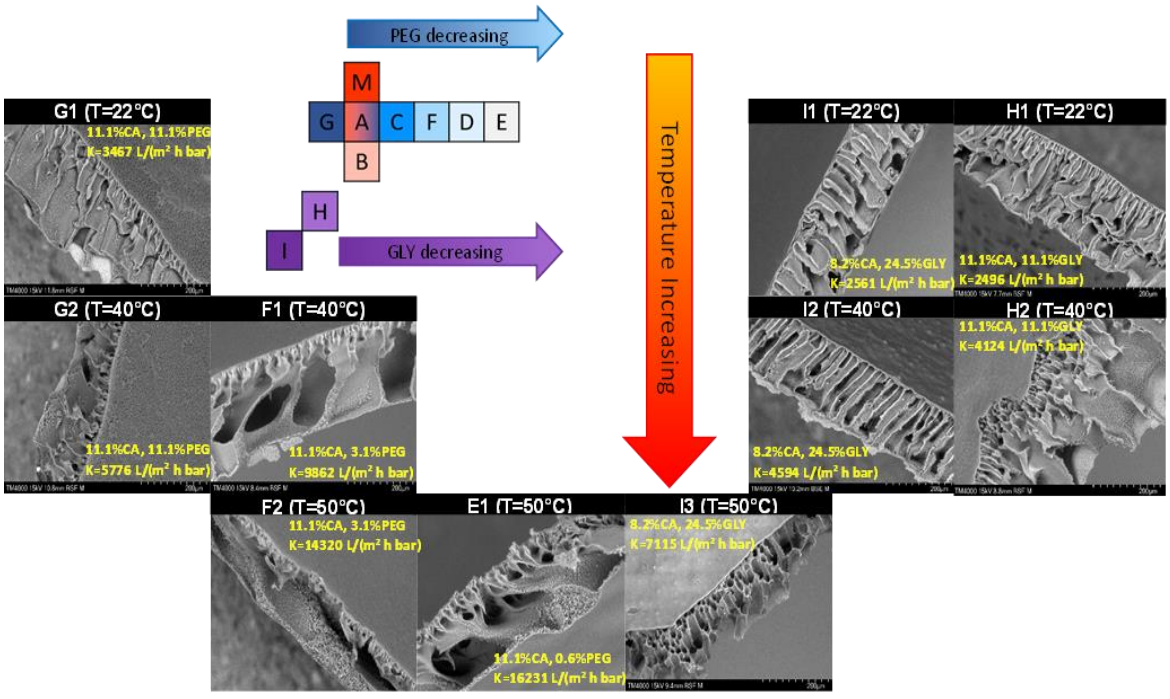


**Figure 35** Section images of membranes G (11.1%CA, 11.1%PEG), F (11.1%CA, 3.1%PEG), E (11.1%CA, 0.6%PEG), H (11.1%CA, 11.1%GLY) and I (8.2%CA, 24.5%GLY) at the different coagulation bath temperature $T_{bath}$=40°C and $T_{bath}$=50°C at scale of 200 µm.

## 3.7 Impact of zeolite dispersion in the composite membrane

The adsorbent powder dispersed into the polymeric matrix has an impact on the membrane fabrication. In fact, MMMAs are composites and their characteristics are different of the pristine membrane. For this reason, it is important to assess the variation of the parameters of interest, such as permeability, morphology and adsorption capacity, with the introduction of the adsorbent, in order to quantify the drop in membrane performance as a function of the amount of filler dispersed.

For this reason, several MMMAs with the same polymer and porogen concentration were fabricated, dispersing different amount of adsorbent.

Of all the zeolites tested only two types of zeolites were used as adsorbent to prepare the composite membrane: ZFA and ZY because they showed highest adsorption capacity (higher $q_{ads}$, during static adsorption test).

In fact, the membranes chosen to produce MMMAs are A, F and I. These are the membranes with high permeability and a porosity that offers high surface area. Nonetheless, they differ for the morphology of the microstructure: sample A shows a classic finger-like porosity throughout the thickness of the membrane from top to bottom, while F owns a massive macrovoid between the skin layer and a spongy microporosity in the bottom of the layer. Sample I, instead, shows a regular finger-like porosity, with channels throughout the thickness of the membrane from top to bottom, extending in parallel to each other, with a thin separating wall (**Figure *36***).

Some membranes chosen to produce the MMMAs with adsorbent were fabricated changing the coagulation bath temperature (T=40°C and T=50°C for membranes I and F, respectively).

A summary of the MMMAs produced and tested is reported in **Table *5*** .

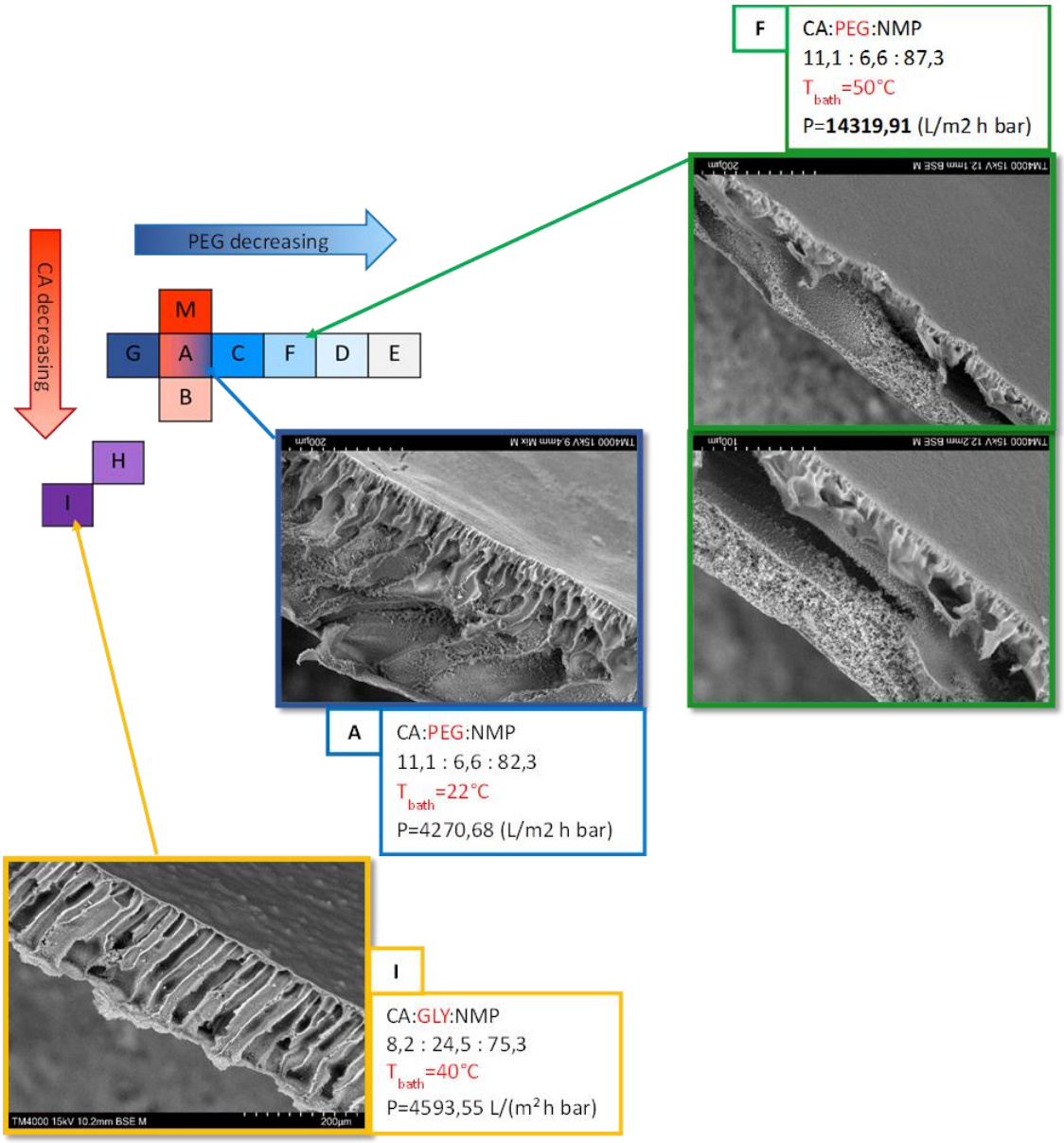


**Figure 36** Summary diagram of the properties of the membranes chosen to produce MMMAs.

In membrane A (11.1% CA, 6.6% PEG), ZY is used as a filler with three different mass percentages to analyse how the adsorbent concentration influences the membrane. In composites AA, AB and AC, 5 wt%, 10 wt% and 25 wt% of ZY were used, respectively. As the filler concentration increases from 0% to 25%, the permeability decreases from 4270 to 1195 L/(m$^2$ h bar) (**Figure *37***). The percentage reduction in permeability is 17.9% for 5 wt% ZY (AA), 45.3% for 10 wt% ZY (AB) and 72% for 25 wt% ZY (AC).

SEM images of AA, AB and AC membranes (**Figure *38***) show that the adsorbent is homogeneously dispersed both on the surface and in the thickness, and the morphology of

the membrane does not undergo a strong change. However, the surface of the channels and macrovoids appears denser, lacking microporosity due to the introduction of the adsorbent particles into the porosity.

In fact, in the cross-section there is a “finger like” porosity up to half the thickness and in the bottom of the membrane there are macrovoids. Comparing the pristine membrane (A) and all the MMMAs (AA, AB and AC); the macrovoids in MMMAs are smaller in size than those in pristine membrane (A). This morphological difference explains the reason for the reduction in permeability, so the addition of particles in the membrane is responsible for a reduction in the size of the macrovoids and the empty volumes available to water flow and the permeability decreases.

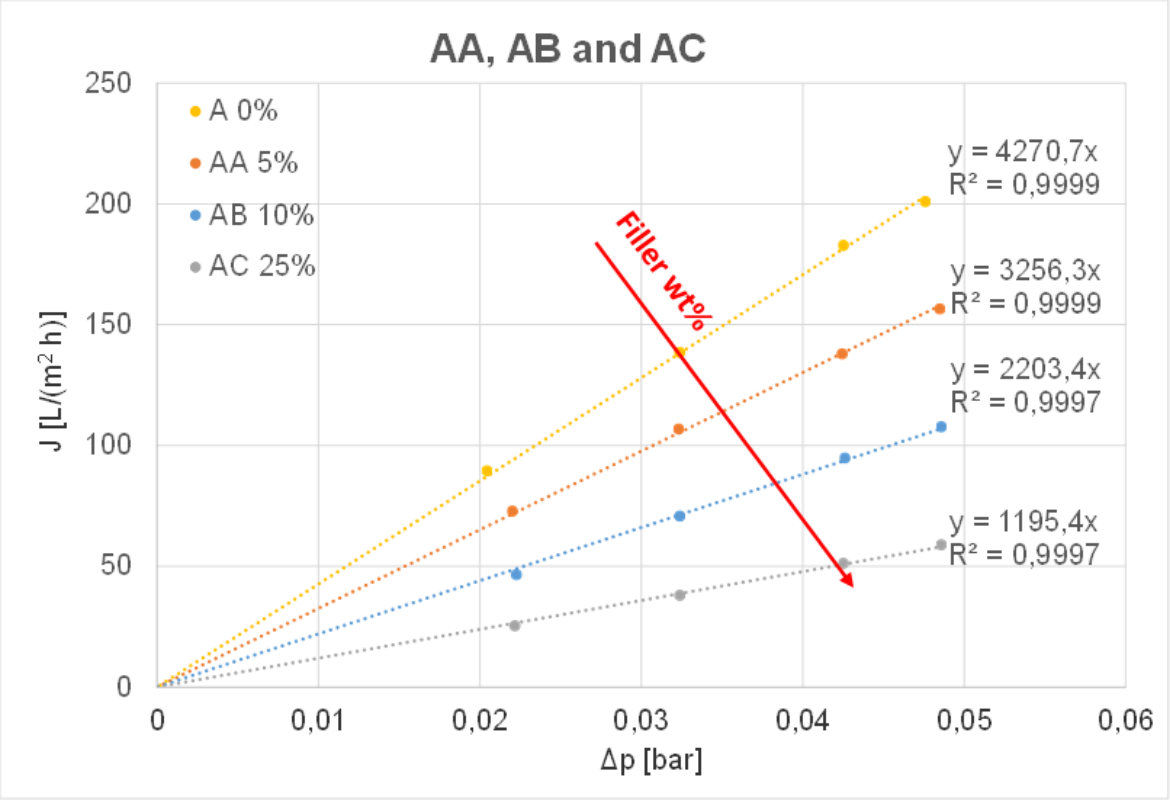


**Figure 37** Flux vs pressure drop for membrane at different ZY wt%.

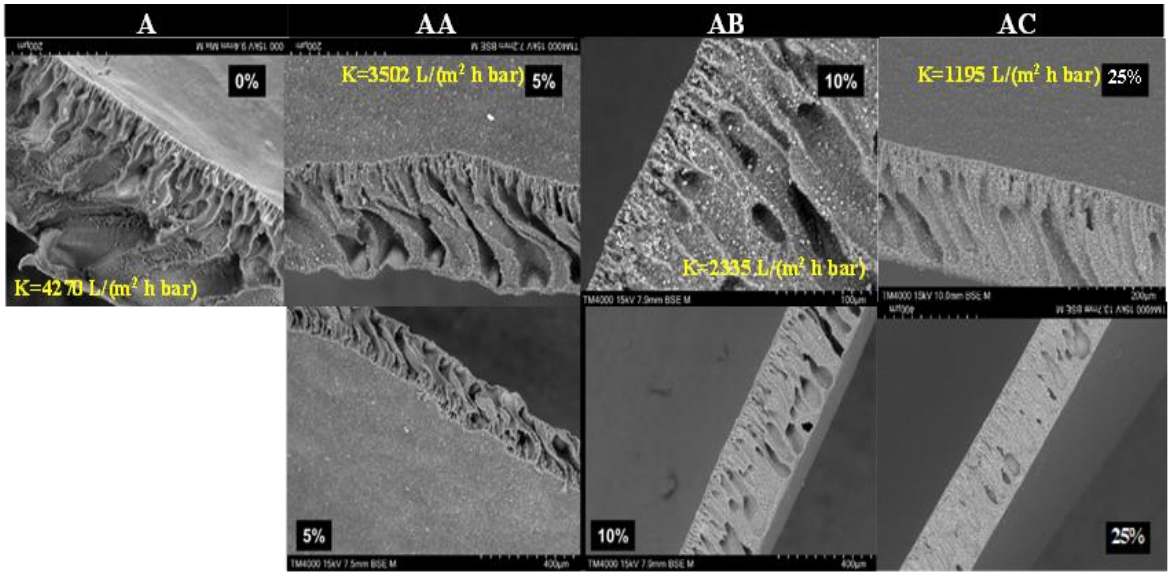


**Figure 38** Section images of membranes A (11.1%CA, 6.6%PEG) with 0% filler, AA with 5% filler, AB with 10% filler and AC with 25% filler at scale of 2000 µm and 400 µm.

In membrane F (11.1% CA, 3.1%PEG) and I (8.2% CA, 24.5%PEG), ZFA is used at a fixed concentration of 10 wt%.

Similarly to the previous case, the permeability decreases with the introduction of the filler into the membrane. Permeability reduces from a value of 14320 L/($m^2$ h bar) to 4120 L/($m^2$ h bar) bar and from a value of 4594 L/($m^2$ h bar) to 4269 L/($m^2$ h bar) for membranes F and I, respectively. Therefore, the MMMAs FB and IB membranes, the percentage reduction in permeability compared to the F and I membranes are 71.2% and 7.07% respectively (**Figure 39** and **Figure 40**).

From the SEM images (**Figure 41** and **Figure 42**), a more obvious change in morphology of the membrane cross-section is observed for sample FB (F + 10% ZFA), the macrovoids at the bottom of the membrane are very small compared to the pristine membrane (F). The membrane IB (I + 10% ZFA) has a very different morphology with respect to membrane I.

In fact, a finger like porosity is still present, but it is no longer homogeneous throughout its thickness from top to bottom. In the region closer the skin layer, there is a finer porosity while in the bottom few larger cavities appear. Again, the change in permeability is clearly caused by a change in membrane morphology.

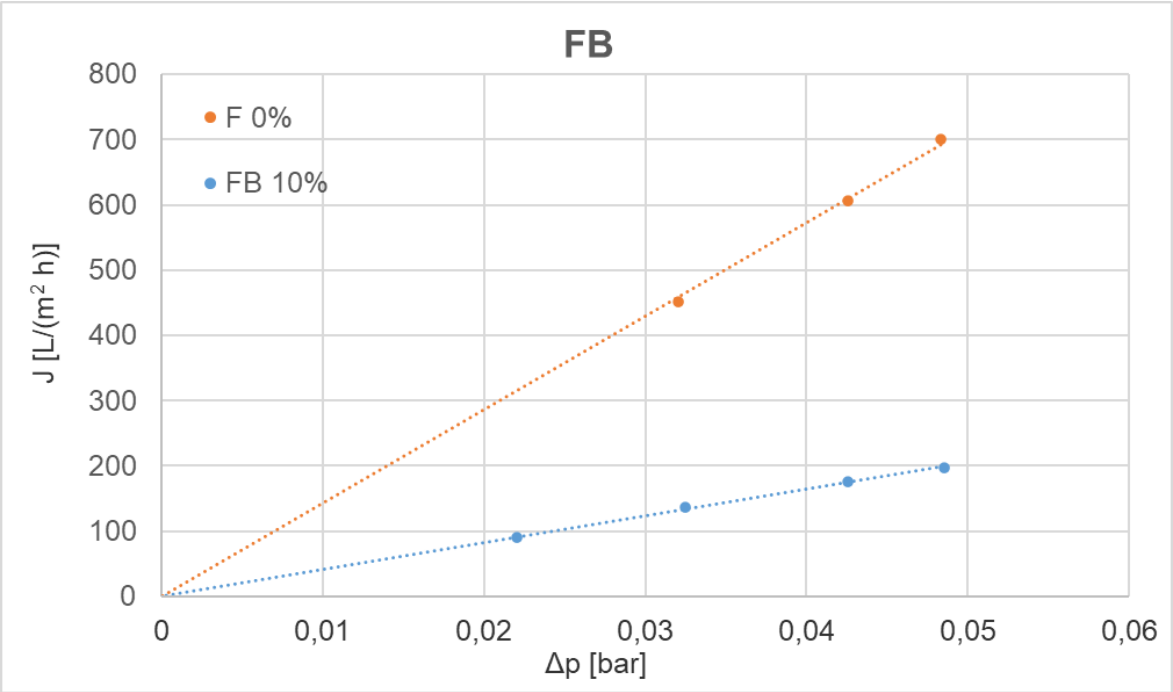


**Figure 39** Comparison of water flux of membrane F: effect of 10% filler.

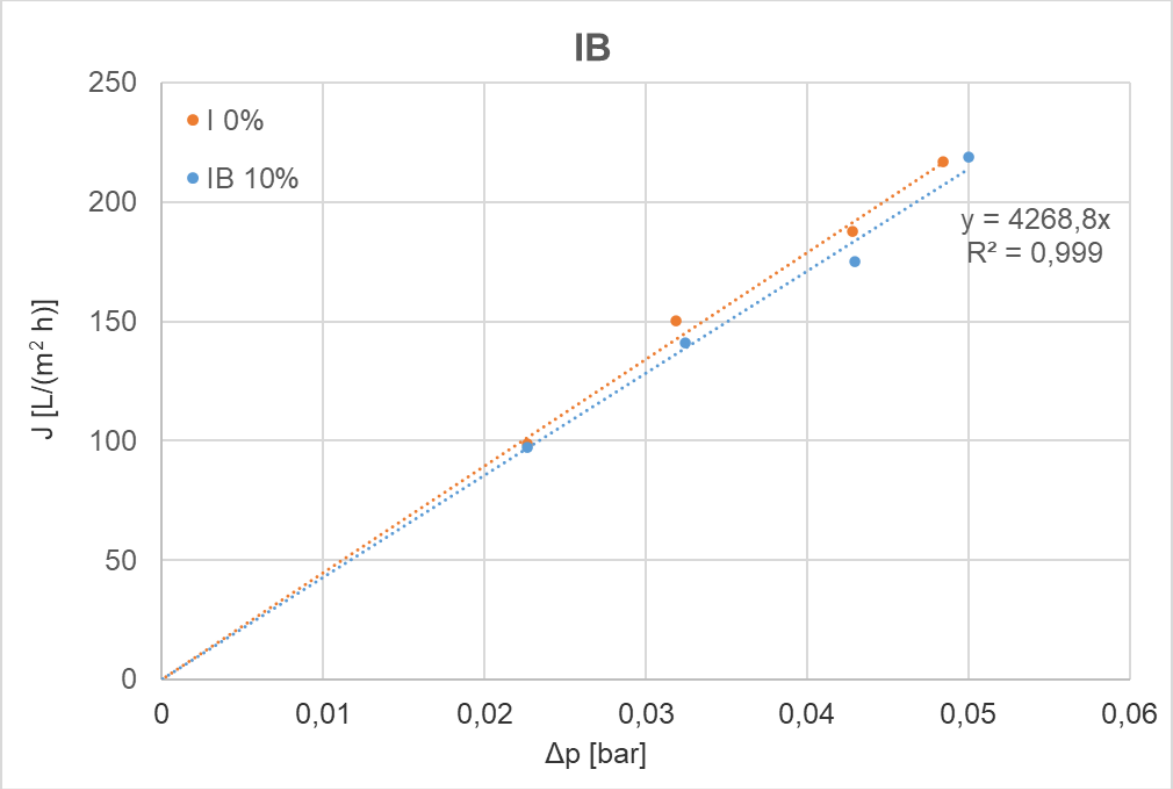


**Figure 40** Comparison of water flux of membrane I: effect of 10% filler.

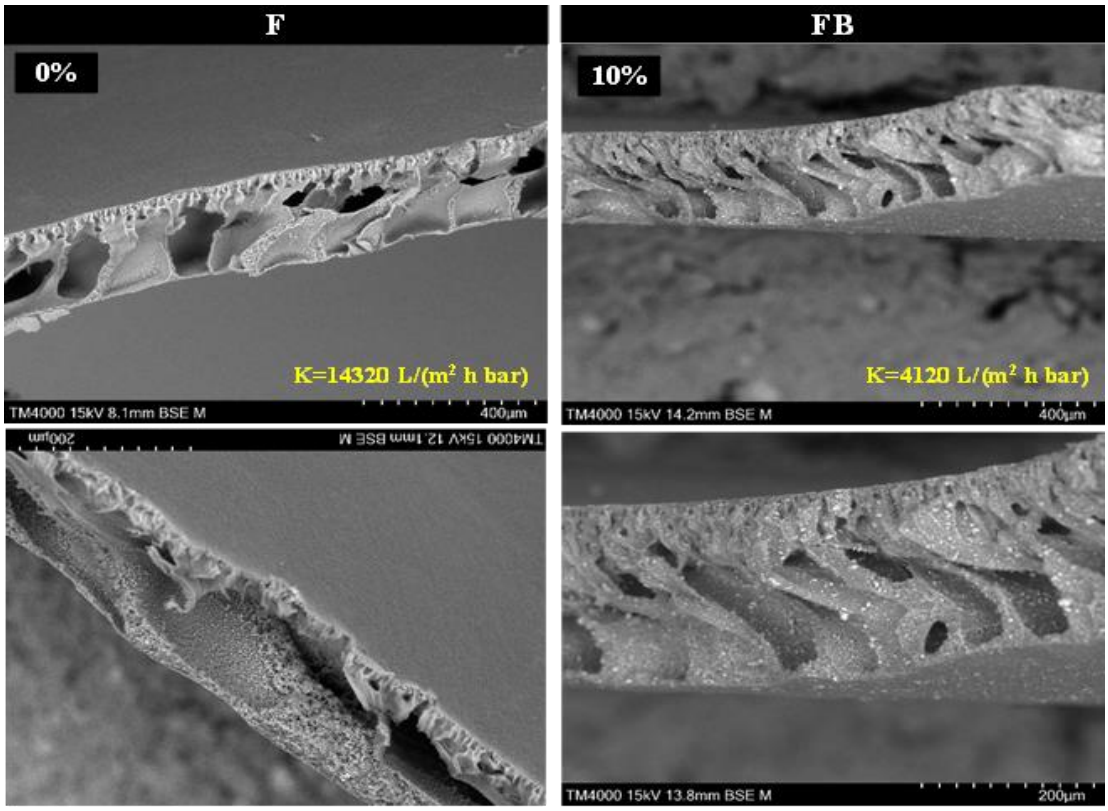


**Figure 41** Membrane section images F (11.1%AC, 3.1%PEG) with 0% filler, FB with 10% filler at scale of 200 µm and 400 µm.

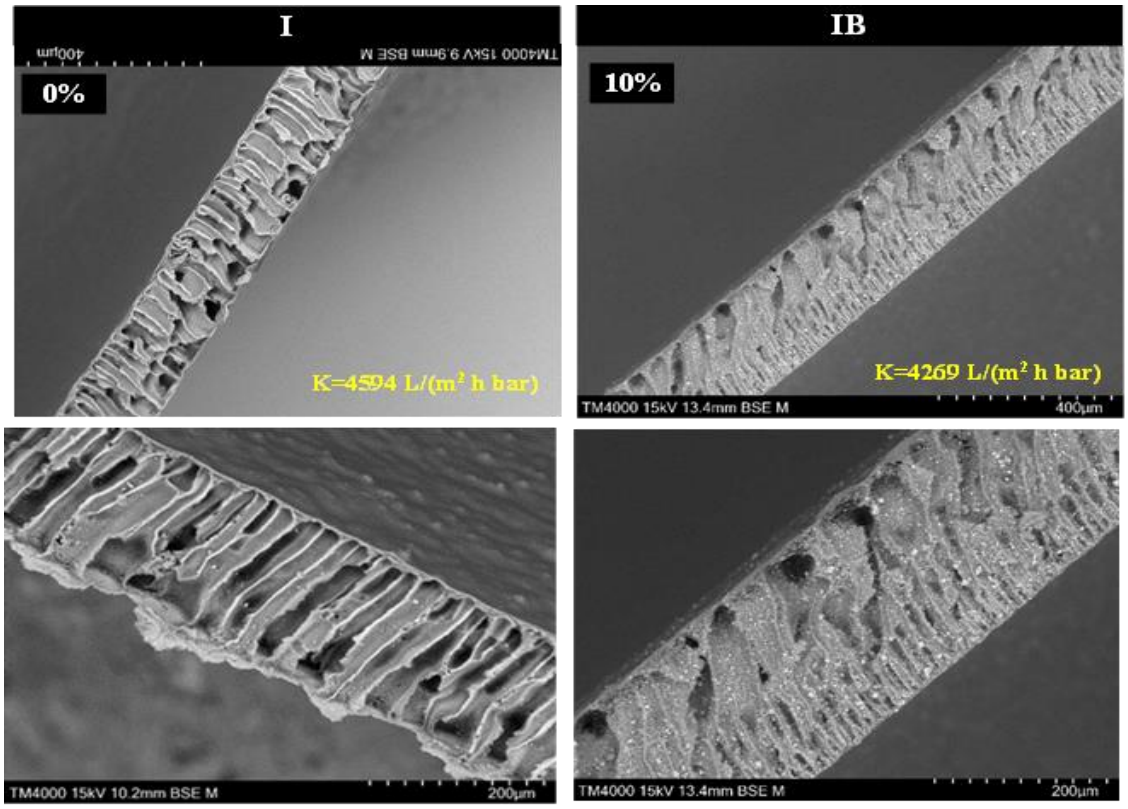


**Figure 42** Membrane section images I (8.2%AC, 24.5%GLY) with 0% filler, IB with 10% filler at scale of 200 µm and 400 µm.

A comparison of the water flux of the three different MMMAs prepared with 10% filler is shown in **Figure *43***. In this way, the performance of the different membranes can be compared and thus an assessment can be made of how and how much the presence of the adsorbent introduced in the different membranes influences the water flux and thus their permeability.

Using the same filler concentration, membranes FB and IB have very similar permeabilities, although membrane F initially has a much higher permeability than membrane I, an order of magnitude higher, specifically 14320 L/($m^2$ h bar) and 4594 L/($m^2$ h bar) respectively. Therefore, the presence of the adsorbent causes a much greater reduction of permeability in membrane FB than IB, 71.2% and 7.07%, thus almost 10 times higher. Membrane AB has much lower permeability values than FB and IB, although membranes A and I initially have very similar permeability values 4270.68 L/($m^2$ h bar) and 4593.55 L/($m^2$ h bar), the membrane AB undergoes a greater reduction in permeability due to the presence of the filler.

In conclusion, all membranes undergo a change of permeability and especially an inevitable change in the morphology of the membrane section with the introduction of filler. High amounts of filler as 25% in mass completely destroy the porosity present in the membrane without filler, collapsing the structure and making the membrane extremely dense and almost without porosity. This can be justified by the adsorbent as a powder with average particle size less than 2 μm that deform the structure of the pristine membrane.

More in detail, comparing the morphology of all MMMAs with 10% filler (AB, FB and IB), we can observe that membrane AB (11.1%AC, 6.6%PEG and 10% ZY) undergoes less morphological changes than membrane FB (11.1%AC, 3. 1%PEG and 10% ZFA). In fact, membrane F (FB with 0%filler) initially had small cavities even in the parts of the membrane that constituted the pore walls, but the presence of the filler induces the disruption and the deformation of the porosity, resulting in a denser membrane. In this way, very large macrovoids generate smaller pores due to the formation of dense walls and the structure collapses. This phenomenon is not observed with the same importance in membrane AB because membrane A (AB with 0% filler) initially is not characterized by the presence of small cavities in the pore walls that can be obstructed, but the pure polymeric membrane is denser.

This explains why at the same filler concentration, FB membrane has a higher percent reduction in permeability than AB membrane. Finally, IB (8.2%AC, 24.5% PEG and 10%

ZFA) membrane manages to retain a finger like porosity, but with smaller pore size (10µm) in the top of the section, macrovoids are formed in the bottom of the section that were not initially present in the membrane without filler. This is motivated by the different morphology that membrane I (AB with 0%filler) had, i.e., the pore walls were very thin and with very small cavities, therefore the presence of filler obstructs the microcavities and the membrane collapses only partially. This justifies the very low percentage reduction in permeability, between the membrane without and with filler compared to all other membranes.

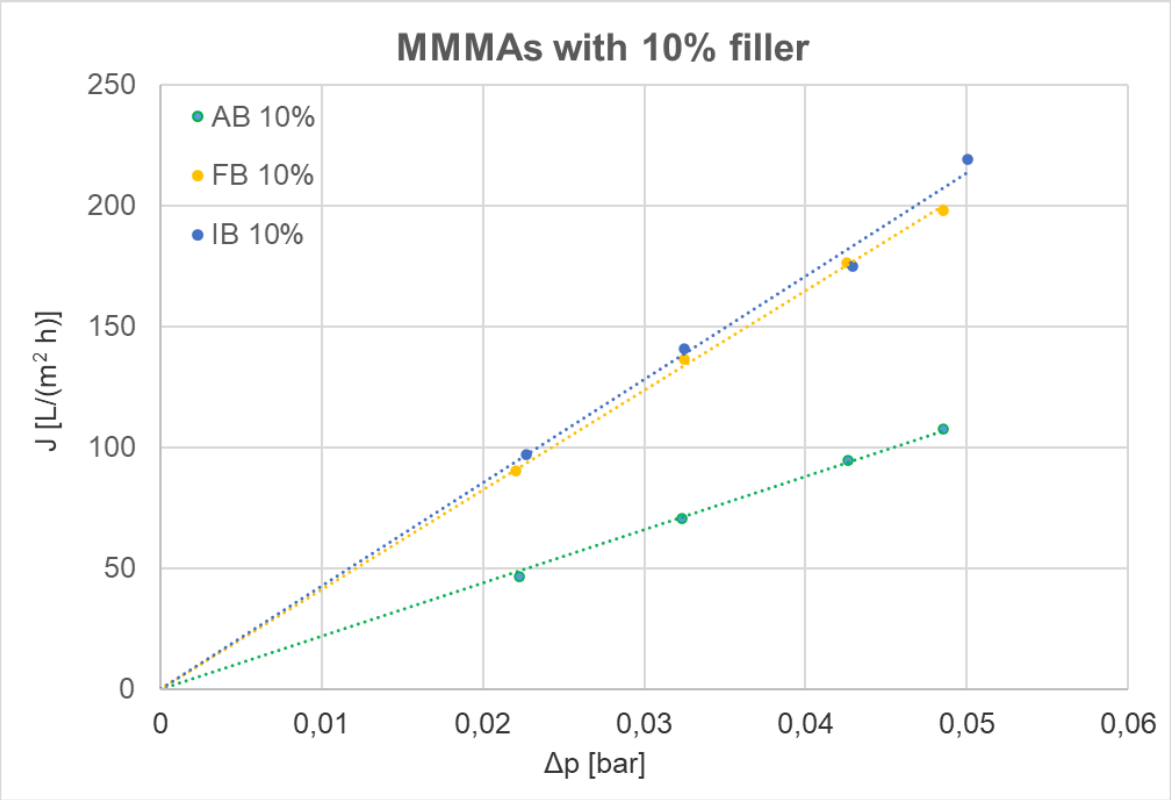


**Figure 43** Comparison of the water flux of different MMMAs with 10% filler concentration.

## 3.8 MMMAs adsorption tests

Adsorption tests on MMMAs are intended to evaluate the adsorption capacity of the composite material with adsorbent. This is an important evaluation because the binding capacity of a pure powdered adsorbent often changes when the same adsorbent is introduced into a matrix. The binding capacity of the free adsorbent is a parameter to identify the adsorbent material with greater adsorptive properties, while the adsorption capacity of the

adsorbent in the membrane is intended to verify that the composite material still retains good adsorptive capacity and is suitable for the purpose of this study removal of uremic toxins from the spent dialysate.

**Figure *44*** shows the static adsorption test in which the $q_{ads}$ (mg/(g/cm$^3$)) is defined as the mass of urea adsorbed over the density of the adsorbent in the membrane used for the test. The volume and density values used in the calculation are given in **Table *10***. From the graph it can be observed that membrane AC (11.1% CA; 6.6% PEG + 25% ZY) has the highest $q_{ads}$ of 17.7 mg/cm$^3$ and the adsorption values of membranes AB (11.1% CA; 6.6% PEG + 10% ZY) and AA (11.1% CA; 6.6% PEG + 5% ZY) decrease to values of 17.2 and 14.4 mg/mL, respectively. This behaviour is consistent with the amount of filler in membranes AA, AB and AC (same concentration of CA and PEG and same $T_{bath}$), sharing the same composition, the same type of adsorbent but increasing mass percentage concentrations of zeolite. Therefore, by increasing the amount of filler introduced into the membrane, the adsorption capacity per unit volume increases because there is more adsorbent in the same unit volume. It is also observed that the increase in $q_{ads}$ values as a function of the amount of filler introduced is greater at low concentrations of zeolite, for very high amounts of zeolite there is no further increase in $q_{ads}$. In fact, increasing the amount of zeolite from 5% to 10% in mass of ZY in the AB and AC membranes results in a 16% increase in $q_{ads}$, whereas increasing the amount of zeolite from 10% to 25% results in only a 2.8% increase in $q_{ads}$.

The FB (11.1% CA; 3.1% PEG +10% ZFA) and IB (8.2% CA; 24.5% PEG +10% ZFA) membranes have the same amount in mass and the same type of zeolite but different types of matrix into which the filler is introduced (the concentrations of CA and PEG are different). These membranes show no particular difference on the adsorption capacity and therefore the matrix composition has little effect on the $q_{ads}$. Furthermore, the FB, IB and AB membranes have the same concentration of 10% adsorbent, but different types of zeolite used, from this it can be deduced that the type of zeolite has little effect on the $q_{ads}$ of the MMMAs, in fact adsorption capacity values for all three membranes FB, IB and AB are in the range of 16-17 mg/cm$^3$.

Finally, the **Figure *45*** adsorption values defined as the mass of urea adsorbed on the adsorbent density used in the MMMAs are shown. The $q_{ads}$ values are reversed from those shown in **Figure *44***, i.e. membranes AA, AB and AC in this order have decreasing adsorption values of 27, 15 and 8 mg/(g/cm$^3$) respectively and membrane FB has an

adsorption value of 15.4 mg/(g/cm$^3$) compared to the highest value of 18 mg/(g/cm$^3$) of membrane IB. However, the $q_{ads}$ values of membranes AB, FB and IB continue to be similar values in the range of 18-15 mg/(g/cm$^3$).

The masses of adsorbent present in the membrane calculated as described in the paragraph 2.4.5 and used to calculate the adsorption capacity are shown below in the **Table *10***.

**Table 10** Mass values of membranes with adsorbent ($m_{MMMA}$), of membranes without adsorbent ($m_{mem}$) and of zeolite contained in the membrane ($m_{adsorbent}$). Thickness, volume and density values of membranes with a discoidal cross-section and a diameter of 2.5 cm.

| Membrane name | **AA** 11,1% CA 6,6% PEG + 5% ZY | **AB** 11,1% CA 6,6% PEG + 10% ZY | **AC** 11,1% CA 6,6% PEG + 25% ZY | **FB** 11,1% CA 3,1% PEG + 10% ZFA | **IB** 8,2% CA 24,5% PEG + 10% ZFA |
|---|---|---|---|---|---|
| **$m_{MMMA}$** [mg] | 24,4 | 35,3 | 54,6 | 32 | 25,1 |
| **$M_{mem}$** [mg] | 14,9 | 14,9 | 14,9 | 14,1 | 12,8 |
| **$m_{adsorbent}$** [mg] | 9,5 | 20,4 | 39,7 | 17,9 | 12,3 |
| **Thickness** [cm] | 0,0271 | 0,0271 | 0,0271 | 0,0264 | 0,024 |
| **Volume** [cm$^{3]}$ | 0,133 | 0,133 | 0,133 | 0,130 | 0,118 |
| **Density** [mg/cm$^3$] | 71,41 | 153,35 | 298,44 | 138,13 | 104,41 |

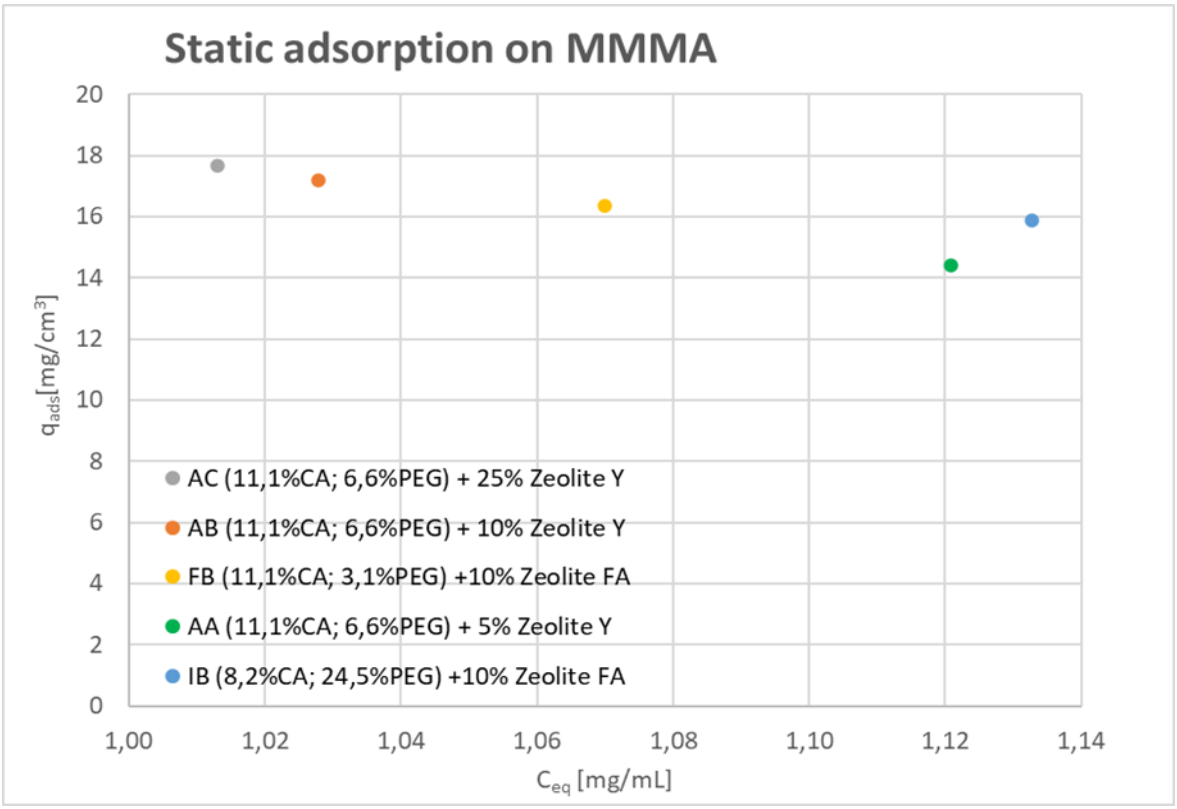


**Figure 44** Static adsorption of MMMAs (AA, AB, AC, FB and IB) where adsorption capacity is defined as mass of adsorbent over membrane volume.

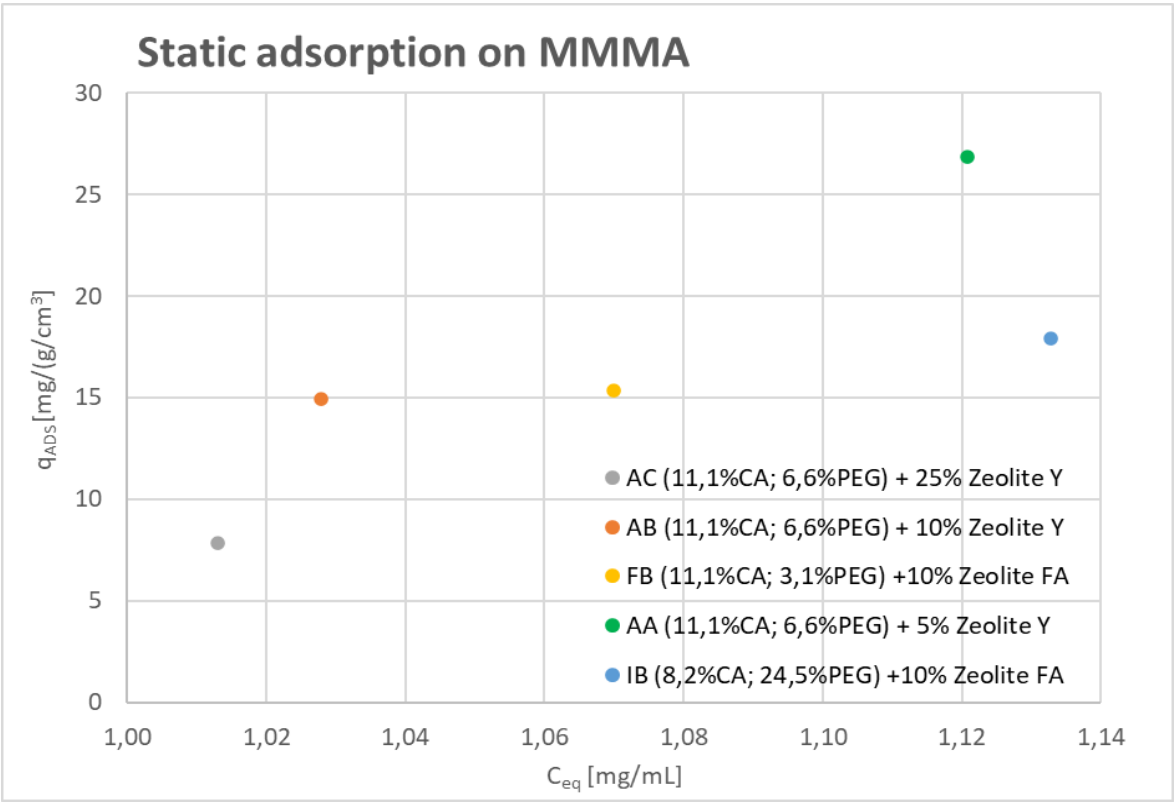


**Figure 45** Static adsorption of MMMAs (AA, AB, AC, FB and IB) where adsorption capacity is defined as mass of adsorbent over density of adsorbent in the membrane.

By comparing the results in **Figure *44*** with those in **Figure *45***, it can be deduced that not only the amount of adsorbent used is important but also how the adsorbent powder is dispersed and trapped in the matrix. In fact, the AC membrane has a higher $q_{ads}$ value ($mg/cm^3$) evaluated on the membrane volume unit than all other membranes but has a lower $q_{ads}$ value ($mg/(g/cm^3)$) evaluated on the density of adsorbent in the membrane. This is justified because in the first case it is assessed how much mass of urea has been adsorbed per unit volume of membrane but the effective surface area of the zeolite trapped in the membrane still available to adsorb urea is not considered. When the adsorbent is introduced as a filler in the membrane, not all of its surface area will be available to bind urea as in the case of a free adsorbent and not introduced in a matrix, because necessarily part of its surface area will be in contact with the membrane polymer so that the zeolite remains attached to the composite material. Thus, in the case of MMMAs (such as AC) where there is a high zeolite concentration, a great amount of the adsorbent is completely embedded in the membrane polymer and its surface area is not available for adsorption because it is not accessible to urea. In contrast to the AC membrane, the AA membrane, which has the same volume and type of matrix and zeolite as AC, but a much lower concentration of filler than AC, has a very high $q_{ads}$ over density of adsorbent because although the amount of zeolite contained in the membrane is very low, the surface area of the zeolite available to bind with urea is greater.

In conclusion, there is no further benefit on the adsorption capacity by introducing quantities of adsorbent much higher than 10% in mass.

For the purposes of adsorption capacity alone, without evaluating other properties such as permeability, the AA membrane is potentially the best composite material to use as it has a high adsorption capacity even if the adsorbent concentration is the lowest of all the other MMMAs.

In conclusion, considering both adsorptive properties and fluidodynamic features that characterise an MMMAs, the optimal membrane for the purposes of this work is IB In fact, IB membrane has both the highest adsorption capacity and permeability of all the other MMMAs tested in this work (AA, AB, AC, FB). In particular, IB has a permeability value of 4269 $L/(m^2\ h\ bar)$ (**Figure *43***) and has a $q_{ads}$ of 18 $mg/(g/cm^3)$.

# 4 Conclusions and future prospects

This work aimed the fabrication and the optimization of mixed matrix membranes (MMMAs) for dialysate regeneration in haemodialysis, with a special focus on urea capture. This represents a challenge to reduce the water consumption of haemodialysis, promoting home haemodialysis, home nocturne haemodialysis or designing a new wearable artificial kidney. Such transition would improve life of patient with chronic kidney failure. Not only is the amount of water needed for haemodialysis reduced, but the side effects on other organs due to discontinuous haemodialysis treatment (in-centre haemodialysis) are also reduced.

The optimal MMMA for this application has a large surface area, to expose larger quantities of adsorbent and thus adsorb larger quantities of toxin with a faster kinetics. To be able to do this, it will be necessary to have high-performance membranes and fillers with good toxin adsorption capacity. These are two fundamental requirements in order to obtain MMMAs for use in membrane modules, which retain good permeability and good binding capacity, suitable for supporting haemodialysis carried out regenerating small volumes of dialyzate.

An easy one-step protocol for membrane fabrication, through the NIPS technique, was developed. The membranes' properties were optimized by changing compositions of polymer and porogen, using glycerol or PEG as porogen, and studying the impact of the coagulation bath temperature.

Membranes of cellulose acetate produced revealed to not retain any solvent or porogen.

The membranes showed to have satisfactory properties and characteristics. The mechanical resistance is sufficient to prevent crushing and rupture of the membrane up to an maximum pressure of 0.05 bar, exerted on the membrane for up to 5 h, making the membrane self-standing. The permeability values have a range of 2000-16200 L/($m^2$ h bar) for membranes without filler and a range of 1100-4200 L/($m^2$ h bar) for MMMAs, depending on the composition of the membrane (polymer and porogen concentrations, type of porogen and temperature of the coagulation bath) and the type and quantity of filler introduced into it. The zeolites reached a maximum adsorption capacity of 26 mg/g and 16 mg/g (mg of urea adsorbed per g of adsorbent) at the equilibrium concentration of around 6 mg/mL for the zeolites Ferrierite Ammonium and zeolite Y respectively, values comparable with those reported in (De Pascale, 2021). These zeolites were found to be the best zeolites tested in

this work. In addition, all zeolites tested, including zeolite Ferrierite Ammonium and zeolite Y have very fast adsorption kinetics, reaching equilibrium just about 15-20 min after contact with urea. For these reasons, zeolite ferrierite Ammonium and zeolite Y were used to fabricate the MMMAs.

Membranes with glycerol as a filler, 11.1%CA and 11.1%GLY (H) and 8.2%CA and 24.5%GLY (I) had been produced demonstrating that glycerol concentrations have a strong effect on morphology but not on permeability, in fact the H and I membranes have the same permeability values of approximately 2500 L/($m^2$ h bar) at $T_{bath}$= 22°C or approximately 4000 L/($m^2$ h bar) at $T_{bath}$= 40°C. Furthermore, membranes with glycerol as filler have lower permeability values than those obtained with PEG as filler with the same concentrations and bath temperature, in fact, membrane 11.1%CA and 11.1%PEG (G) has a permeability of 3467 L/(m2 h bar) compared to 2497 L/(m2 h bar) of membrane H.

It was observed that the temperature of the coagulation bath is the factor that most influences both permeability and membrane morphology. Membranes casted at a bath temperature of 50°C have higher permeability values than the same membranes casted at a lower bath temperature such as 22°C, e.g. membrane A has values of 16257 and 4271 L/(m2 h bar) at 50°C and 22°C, respectively. In general, the permeability increases with increasing temperature.

The introduction of the filler in the membrane influences the permeability values. In fact, the permeability decreases with the filler introduction, a reduction of 17.9% of permeability was observed with 5% filler (membrane AA), while increasing the amount of filler up to 10% filler (membrane AB), a permeability dropped of 45.3%. Interestingly the reduction for membrane IB with 10% filler was only 7%. The permeability values of the MMMAs filler concentrations not exceeding 10% were in the range of 2336 - 4248 L/($m^2$ h bar).

It can be seen from the adsorption tests on the MMMA that it is not only the amount of filler introduced that is important for the adsorption capacity, but also its distribution and adhesion with the polymer in the membrane. Further increases above 10% zeolite do not bring significant increases in adsorption capacity, from 5% (AA) to 10% (AB) zeolite $q_{ads}$ increases of 16%, whereas from 10% (AB) to 25% (AC) zeolite the increase in $q_{ads}$ is only 2.8%. Therefore, a membrane with 5% filler (AA) has a high adsorption capacity measured with respect to the density of adsorbent in the membrane of 27 mg/(g/$cm^3$) compared to the

same membrane with 25% zeolite (AC) with $q_{ads}$ of 8 mg/(g/cm$^3$) due to a higher surface area available for adsorption and accessible to urea.

SEM images showed a very thin skin layer with a uniform pore size distribution of 5 µm on average. A *finger-like* microstructure is observed in most of the samples. Nonetheless, it has been shown that changing the amount of porogen does not have a great effect on the morphology of the membrane section. In contrast, the different type of porogen, PEG-400 or glycerol, had a strong effect on the morphology, making significant changes in the membrane structure. When glycerol is used as a porogen, the major differences are recognized in the regularity and size of the finger like poroes along the section and in the size of the macrovoids at the bottom of the membrane.

The MMMAs showed a homogeneous dispersion of the adsorbent in the membrane and demonstrated that the morphology did not undergo a major change at the microscopic level, even after the introduction of the filler at 5%wt concentrations, which justifies the moderate reduction in permeability achieved. Interestingly, the use of 10% powder in MMMAs with 11.1% CA, 3.1% PEG (FB) and with 8.2%AC, 24.5% GLY (IB) has a strong impact on the structure, whereas for the 11.1%CA, 6.6% PEG (AB) membrane the structure remains the same.

For all MMMAs, increasing the filler concentration increased the membrane the density of to the point of causing the microstructure to collapse for high filler concentrations.

According to what was obtained in this study, the MMMA that optimises permeability and adsorption capacity is IB (8.2% CA; 24.5%GLY + 10% zeolite Ferrierite Ammonium; $T_{bath}$=40°C). This has the highest permeability of all MMMA with 10% filler of 4269 L/(m$^2$ h bar) and an excellent adsorption capacity of 18 mg/(g/cm$^3$) (mass of adsorbed urea on density of zeolite in the membrane, i.e. mass of zeolite on volume of membrane).

Despite the satisfactory results in terms of permeability and adsorption capacity, MMMAs for this application can be further optimised.

The membranes might be improved, increasing the surface area and/or obtaining “sponge like” porosity, by using different bath compositions and conditions, (e.g. by using different non-solvent, temperature or pH), or changing the mode of pore formation, (e.g. by using a salt such as $CaCO_3$).

This work has focused on improving the chemical-physiological and mechanical properties of membranes, however, at present, the known adsorbent materials suitable for this type of application do not have a good ability to capture urea effectively selectively enough, therefore filler selection is still a challenge.

# Reference


Avramescu, M.-E. *et al.* (2003) 'Preparation of mixed matrix adsorber membranes for protein recovery', *Journal of Membrane Science*, 218(1), pp. 219–233. Available at: https://doi.org/10.1016/S0376-7388(03)00178-9.

Azar, A.T. and Canaud, B. (no date) 'Hemodialysis System', in *Modelling and Control of Dialysis Systems*. Berlin, Heidelberg: Springer Berlin Heidelberg (Studies in Computational Intelligence), pp. 99–166. Available at: https://doi.org/10.1007/978-3-642-27458-9_3.

Bauer, C., Melamed, M.L. and Hostetter, T.H. (2008) 'Staging of Chronic Kidney Disease: Time for a Course Correction', *Journal of the American Society of Nephrology*, 19(5), p. 844. Available at: https://doi.org/10.1681/ASN.2008010110.

Cheah, W.-K., Sim, Y.-L. and Yeoh, F.-Y. (2016) 'Amine-functionalized mesoporous silica for urea adsorption', *Materials Chemistry and Physics*, 175, pp. 151–157. Available at: https://doi.org/10.1016/j.matchemphys.2016.03.007.

Couser, W.G. *et al.* (2011) 'The contribution of chronic kidney disease to the global burden of major noncommunicable diseases', *Kidney International*, 80(12), pp. 1258–1270. Available at: https://doi.org/10.1038/ki.2011.368.

De Pascale, M. <1992> (2021) *Novel membranes for hemodialysis application*. Doctoral Thesis. Alma Mater Studiorum - Università di Bologna. Available at: http://amsdottorato.unibo.it/9605/ (Accessed: 20 June 2022).

'FTIR.pdf' (no date). Available at: http://webusers.fis.uniroma3.it/iucci/gio/FTIR.pdf (Accessed: 15 January 2023).

Galarneau, A. *et al.* (2001) 'True Microporosity and Surface Area of Mesoporous SBA-15 Silicas as a Function of Synthesis Temperature', *Langmuir*, 17(26), pp. 8328–8335. Available at: https://doi.org/10.1021/la0105477.

van Gelder, M.K. *et al.* (2018) 'From portable dialysis to a bioengineered kidney', *Expert Review of Medical Devices*, 15(5), pp. 323–336. Available at: https://doi.org/10.1080/17434440.2018.1462697.

van Gelder, M.K. *et al.* (2020) 'Urea removal strategies for dialysate regeneration in a wearable artificial kidney', *Biomaterials*, 234, p. 119735. Available at: https://doi.org/10.1016/j.biomaterials.2019.119735.

Geremia, I. *et al.* (2021) 'New mixed matrix membrane for the removal of urea from dialysate solution', *Separation and purification technology*, 277, p. 119408. Available at: https://doi.org/10.1016/j.seppur.2021.119408.

Health, C. for D. and R. (2020) *Quality Assurance Guidelines for Hemodialysis Devices, U.S. Food and Drug Administration*. FDA. Available at: https://www.fda.gov/regulatory-information/search-fda-guidance-documents/quality-assurance-guidelines-hemodialysis-devices (Accessed: 23 February 2023).

*Hemodialysis - ClinicalKey* (2020). Available at: https://www-clinicalkey-com.ezproxy.is.ed.ac.uk/#!/content/book/3-s2.0-B9780323532655000630 (Accessed: 10 June 2022).

Hosten, A.O. (1990) 'BUN and Creatinine', in H.K. Walker, W.D. Hall, and J.W. Hurst (eds) *Clinical Methods: The History, Physical, and Laboratory Examinations*. 3rd edn. Boston: Butterworths. Available at: http://www.ncbi.nlm.nih.gov/books/NBK305/ (Accessed: 17 November 2022).

Innovation, A. for C. (2014) *Water for dialysis: A guide for in-centre, satellite and home haemodialysis in NSW, Agency for Clinical Innovation*. Agency for Clinical Innovation (ACI). Available at: https://aci.health.nsw.gov.au/resources/renal/dialysis (Accessed: 23 February 2023).

Jane Y. Yeun, Brian Young, Thomas A. Depner e Andrew A. Chin (2020) *Hemodialysis - ClinicalKey*. Available at: https://www-clinicalkey-com.ezproxy.is.ed.ac.uk/#!/content/book/3-s2.0-B9780323532655000630?scrollTo=%23hl0000849 (Accessed: 18 January 2023).

Klarenbach, S. and Manns, B. (2009) 'Economic Evaluation of Dialysis Therapies', *Seminars in Nephrology*, 29(5), pp. 524–532. Available at: https://doi.org/10.1016/j.semnephrol.2009.06.009.

Lehmann, H.D., Marten, R. and Gullberg, C.A. (1981) 'How To Catch Urea? Considerations on Urea Removal from Hemofiltrate', *Artificial Organs*, 5(3), pp. 278–285. Available at: https://doi.org/10.1111/j.1525-1594.1981.tb04002.x.

Maduell, F. (2018) 'Hemodiafiltration versus conventional hemodialysis: Should "conventional" be redefined?', *Seminars in Dialysis*, 31(6), pp. 625–632. Available at: https://doi.org/10.1111/sdi.12715.

Mazinani, S. *et al.* (2017) 'Phase separation analysis of Extem/solvent/non-solvent systems and relation with membrane morphology', *Journal of Membrane Science*, 526, pp. 301–314. Available at: https://doi.org/10.1016/j.memsci.2016.12.031.

Mcfarlane, P.A., Pierratos, A. and Redelmeier, D.A. (2002) 'Cost savings of home nocturnal versus conventional in-center hemodialysis', *Kidney International*, 62(6), pp. 2216–2222. Available at: https://doi.org/10.1046/j.1523-1755.2002.00678.x.

Miliani, M.R. (2020) '"L'azotemia che cos'è?": la risposta alle domande più frequenti.', *Fondazione Italiana del Rene*, 29 January. Available at: https://www.fondazioneitalianadelrene.org/azotemia-che-cose/ (Accessed: 10 February 2023).

miriana (2021) 'Quali sono gli stadi della malattia renale cronica?', *Fondazione Italiana del Rene*, 7 June. Available at: https://www.fondazioneitalianadelrene.org/quali-sono-gli-stadi-della-malattia-renale-cronica/ (Accessed: 27 February 2023).

Mowatt, G., Vale, L. and MacLeod, A. (2004) 'Systematic review of the effectiveness of home versus hospital or satellite unit hemodialysis for people with end-stage renal failure', *International Journal of Technology Assessment in Health Care*, 20(3), pp. 258–268. Available at: https://doi.org/10.1017/s0266462304001060.

Mulder, M. (1996) *Basic Principles of Membrane Technology*. Dordrecht, NETHERLANDS, THE: Springer Netherlands. Available at: https://link.springer.com/book/10.1007/978-94-009-1766-8 (Accessed: 10 May 2022).

Nguyen, C.H. *et al.* (2021) 'Enhanced and selective adsorption of urea and creatinine on amine-functionalized mesoporous silica SBA-15 via hydrogen bonding', *Microporous and Mesoporous Materials*, 311, p. 110733. Available at: https://doi.org/10.1016/j.micromeso.2020.110733.

Olesberg, J.T., Arnold, M.A. and Flanigan, M.J. (2004) 'Online Measurement of Urea Concentration in Spent Dialysate during Hemodialysis', *Clinical Chemistry*, 50(1), pp. 175–181. Available at: https://doi.org/10.1373/clinchem.2003.025569.

'Phosphate-buffered saline (PBS)' (2006) *Cold Spring Harbor Protocols*, 2006(1), p. pdb.rec8247. Available at: https://doi.org/10.1101/pdb.rec8247.

Raymond M. Hakim and Sharmeela Saha (2013) *Dialysis frequency versus dialysis time, that is the question | Elsevier Enhanced Reader*. Available at: https://doi.org/10.1038/ki.2013.474.

Roberts, M. *et al.* (2000) 'THE REDY® RECIRCULATING DIALYSIS SORBENT SYSTEM: STRATEGIES TO INCREASE CLEARANCES', *ASAIO Journal*, 46(2), p. 212.

Romay, M., Diban, N. and Urtiaga, A. (2021) 'Thermodynamic Modeling and Validation of the Temperature Influence in Ternary Phase Polymer Systems', *Polymers*, 13(5), p. 678. Available at: https://doi.org/10.3390/polym13050678.

Saljoughi (2009) *Effect of preparation variables on morphology and pure water permeation flux through asymmetric cellulose acetate membranes*. Available at: https://doi.org/10.1016/j.memsci.2008.10.044.

Saljoughi, E., Amirilargani, M. and Mohammadi, T. (2010) 'Effect of PEG additive and coagulation bath temperature on the morphology, permeability and thermal/chemical stability of asymmetric CA membranes', *Desalination*, 262(1), pp. 72–78. Available at: https://doi.org/10.1016/j.desal.2010.05.046.

Shinaberger, C.S. *et al.* (2006) 'Longitudinal Associations Between Dietary Protein Intake and Survival in Hemodialysis Patients', *American Journal of Kidney Diseases*, 48(1), pp. 37–49. Available at: https://doi.org/10.1053/j.ajkd.2006.03.049.

Stokes, J.B. (2011) 'Consequences of Frequent Hemodialysis: Comparison to Conventional Hemodialysis and Transplantation', *Transactions of the American Clinical and Climatological Association*, 122, pp. 124–136.

Tarrass, F. *et al.* (2010) 'Water Conservation: An Emerging but Vital Issue in Hemodialysis Therapy', *Blood Purification*, 30(3), pp. 181–185. Available at: https://doi.org/10.1159/000321485.

Vanholder, R., Gryp, T. and Glorieux, G. (2018) 'Urea and chronic kidney disease: the comeback of the century? (in uraemia research)', *Nephrology Dialysis Transplantation*, 33(1), pp. 4–12. Available at: https://doi.org/10.1093/ndt/gfx039.

Weiner, I.D., Mitch, W.E. and Sands, J.M. (2015) 'Urea and ammonia metabolism and the control of renal nitrogen excretion', *Clinical Journal of the American Society of Nephrology*, 10(8), pp. 1444–1458. Available at: https://doi.org/10.2215/CJN.10311013.

Wernert, V. *et al.* (2005) 'Adsorption properties of zeolites for artificial kidney applications', *Microporous and Mesoporous Materials*, 83(1), pp. 101–113. Available at: https://doi.org/10.1016/j.micromeso.2005.03.018.

Yang, J. and He, W. (eds) (2020) *Chronic Kidney Disease: Diagnosis and Treatment*. Singapore: Springer Singapore. Available at: https://doi.org/10.1007/978-981-32-9131-7.

Yi Suen, S. (2015) 'Mixed Matrix Membranes for Adsorption Application', *Journal of Chemical Engineering & Process Technology*, 06(01). Available at: https://doi.org/10.4172/2157-7048.1000e119.

# Appendix

In order to obtain the adsorption values as binding capacity, it is first necessary to obtain spectra and calibration curves of the toxins for the identification of the optimal values for the *m* and *q* parameters as explained in detail in the section 2.2.3.

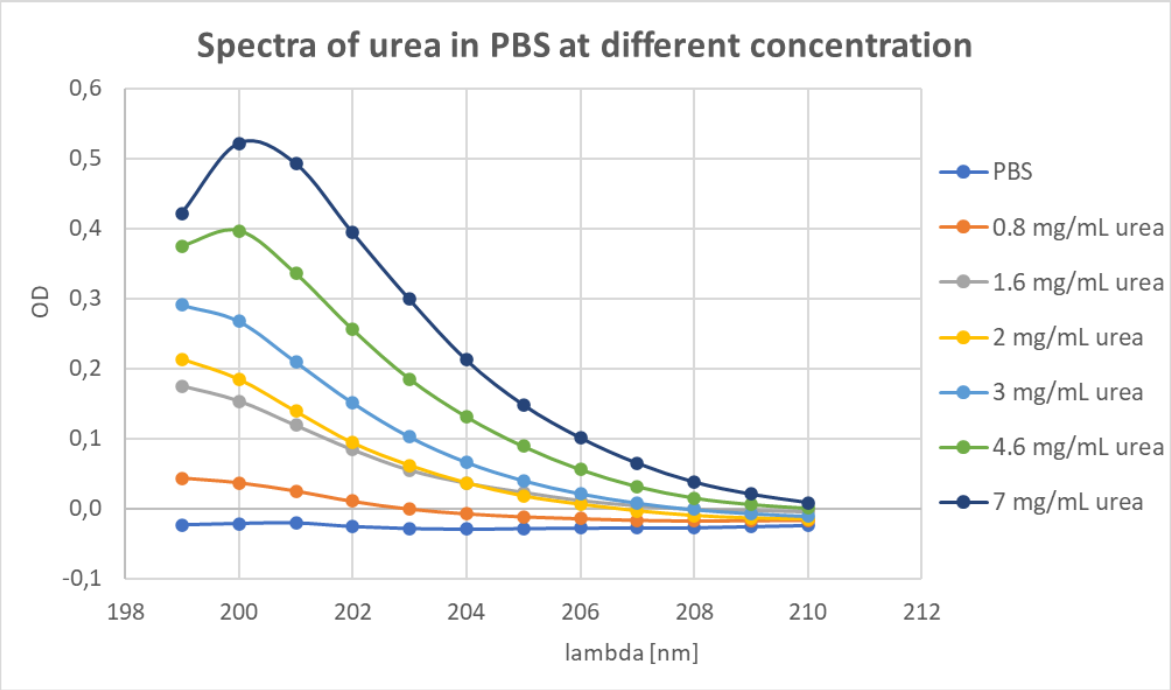


**Figure A.1** Spectra of urea in PBS at different urea concentrations.

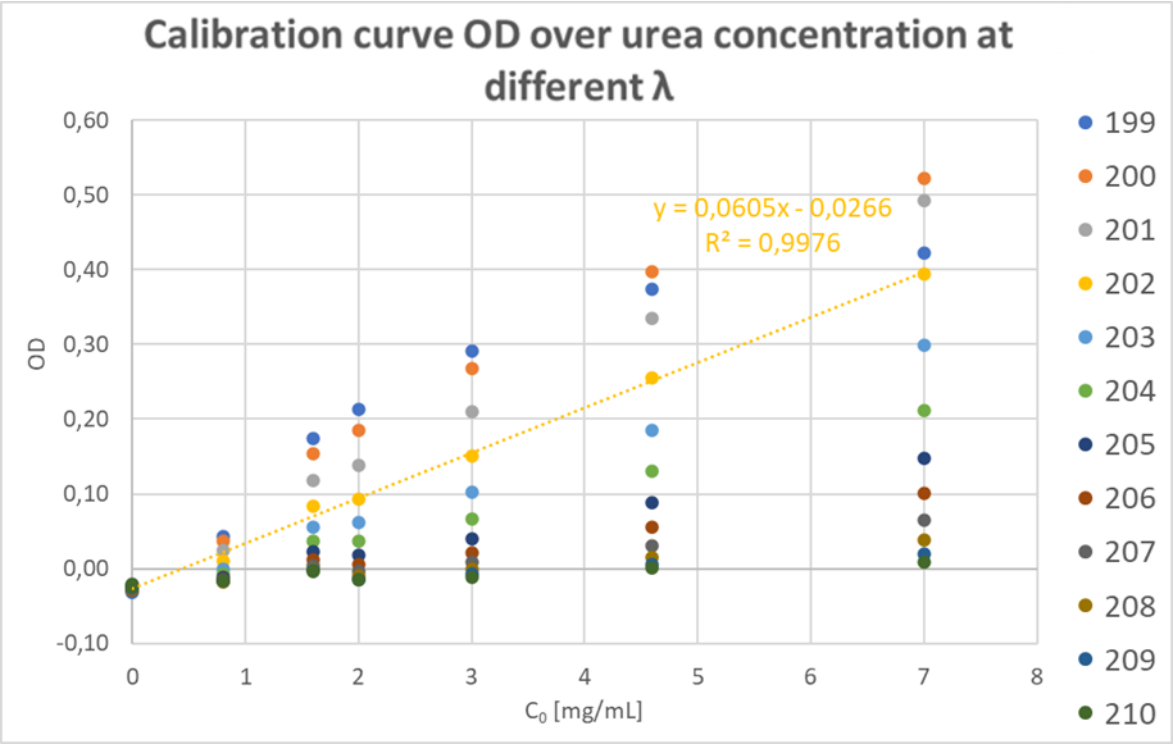


**Figure A.2** Calibration curve OD over urea concentration.

**Figure A.1** shows the urea calibration curve at different wavelengths in which the OD is shown in the abscissae and the initial urea concentrations from 0 to 7 mg/mL in the ordinates in contrast to **Figure A.2**. The graph shown in **Figure A.3** is more functional in practice to obtain the values of m and q immediately without further calculation. Once the adsorption process has been completed, the parameters m and q are then used to obtain the concentration at equilibrium of urea $C_{eq}$, knowing the OD values from the nanodrop examination of the sample (for calculation details refer to the section 2.2.3).

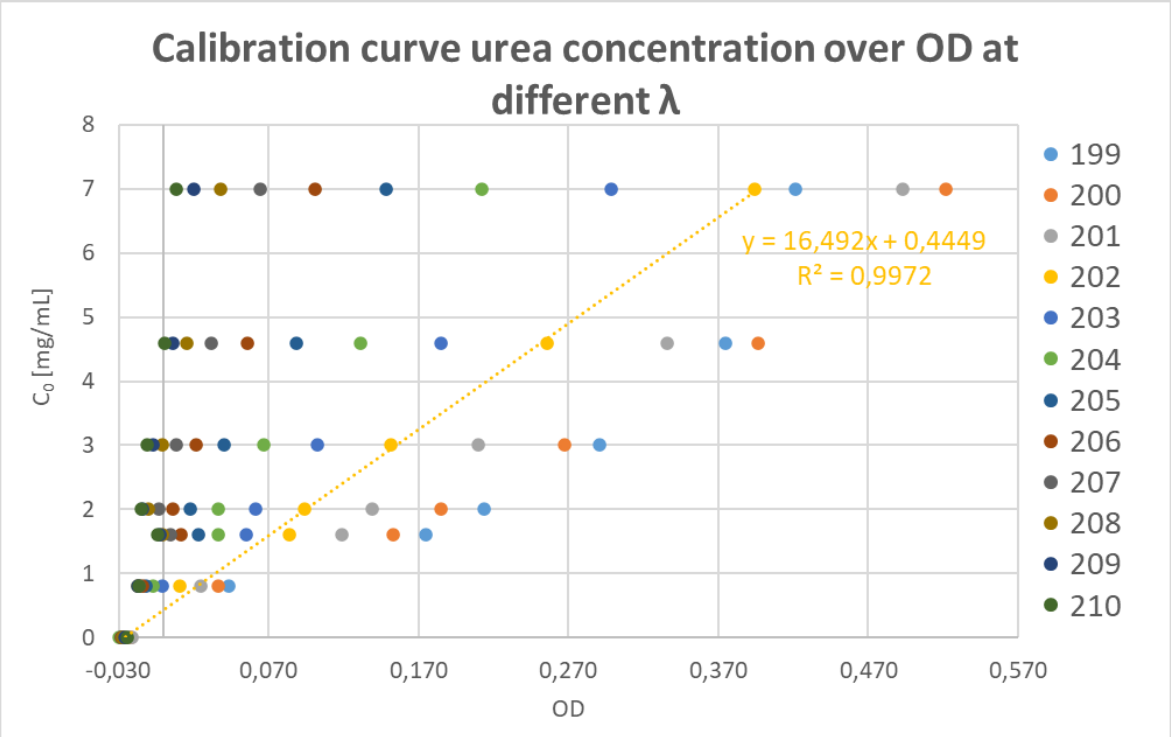


**Figure A.3** Calibration curve urea concentration over OD.

The creatinine spectra as a function of OD and wavelengths are shown in the **Figure A.4**. The spectra at concentrations of 0.5 and 1 mg/mL creatinine in PBS show two peaks since out of the linearity range.

As for urea, **Figure A.5** and **Figure A.6** show the OD values as a function of initial creatinine concentration at the various wavelengths to identify the wavelength at which there is greater linearity and thus obtain the parameters of the calibration line (*m* and *q*).

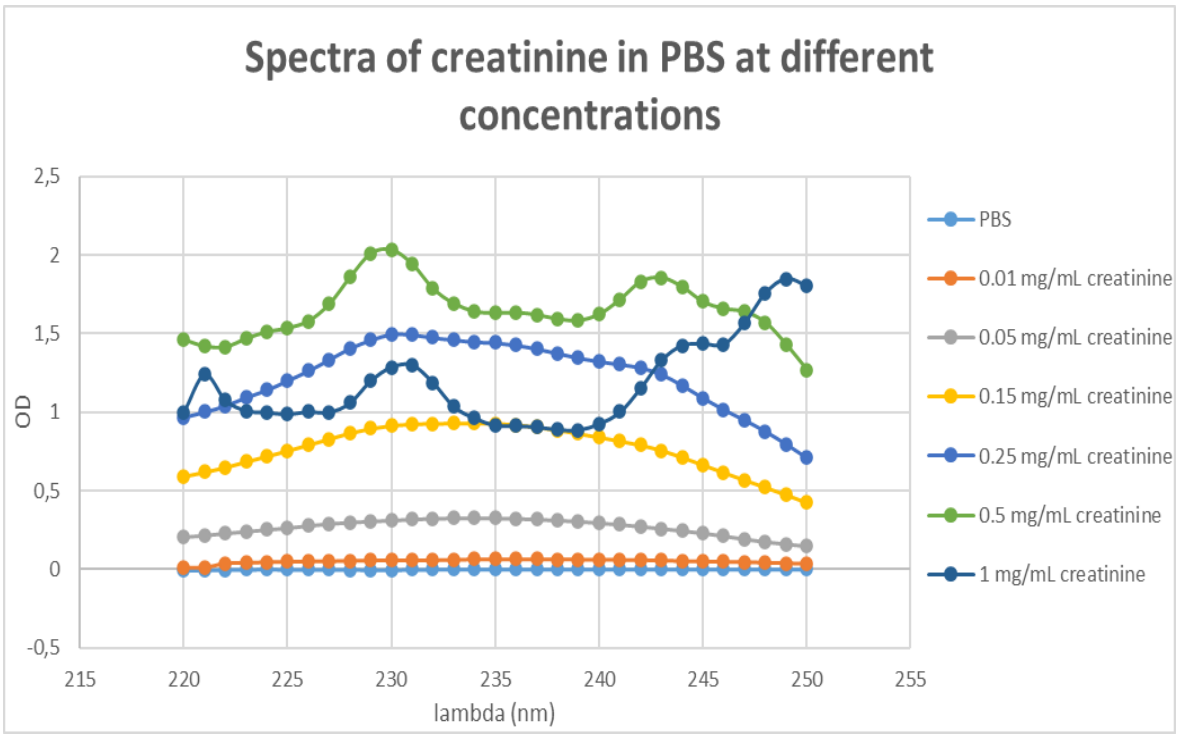


**Figure A.4** Spectra of creatinine in PBS at different urea concentrations.

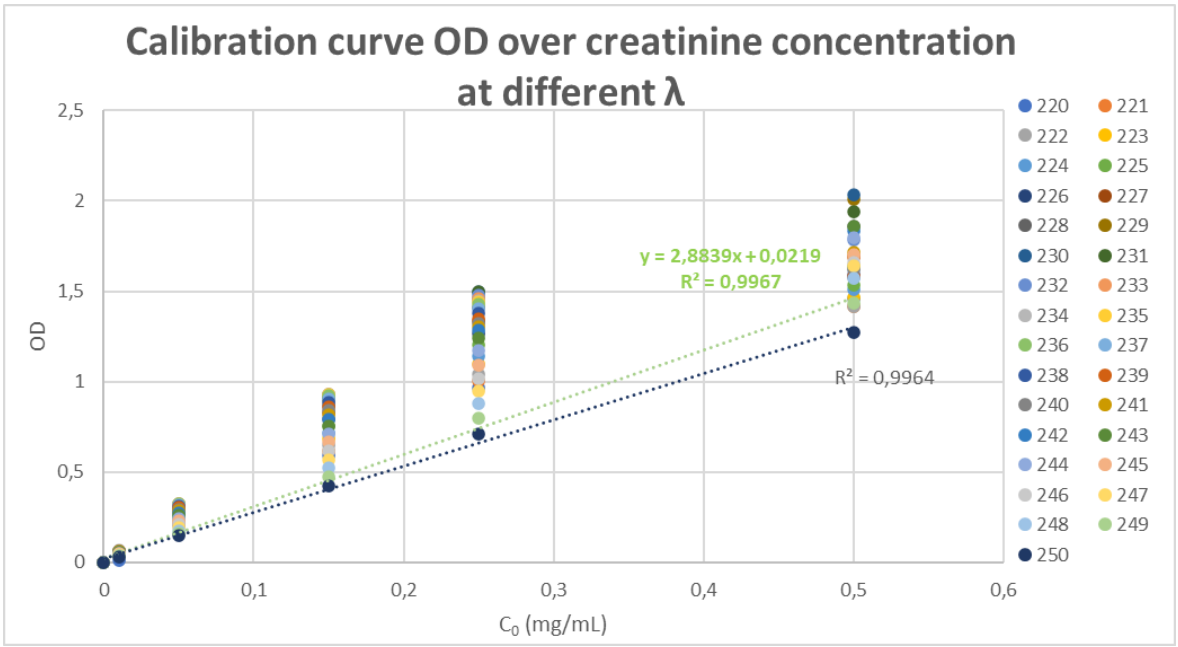


**Figure A.5** Calibration curve OD over creatinine concentration.

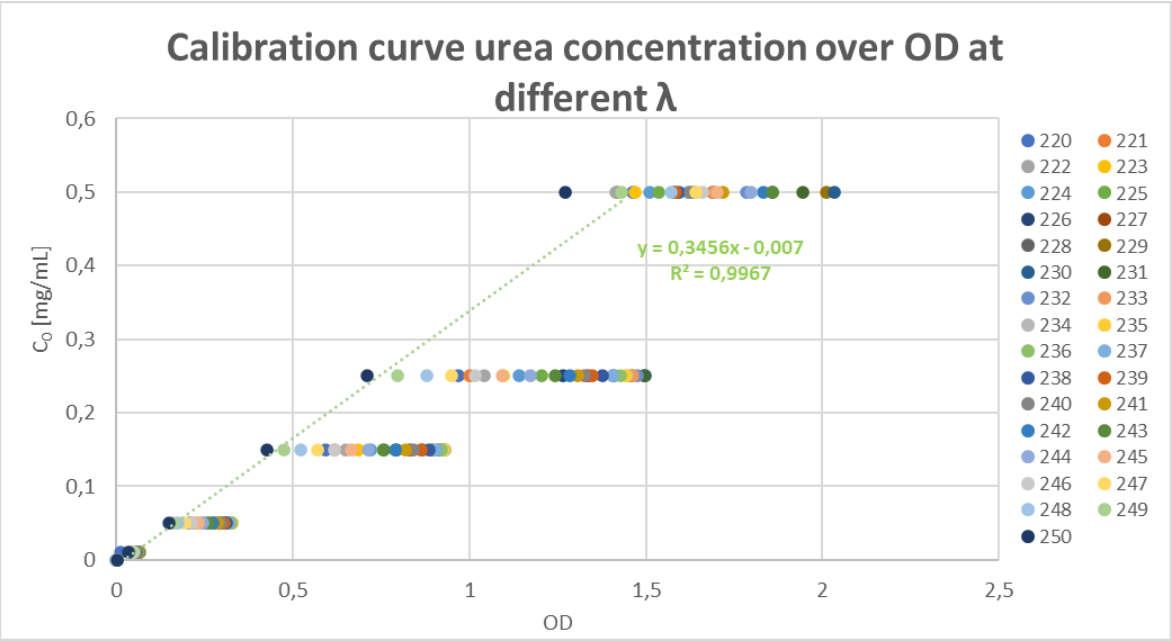


**Figure A.6** Calibration curve creatinine concentration over OD.